LEVEL D

FLOW RESEARCH COMPANY

A DIVISION OF FLOW INDUSTRIES, INC.

(14) FLOW-RR-69

(1)

A067 195

(9) [redacted] Research Report, [redacted]

(6) # Turbulent Flow Past A Self-Propelled Vehicle. I. Formulation. Revision.

(12) 112 p.

(10) W. J. Grabowski, R. L. Gran, R. E. Robins, T. Kubota, James J. Riley, D. R. S. Ko, and S. M. Bernstein

December 1976 (Revised December 1977 and December 1978)

(11) Dec 78

Sponsored by:

Defense Advanced Research Projects Agency
ARPA Order No. 1910

(15) [redacted] N00014-76-C-0564 ARPA Order-1910
Program Code No. NR 062-541/12-11-75
Name of Contractor: Flow Research Company
A Division of Flow Industries, Inc.
Principal Investigator and Phone Number: Dr. James J. Riley
(206) 854-1370

Scientific Officer: Dr. Philip A. Selwyn
Effective Date of Contract: 1 February 1976
Contract Expiration Date: 31 October 1977
Amount of Contract: $107,940.00
Short Title of Work: Turbulent Wake Flow

79 08 14 036

390 409 79 08 20 033 alt

Abstract

This report describes the formulation of a numerical procedure for simulating the turbulent, incompressible flow over and behind an axisymmetric, self-propelled body. The flow is treated in three parts: (i) over the body, (ii) through the propeller, and (iii) in the very near wake of the body, where axial gradients cannot be ignored.

Over most of the body, the flow is easily available from the Reynold's number of the flow and the body shape, but near the body's tail, a special treatment is required. The non-radial components of the mean flow through the propeller are obtained from a computer code based on a classical blade element analysis, while the radial component is obtained analytically in terms of the non-radial components. The effect of the propeller on the aft-body boundary layer turbulence is obtained by integrating the very near wake turbulence model equations across the plane of the propeller.

In the very near wake, the flow is computed from the time-averaged Navier-Stokes equations, closed with a second-order model for the turbulence correlations. This system of equations is elliptic, so conditions at all boundaries of the very near wake region are required. In order to choose a sufficiently large solution domain without sacrificing adequate resolution just behind the propeller, the equations are transformed logarithmically. A uniformly discretized version of the transformed equations is solved using an ADI (Alternating-Direction-Implicit) procedure. The flow is treated as transient and is allowed to evolve to a steady state.

Three sample calculations are presented with comparisons to experimental data which are generally favorable.

Foreword

The purpose of this foreword is to clarify the roles of each of the authors in the writing of this report. It should be understood that the persons associated with the writing are the ones who performed the work being reported.

The primary contributions are due to Grabowski who wrote Section 3 and the related Appendices, and to a group from Physical Dynamics, Inc. (PDI), composed of Gran, Kubota, and Ko, who wrote Section 2 and the related Appendix. The PDI group was supported by a subcontract from Flow Research, Inc., contract No. PDI-1-ICWAKE. Sections 4 and 5 are due to Grabowski and Robins, and Section 1 is due to Riley, Robins, Grabowski and the PDI group. Bernstein contributed the details of the Flow Research propeller analysis to Section 2, and the overall coordination and editing was handled by Robins.

One outcome of this diversity of authors is that the nomenclature is not uniform throughout the report. For example, Section 2 uses coordinates and symbols appropriate for boundary layer flows, Section 3 uses coordinates and symbols appropriate for wake flows, and Appendix A uses notation that is convenient for the analysis contained therein. Confusion resulting from the nonuniform nomenclature should be minimal, however, since all symbols are clearly defined within the context of their use.

One further note is that the work reported herein was accomplished with a level of support approximately equal to 80 percent of the contract dollar amount.

A special acknowledgement is due Walt Reddall of Aerospace, Corp., who painstakingly reviewed a preliminary draft of the report and made many important suggestions.

Table of Contents

Table of Contents (Cont.)

1. Introduction

When modeling the flow around and behind a self-propelled body, it is convenient to divide the domain of the flow into two regions (see Figure 1.1). These regions are Region I, which contains the flow around the body and in its very near wake, where axial gradients of flow quantities are important, and Region II, the downstream portion of the wake, where axial gradients can be neglected. This division has important economic consequences, since an expensive detailed calculation of the flow is needed only in Region I, the results of which can be used to provide a plane of initial conditions for a relatively inexpensive, marching type calculation in Region II.

The phenomena associated with the boundary-layer, propeller, and near-wake portions of Region I (what we have termed region I½ in Figure 1.1) have, until now, received little attention, but accurate flow calculations in this region are essential in order to correctly initialize calculations in Region II. It is the purpose of this report to describe a method for modeling the flow in Region I½, the key elements of which include (Figure 1.2): (1) the boundary-layer flow near the stern of the body ($z < 0$), (2) the flow through the propeller ($0^- < z < 0^+$), and (3) the flow in the near-wake region ($0^+ < z < z_o$). Here, z is the distance downstream of the body's tail and z_o marks the beginning of Region II.* The above flow elements are treated in Sections 2.1, 2.2, and Section 3, respectively, of this report. Before proceeding to these discussions, we first briefly summarize the characteristics of each element.

The body boundary-layer flow is, in general, easily computed or estimated from the flow Reynolds number and body shape. Near the stern of the body, however, where the body radius becomes small compared with the turbulent boundary-layer thickness, the flow evaluation is not straight-forward and a special treatment is required. As the flow passes through the propeller, both the mean and the turbulent flow fields are altered. The flow at $z = 0^+$, required for the near-wake calculation, is evaluated in three parts: (a) the mean axial and swirl

---

*A typical value for z_o, based on Flow Research Laboratory results (Lin, et. al (1974)), is 12 body radii behind the body tail.

velocities, (b) the mean radial velocity, and (c) the Reynolds stresses. In the near-wake region, the flow is characterized by relatively large radial and axial mean shears and high energy exchange rates; it is strongly influenced by the body and propeller configurations. In particular, significant production of turbulent energy arises from the swirl induced velocity gradients and the non-uniformities in the axial flow. Accompanying the increasing turbulent energy is an increase in the rate at which turbulent energy is dissipated into heat. In fact, according to the measurements of Gran (1972), the bulk of the excess energy input to the flow field by the propeller is dissipated in the near-wake region.

A computer code, ICWAKE, based on the methods described in this report has been written to compute the flow in Region I½ and thus provide initial conditions for the Region II calculation. The code is described by Grabowski and Robins (1976).

2. Propeller Region

2.1 Aft-Body Boundary-Layer Characterization

In order to estimate the fluid flow velocities in the near wake, consideration must first be given to the boundary-layer flow field which envelopes the surface of the body. The body shape is assumed to be axisymmetric and slender in the sense that the body length is considerably larger than its maximum frontal diameter. A typical characterization of the body shape is given by a Rankine Ovoid with a length-to-diameter ratio of about 10. Often, the aft-end of the body is more gradually tapered than a Rankine Ovoid in order to alleviate the tendency for the boundary layer to separate. The orientation of the major axis of the body is assumed to coincide with the direction of the approaching flow. Slight deviations (i.e., small angles of attack) are not expected to grossly affect the wake flow field.

The boundary layer which develops on the body is assumed to be fully turbulent well ahead of the mid-section which implies that the Reynolds number (based on the speed of the body and its frontal diameter) is in excess of 10^6. Over most of the body surface, the description of the boundary layer is amenable to conventional analysis because it is usually thin in comparison with the local body radius ($\delta/R \ll 1$). Near the stern of the body, its description becomes difficult. This difficulty arises because of two separate but concurrent effects: because of the decreasing cross-section body radius, the boundary layer undergoes a change from a flat-plate-like flow ($\delta/R \ll 1$) to one where axisymmetric effects dominate and $\delta/R \to \infty$; and because there exists substantial interaction between the thick boundary layer near the aft end of the body and the potential flow outside it, the boundary layer is subjected to both streamwise and transverse pressure gradients. Thus, several assumptions required by conventional boundary-layer theory are violated. Despite the considerable amount of effort which has been devoted to the development of an analytical model to describe the aft-body boundary-layer characteristics (e.g., Patel 1973a and 1973b), these tools have not yet been shown to be reliable for practical use at very high Reynolds numbers.

In lieu of employing unproven computer codes to calculate the aft-body boundary layer flow, we have examined the available experimental data and employed somewhat more conventional extrapolation procedures in order to estimate the boundary-layer characteristics of a body immersed in a very high Reynolds number flow. In the following we first examine the mean flow field characteristics and, then, examine the turbulence characteristics.

2.1.1 Mean Flow Field

In our first attempt at correlating the mean velocity profile of the aft-body boundary layer, we employed the conventional boundary-layer correlation schemes such as plotting $\frac{w}{w_e}$ (y/δ) , $\frac{w}{u_\tau}$ $(\frac{yu_\tau}{\nu})$ and $\frac{w-w_e}{u_\tau}$ (y/δ) where w is the streamwise fluid speed, w_e is the local freestream speed, u_τ is the friction velocity, y is the distance measured normal to and from the body surface and δ is the local boundary-layer thickness. Such graphs (using Patel's 1974 experimental data) failed to display any noticeable degree of collapse to a single curve. The lack of collapse can be attributed to the boundary-layer/mean-flow interaction and to the failure of the flow to satisfy the boundary-layer assumption $\delta/R<<1$ at the trailing edge.

We then hypothesized that, in spite of the complex dynamics of the flow in the aft-body region, the mechanisms whereby the total mean flow energy is converted to turbulent energy might not be drastically different from the mechanisms which act in a flat-plate boundary layer. To test this hypothesis, Patel's (1974) very extensive measurements of the aft-body boundary layer were used to compute the total mean flow energy (i.e., $(p/\rho)+(q^2/2)$, where the pressure term, p/ρ , represents the potential energy of the fluid and the velocity term $q^2/2$ represents the kinetic energy of the fluid) for each streamline at a number of measurement stations along the surface of the body which he utilized. A graph of this reduction of Patel's data is shown in Figure 2.1 where the ordinate is the square root of the stagnation pressure coefficient $(C_p = \frac{p-p_\infty}{\frac{1}{2}\rho w_\infty^2} + \left(\frac{q}{w_\infty}\right)^2)$, and the abscissa is the streamfunction ψ ,

normalized by streamfunction, ψ_e, at the "edge" of the boundary layer (where $C_p = 0.99$). Here the subscript ∞ denotes free-stream values. The value of ψ at any survey location was determined from Patel's data from

$$\psi = \int_0^y 2\pi(y'+y_b)\bar{q}\cdot\bar{n}\, dy'$$

where y_b is the distance from the body axis to the body surface measured along the local normal and $\bar{n}$ is a unit vector parallel to the body surface at the point where the normal intersects it.

The rationale for this particular choice of coordinate scales will be discussed below. It is evident from Figure 2.1 that all of the computed values lie within a very narrow band in spite of the fact that the local pressure gradient and ratio of boundary-layer thickness to body radius both change markedly over the range of survey stations (the numbers shown next to the tabulated symbols represent the fraction of the body length measured from the leading edge where the boundary-layer survey was conducted). At $z^*/L = 0.662$, for example, the streamwise pressure gradient is negligible and $\delta/R \doteq 0.15$, whereas beyond $z^*/L = 0.80$ the boundary layer is subject to an adverse pressure gradient and at $z^*/L = 0.99$, $\delta/R \doteq 13$. Here, L is the body length and z^* is the distance behind the body nose.

In order to lend additional credence to this correlation, the universal, flat-plate, boundary-layer profile given by Coles and Hirst (1969) is shown by the heavy line in Figure 2.1 after converting it to the coordinates used in the figure.* The close correspondence between Coles' flat-plate profile and the aft-body boundary-layer measurements taken by Patel supports the original hypothesis. Two examples of one other flat-plate boundary layer correlation scheme are also shown in Figure 2.1; these examples are for the case where the velocity profile is approximated by

---

*A representative value of the friction coefficient C_f measured by Patel has been used to compute this curve; it should be noted that the measured C_f is some 30% lower than would be estimated for a flat-plate boundary layer at a Reynolds number based on the body half-length. This deviation is most likely a result of the boundary layer being tripped near the leading edge.

$$w/w_e = (y/\delta)^{1/n} .$$

Profiles of this representation for n = 5 and 7 are indicated by the dashed lines when computed in the coordinates shown in Figure 2.1. Although this representation has less theoretical basis than Coles', the case for n = 5 appears to fit the data quite well, at least for the inner 50% of the boundary-layer mass flux. The fact that the 1/7th power law profile appears to represent the data somewhat better in the outer region again may be attributed to the boundary-layer trips.

The comparison between these analytic velocity profiles and the experimental data gives an indication as to why the particular coordinates were chosen to plot the data and the curves. For a flat-plate boundary-layer, the abscissa represents nothing more than the velocity ratio within the boundary layer since $p = p_\infty$. This would be true also of the aft-body boundary layer if the flow were to be inviscid and were to turn parallel to the body axis with the static pressure recovering to the free stream pressure. If one desires the boundary-layer velocity profile in the aft-body region, it is necessary that the pressure distribution be known a priori. Often this is not known, however, because of the influence of some other phenomenon such as a marine propeller mounted at the trailing edge. Even if this could be estimated by some technique, the correlation shown in Figure 2.1 would only permit the calculation of the magnitude of the fluid velocity within the boundary layer; the flow direction could not be computed.

It should be added that some of the other data obtained by Patel, et al., indicate that the flow direction within the boundary layer varies linearly, from being parallel to the surface at the body to being parallel to the undisturbed flow at the boundary layer edge.

The normalization of the abscissa by ψ_e simply accounts for the fact that even a flat-plate boundary layer entrains fluid as it develops downstream. Manual calculations (not shown here) of the entrainment rate for a flat-plate boundary layer and for an aft-body boundary layer indicated that each entrains fluid at about the same rate in spite of the geometric and pressure gradient differences between them. Thus, using the flat-plate computation of the amount of entrained

fluid, the quantity ψ_e can be estimated at any location along the body surface from (see Appendix A.1)

$$\psi_e(z^*) \doteq 4\, w_e\, A(z^*)(C_F)_{F.P.}$$

where: $A(z^*)$ is the wetted surface area of the body between the leading edge and the location z^*.
$(C_F)_{F.P.}$ is the flat-plate value of the total friction coefficient computed using the Reynolds number $w_e z^*/\delta$ (possibly modified in the event a boundarylayer trip is employed).

The line of reasoning for the apparent independence of the entrainment rate on surface geometry is that it is roughly proportional to the turbulent intensity. For a flat-plate boundary-layer it has also been observed that the turbulent intensity is about three times the local friction velocity ($u_\tau = w_e\sqrt{C_f/2}$). For the aft-body flow, however, Patel's measurements indicate that this latter relation is no longer valid but that the turbulent intensity remains at about the same level even though C_f is considerably smaller.

In spite of the apparent success of the correlation of the aft-body boundary-layer data with flat-plate predictions, the calculation of the physical velocity profile (i.e., w/w_e (r)) is not a trivial matter even if the turning of the flow parallel to the axis and the recovery of the static pressure (with viscous effects neglected) could be approximated (this turning and pressure recovery is exactly what is usually assumed for computing the flow through a marine propeller such as that given in Section 2.2). In this event, the streamline location can be computed from

$$\frac{\psi e}{w_e}\int_0^{\psi(r)} \frac{d\psi'/\psi e}{w/w_e} = \pi r^2$$

and, by cross-plotting, the velocity profile $w/w_e(r)$ can then be determined. If a power-law boundary-layer velocity profile correlation were adequate so that

$$\frac{w}{w_e} = \left(\frac{\psi}{\psi e}\right)^{\frac{1}{n+1}},$$

then at the trailing edge of the body, the above integral may be evaluated with the result that

$$\frac{w}{w_e} = \left(\frac{r}{\delta}\right)^{2/n}$$

where

$$\delta = \left[\frac{1}{\pi}\left(\frac{n+1}{n}\right)\frac{\psi_e}{w_e}\right]^{\frac{1}{2}}$$

$$= \left[\frac{4}{\pi}\left(\frac{n+1}{n}\right)AC_F\right]^{\frac{1}{2}} .$$

Note that this implies that the velocity profile when expressed as a function of r/δ is less full than a flat-plate profile expressed as a function of y/δ .

2.1.2 Turbulence Characteristics

The data of Patel, et al. (1974) have also been examined to estimate the characteristics of the turbulence within the aft-body boundary layer. This effort has involved converting Patel's measurements into the form of the dependent variables which are used in the ICWAKE code. The reader is referred to Section 3 for the precise definition of these dependent variables. For the purposes here, it is noted that R_{zz} represents the expected value of the mean-square velocity fluctuation in the direction parallel to the body axis. The quantities $R_{\theta\theta}$, R_{rr} , R_{rz} , and the others are defined similarily.

In our effort to correlate these data, we have taken the liberty to incorporate some Reynolds number scaling into the graphs discussed below. This involves nothing more than incorporating the approximate Reynolds number scaling for flat-plate boundary layers where all turbulent stresses are proportional to the square of the flat-plate friction velocity into the aft-body boundary-layer correlations. That is, in a flat-plate boundary layer it is found that R_{zz}/u_τ^2 is a function of y/δ.

Based on the reasoning presented in Section 2.1.1 regarding the turbulent entrainment rate, we assume here that even in the aft-body

boundary layer the magnitudes of the turbulent stresses are proportional to the flat-plate friction velocity computed at the Reynolds number $w_\infty z^*/\nu$. The justification for this assumption is that it works for flat-plate boundary layers and that it agrees fairly well with the turbulent entrainment rate for the aft-body boundary layer. It should be noted that this Reynolds number scaling only introduces a slight correction to the stresses since $u_\tau^2 \sim (C_f)_{F.P.}$ and the local flat-plate friction coefficient, C_F , only changes a factor of two or so over several orders of magnitude change in Reynolds number.

The distribution of the turbulent intensity across the aft-body boundary layer as measured by Patel, et al., is shown in Figure 2.2. On this figure the turbulent intensity (defined as the square root of one-half the sum of the three turbulent normal stresses) is plotted as a function of the fractional distance across the local boundary-layer thickness for the four survey stations reported by Patel (and represented by the open symbols). Klebanoff's (1955) flat-plate measurements which are represented by the solid circles are also shown in Figure 2.2. Except for the region near the body surface ($(y-y_b)/\delta \lesssim 0.2$) at the trailing edge, these data all lie within a band whose mean is indicated by the solid line shown in Figure 2.2.

The degree of anisotropy of the aft-body boundary-layer turbulence is shown in Figure 2.3 where the ratio of the radial to the axial and the ratio of the circumferential to axial turbulent intensities are shown as a function of position within the boundary layer. Although there is considerable scatter in both of these sets of data, the crude approximation that both the radial and the circumferential intensities are about 60 percent of the axial turbulent intensity over most of the aft-body boundary layer is not too unreasonable.

The distribution of turbulent shear stress R_{rz} across the aft-body boundary layer is shown in Figure 2.4. After several other correlation attempts (such as estimating the eddy viscosity rather than the turbulent stress), it was our opinion that Bradshaw's (1967) normalization, in which the stress is assumed proportional to the turbulent energy, appeared to give the best correlation of Patel's data. It should be observed that for the data at $z^*/L = 0.662$ (where the boundary layer is thin and the pressure gradient is small), Patel's

data agree quite well with Bradshaw's estimate. As the boundary layer thickens and decelerates toward the aft-end of the body, the shear stress in the outer portion of the boundary layer decreases relative to Bradshaw's flat-plate boundary-layer correlation. Patel's turbulent shear stress data appear to be reasonably correlated by the heavy dashed line shown in Figure 2.4. A Reynolds number scaling of the shear stress data shown in Figure 2.4 is implicit in that the shear stress normalization quantity k^2 is scaled with u_τ^2 (Figure 2.2).

The other two turbulent shear stresses $R_{r\theta}$ and $R_{z\theta}$ are zero within the boundary layer. It should be remarked that if the turbulence passes through a marine propeller (which exerts a step change in the swirl velocity at the plane of the propeller), these two stress components will no longer be identically zero. The effect of a propeller on all of the turbulent velocity correlations is discussed further in Section 2.2.2.

By far the most difficult correlation that was to be extracted from Patel's data was for the turbulent dissipation rate. The initial distribution of this quantity aft of the propeller is required by the ICWAKE code in Section 3. This quantity was not measured nor could it be inferred directly from, say, the decay rate of the turbulent intensity along a given streamline. To proceed, we adopted a model for the local turbulent dissipation rate, such as given by Tennekes and Lumley (1973). Basically, this assumes that the dissipation rate ε is

$$\varepsilon = R_{zz}^{3/2}/\Lambda$$

where Λ is the longitudinal integral scale size of the turbulent velocity fluctuations. In the aft-body region we have assumed that Λ is no longer proportional to the actual boundary-layer thickness but, rather, it is proportional to the thickness of an undistorted boundary layer. Furthermore, the quantity R_{zz} has been assumed to be proportional to $(u_\tau^2)_{F.P.}$ according to the correlation shown in Figure 2.2. With this line of reasoning, one is then led to the conjecture that

$$\frac{\varepsilon\delta_{FP}}{(u_\tau^3)_{FP}} = \text{fcn}\left(\frac{y - y_b}{\delta}\right) .$$

To test this contention, Patel's data were used to compute the left-hand-side of the equation (which is nearly $k^{3/2}$ times a very weak function of Reynolds number to account for the slight change in $(u_\tau)_{F.P.}$ and $\delta_{F.P.}$ for the different survey stations examined by Patel). The results of this computation are shown in Figure 2.5. Note that the scatter of the data is considerable and that it is also somewhat different than the data for a flat-plate boundary layer. In spite of this, we have attempted to estimate the turbulent dissipation rate distribution across the aft-body boundary layer in a manner indicated by the heavier dashed line. Obviously, an improved correlation would require not only a better underlying scheme but more detailed and varied measurements. Whether a better correlation than that given above is really needed or not depends on how sensitive the wake calculations are with respect to this quantity.

2.2 Influence of a Marine Propeller on the Aft-Body Boundary Layer

In the previous subsection of this report, the characteristics of the aft-body boundary layer were examined and correlated so that one could make reasonable estimates of the mean velocity field and turbulence within the fluid prior to the formation of the wake. This correlation scheme, it should be noted, is extracted from data obtained for the flow field of a body whose speed is maintained by towing it through the surrounding fluid. For most cases of practical interest, however, the body propels itself through the surrounding fluid by means of an aft-mounted marine propeller. Because of the presence of a propeller one might question the applicability of the towed-body, boundary-layer data to a more realistic case.

Experimentally, it has been observed that the upstream influence of a marine propeller is limited to a distance on the order of the propeller diameter. This influence is judged by the change in the surface pressure distribution along the body operating with and without a propeller (see McLemore, 1962, for example). Thus, the development of the body's boundary layer is unaffected by the presence of a propeller upstream of this region which occupies only the last 5 percent or so of the

vehicle's length. The mean flow field and turbulence characteristics described in the previous section are presumably valid over most of the vehicle surface. Within this latter 5 percent of the body length, the influence of the propeller is such that the fluid is accelerated towards the propeller because of the reduced upstream pressure field which accompanies the propeller thrust. A more detailed description of this upstream influence of the propeller will be given in Section 2.2.1. Qualitatively, however, the description here implies that only the mean flow field is affected by the propeller; the turbulence within the aft-body boundary layer is assumed to be simply convected along with the mean flow. Furthermore, because the upstream influence of the propeller is so limited in extent, it is not expected that the energy exchange processes associated with the boundary-layer turbulence will have sufficient time to exert a significant influence on the mean flow. Hence, we assume that the entire flow immediately upstream of the propeller is inviscid (but rotational) and that each turbulence correlation can be treated as a passive scalar. Immediately downstream of the propeller an assumption like this would be invalid since comparatively large velocity gradients exist because of the propeller generated axial and swirl velocities (the latter of which does not exist upstream). These mean flow velocity gradients downstream of the propeller increase the rate of energy exchange from the mean flow to the turbulence thus increasing its intensity and the influence of the dissipative and diffusive effects of the turbulence. This is why a complicated turbulence model computer code is necessary in the near-wake but is unnecessary upstream of the propeller.

2.2.1 Propeller Induced Mean Flow Field

Regarding the influence of a marine propeller on the rotational (but assumed inviscid) flow entering the propeller, a number of analytical investigations have been made. In particular, the analysis developed by Schwartz and Bernstein (1975) was examined. Their model follows the classical propeller analysis of combined blade element, momentum balance, and vortex theory. A computer code (op. cit.) based on their model predicts the induced axial and swirl mean velocities at the propeller plane for a given propeller (size, number and shape of blades, rotational speed) and a given undisturbed upstream boundary-layer velocity profile.

Two-dimensional airfoil theory (with corrections for finite span) is used for calculating the induced velocities within constant radius annuli. The mean radial velocity at the propeller plane is not determined by the Schwartz-Bernstein model.

An alternate derivation of the upstream influence of the propeller is given in Appendix A.2. This analysis leads to an exact solution for the nearly inviscid linearized equations describing the flow through a marine propeller. A significant outcome of this analysis is that it yields an expression for the mean radial velocity at the propeller plane in terms of the induced axial velocity there. This is an important result because it turns out (Appendix A.2), within the approximations of the theory, that the radial flow speed is of the same order of magnitude as the induced axial flow speed, and hence cannot be ignored. (Note that the induced axial flow speed is the change in axial speed from "far" upstream of the propeller to the propeller plane, which, depending on the propeller and its thrust, can be as much as 20 percent of the freestream speed.)

On the other hand, it was determined that even though the new analysis is in some ways more complete than the previous work, the new estimates for the induced axial and swirl velocities do not differ greatly from the previous estimates. Thus, the final computer model for the mean flow in the propeller plane was chosen to be the Schwartz-Bernstein code with the addition of a routine to compute the mean radial flow speed. The equation that relates the radial flow speed to the axial flow speed change is (Appendix A.2)

$$u(r) = -\int_0^\infty \Delta w(\rho) G_u(r,\rho) \rho d\rho \ ,$$

where $\Delta w(\rho)$ is the induced axial velocity at the plane of the propeller as a function of radial distance, and is obtained from the Schwartz-Bernstein model,

and $G_u(r,\rho)$ is a "Green's function" given by

$$G_u(r,\rho) = \frac{1}{\pi r}\left[\frac{E(m)}{r-\rho} + \frac{K(m)}{r+\rho}\right] \ ,$$

where $K(m)$ and $E(m)$ are complete elliptic functions of the 1st and

2nd kind, respectively, and the modulus $m \equiv 4\, r\rho/(r + \rho)^2$. Examination of the function G_u shows that an integrable singularity exists at $\rho = r$.

2.2.2 Effect of Propeller on Aft-Body Boundary-Layer Turbulence

As explained in the previous two sections of this report, the turbulence characteristics of the aft-body boundary layer are not expected to change substantially in the region upstream of the propeller. That is, the turbulence is assumed to be simply convected along with the flow through this region until it arrives at the propeller plane. As the turbulence passes through the propeller, however, it could be markedly changed by the mechanical "chopping" of the blades; also the mean propeller flow field could substantially distort the initial wake turbulence and some turbulence could be added to the body wake from the boundary layers on the propeller blades. This is particularly important if the propeller is operating in a regime whereby the blade boundary layers separate from the blade surface. It is the purpose of this section to examine the potential effect on the initial wake turbulence level of each of these three mechanisms; mechanical chopping, distortion of the incoming turbulence, and generation of new turbulence.

Mechanical Chopping

As a turbulent eddy is convected through a marine propeller by the mean flow, it may be cut into two or more segments by a blade. Because the propeller blades are lifting surfaces, the fluid which passes over the suction side of the blade (upstream side) does so in less time than that which passes on the pressure side. Therefore, downstream of the propeller the segments of the eddy do not rejoin but are displaced relative to one another by a distance $\pi\alpha c$ where α is the blade angle-of-attack and c is the blade chord (this estimate is easily made using conventional airfoil theory). Further, the axial distance between the passage of two adjacent blades is $\frac{1}{B}\frac{w_\infty}{2\pi n}$ where B is the number of blades, and n is the propeller rotational speed (in cycles per unit time). If typical values for the number of blades, the blade chord length, etc. are inserted into these relations, it may be estimated that the net displacement of a severed turbulent eddy is on the order of 0.15 D_p and the distance between blade passages is about 0.1 D_p where D_p

is the diameter of the propeller. For eddy sizes much larger than 0.1 D_p the splitting of the eddy is negligible whereas for eddy sizes much less than 0.1 D_p only a small fraction will experience a permanent split. It is concluded that mechanical chopping, at best, only causes a very localized redistribution of the turbulent energy spectrum in the neighborhood of those eddy sizes which are about 0.1 D_p. This effect can, therefore, be ignored for the present purposes.

Generation of Turbulence Within the Propeller Blade Boundary Layers

Estimates have been made of the propeller blade boundary-layer thickness again for several assumed operating conditions. For each of these conditions it is estimated that less than 5% of the total mass flux of fluid passing through the propeller is entrained within the propeller blade boundary layers. Thus, even if the turbulent intensity within the blade boundary layers were appreciably greater than that washing off the body and through the propeller, the change in the amount of turbulent energy in the wake would be small.

If the blade boundary layers were to separate from the blade surfaces, it might alter the above conclusion. It should be recognized, however, that blade boundary layer separation would probably also result in markedly reduced propulsion efficiency since the thrust (i.e., blade lift) decreases and the torque (i.e., blade drag) markedly increases. Thus, extensive boundary layer separation is a pathological case corresponding to operating at an off-design condition.

Distortion of Turbulence Passing Through a Marine Propeller

As demonstrated in the mean flow velocity analysis presented in the appendix, the primary change experienced by each fluid particle passing through the propeller is that it is suddenly given a swirl velocity component. The changes in the axial and radial flow components are much more gradual. This imposition of a swirl velocity component on the turbulent eddies can cause their orientation to change and they may be stretched or compressed. Thus, the turbulence within the aft-body boundary layer can be both redistributed into other components and intensified upon passing through the propeller. Thus, the aft-body boundary-layer turbulence correlations given in Section 2.1.2 could be altered by virtue of the propeller.

In analyzing this change it is assumed that the turbulence model equations presented in Section 3 (and which are used to compute the flow aft of the propeller) remain valid even in the vicinity of the propeller. Thus, these equations can be analytically integrated across the plane of the propeller (i.e., from $z = -\Delta$ to $z = +\Delta$, where Δ is a very small distance relative to the propeller or wake radius). In doing this, it is assumed that each of the turbulent velocity correlations such as R_{zz} (Section 3) could experience a step change from its value ahead of the propeller (say, $(R_{zz})_o$). As was mentioned above, the mean swirl velocity also undergoes a step change, ΔV, being zero ahead of the propeller and finite behind. The radial distribution of the swirl velocity jump is computed from the propeller code described in Section 2.2.1.

The resulting simultaneous algebraic equations for the change in each turbulent quantity (i.e., R_{ij} where $i, j = r, \theta, z$) and the turbulent dissipation rate ε can then be solved. Because this is rather straightforward (but messy) only the final result will be given as follows (see Appendix A.3 for details):

$$R_{rr} = (R_{rr})_o - 0.582 \left(\frac{\Delta V}{W}\right)^2 F(\tilde{r}) ,$$

$$R_{\theta\theta} = (R_{\theta\theta})_o - 1.055 \left(\frac{\Delta V}{W}\right)^2 F(\tilde{r}) ,$$

$$R_{zz} = (R_{zz})_o - 0.364 \left(\frac{\Delta V}{W}\right)^2 F(\tilde{r}) ,$$

$$\varepsilon = (\varepsilon)_o \left[1 - 1.44 \left(\frac{\Delta V}{W}\right)^2 \frac{F(\tilde{r})}{k}\right] ,$$

$$R_{rz} = (R_{rz})_o \left[1 - 0.026 \left(\frac{\Delta V}{W}\right)^2\right] ,$$

$$R_{r\theta} = -0.236 \left(\frac{\Delta V}{W}\right) (R_{rz})_o ,$$

$$R_{\theta z} = \frac{\Delta V}{W} F(\tilde{r}) ,$$

where $F(\tilde{r}) = 0.327 (R_{zz})_o \; 0.018 (R_{\theta\theta})_o \; 0.091 (R_{rr})_o$, $\tilde{r} = r/r_p$ and $k^2 = \frac{1}{2}\left[(R_{zz})_o + (R_{\theta\theta})_o + (R_{rr})_o\right]$. Here, r_p is the propeller radius.

Note that changes in any turbulence quantity are solely the result of the sudden imposition of a swirl velocity to the stream tube passing through the propeller plane.

Most of these changes are proportional to the square of the normalized swirl velocity with the exceptions of the circumferential stresses $R_{r\theta}$ and $R_{\theta z}$ which are proportional to Δv (the constants shown in the above equations result from the turbulence model constants given in Section 3; the subscript "o" in the above denotes the value of that quantity immediately upstream of the propeller). If a typical value of $(\Delta v/w)$ is taken as 20% and typical values of the boundary layer correlations used, it may be shown that the changes to the normal stress components, the dissipation rate and the longitudinal Reynolds stress are each less than 3% of their values upstream of the propeller. The swirling Reynolds stress component $R_{r\theta}$ is increased from zero upstream to about 5% of $(R_{rz})_o$, and the other swirling Reynolds stress component $R_{\theta z}$ is changed the most, going from zero upstream of the propeller to about 90% of $(R_{rz})_o$. Thus, it is concluded that the propeller has, at most, a minimal effect on the turbulence flowing through it except for causing the swirling Reynolds stresses to assume relatively large values.

2.3 Section Summary

For the boundary-layer mean flow near the aft-end of the body a surprisingly universal correlation of Patel's data with a flat-plate boundary layer has been described. This correlation circumvents the problems associated with the large change in the ratio of the boundary-layer thickness to the body radius and with the strong adverse pressure gradients present near the trailing edge. A similar correlation of the boundary-layer turbulence properties was also developed. Thus, given the body speed and size, it is now possible to make estimates of the aft-body boundary-layer profiles just upstream of the propeller.

An examination of the flow through a marine propeller was also conducted. It was concluded that the existing Flow Research computer program provides a fairly accurate estimate of the induced axial and swirl velocities. An alternate approach, presented in Appendix A, provides an expression for the induced radial velocity. Adding a routine to compute this expression to the existing computer program provides

a complete computer model for the mean flow in the propeller plane. The distortion of the boundary-layer turbulence as it passes through the propeller was also investigated. By and large, the changes in the turbulence caused by the propeller appear to be minimal with the exception of the changes in the swirling Reynolds stresses. These stresses, because of the sudden increase in swirl velocity, immediately assume values comparable to the turbulent shear stress within the upstream boundary layer.

3. Near-Wake Region

3.1 Mathematical Model

3.1.1 Mean-Flow Equations

In the near-wake region, we assume that the flow is statistically steady and axisymmetric, and that the effects of variations in density are negligible. We perform Reynolds' decomposition and let U, V and W represent mean (time-averaged) velocity components in the r, θ and z directions of a cylindrical polar coordinate system fixed with respect to the body (Figure 3.1) with its origin at the body tail. The z-axis is located along the body track. We denote the fluctuating velocities by u', v' and w' and correlations of fluctuating components, that is $\overline{u'u'}$, $\overline{u'v'}$, etc., by R_{rr}, $R_{r\theta}$, etc. In non-dimensional form, the radial, circumferential and axial momentum equations are

$$U\frac{\partial U}{\partial r} + W\frac{\partial U}{\partial z} - \frac{V^2}{r} = -\frac{\partial P}{\partial r} + \frac{1}{Re}\left(\frac{\partial^2 U}{\partial r^2} + \frac{1}{r}\frac{\partial U}{\partial r} + \frac{\partial^2 U}{\partial z^2} - \frac{U}{r^2}\right) - \left(\frac{\partial R_{rz}}{\partial z} + \frac{\partial R_{rr}}{\partial r} + \frac{R_{rr} - R_{\theta\theta}}{r}\right), \tag{3.1}$$

$$U\frac{\partial V}{\partial r} + W\frac{\partial V}{\partial z} + \frac{UV}{r} = \frac{1}{Re}\left(\frac{\partial^2 V}{\partial r^2} + \frac{1}{r}\frac{V}{r} + \frac{\partial^2 V}{\partial z^2} - \frac{V}{r^2}\right) - \left(\frac{\partial R_{\theta z}}{\partial z} + \frac{\partial R_{r\theta}}{\partial r} + \frac{2R_{r\theta}}{r}\right), \tag{3.2}$$

and

$$U\frac{\partial W}{\partial r} + W\frac{\partial W}{\partial z} = -\frac{\partial P}{\partial z} + \frac{1}{Re}\left(\frac{\partial^2 W}{\partial r^2} + \frac{1}{r}\frac{\partial W}{\partial r} + \frac{\partial^2 W}{\partial z^2}\right) - \left(\frac{\partial R_{zz}}{\partial z} + \frac{\partial R_{rz}}{\partial r} + \frac{R_{rz}}{r}\right). \tag{3.3}$$

We express mass conservation as

$$\frac{1}{r}\frac{\partial}{\partial r}(Ur) + \frac{\partial W}{\partial z} = 0 \tag{3.4}$$

and

$$\frac{1}{r}\frac{\partial}{\partial r}(u'r) + \frac{\partial w'}{\partial z} + \frac{1}{r}\frac{\partial v'}{\partial \theta} = 0\ *\ . \tag{3.5}$$

---

*Note that by axisymmetric flow we mean that circumferential gradients of mean quantities vanish.

The mean and fluctuating velocity components are non-dimensionalized by a characteristic mean velocity, and lengths by a characteristic radial length scale; these scales are th free-stream velocity, W_∞, and the body radius, R_b, respectively. The pressure, P, is non-dimensionalized by ρW_∞^2, where ρ is the local fluid density, after subtraction of the ambient pressure far from the wake (so that $P \to 0$ as $r \to \infty$). The flow Reynolds number, Re, is defined as $W_\infty R_b/\nu$.

In order that we may determine the pressure, we introduce the Poisson equation for P which is obtained by taking the divergence of the mean momentum equations. This results in an equation of the form

$$\frac{\partial^2 P}{\partial r^2} + \frac{1}{r}\frac{\partial P}{\partial r} + \frac{\partial^2 P}{\partial z^2} = F(U, V, W, R_{rr}, R_{\theta\theta}, \text{etc.}) \qquad (3.6)$$

Since this equation is used in place of the mean-flow continuity equation (Equation 3.4), the formulation and form of the function F require careful consideration. We must ensure that P, as numerically predicted by this equation, be such that the corresponding mean velocity field be divergence free.

3.1.2 Turbulence Model Equations

The mean flow equations require the specification of six turbulent correlations, R_{rr}, $R_{\theta\theta}$, R_{zz}, $R_{r\theta}$, R_{rz}, and $R_{\theta z}$, none of which, in general, vanish in flows with swirl, even with the assumption of axisymmetry. To obtain these correlations, we apply the second-order closure turbulence model which was proposed by Hanjalic and Launder (1972), and extended by Launder, Reece and Rodi (1975). Two factors entered our decision to use a second-order closure model. First, and perhaps foremost, was the lack of success reported by a number of authors (see, for example, Pope and Whitelaw, 1976) in the application of simpler turbulence models, such as the several k-$k\ell$ and k-ϵ two-equation models, to complex turbulent flows which are less complex than flows with swirl. First-order closure models require constitutive relationships between k and $k\ell$ (or ϵ) and the six unknown correlations; typically, the Reynolds stress tensor, τ, is assumed to equal $\mu_e \text{def}\, \vec{U}$, where μ_e is an isotropic eddy viscosity calculated from k and $k\ell$ (or ϵ). Occasionally, an anisotropic

eddy viscosity is generated, although on purely ad hoc grounds (see, for example, Lilley, 1973). For complex flows, these constitutive relationships are not physically well-founded.

The second factor derives directly from the motivation for this study. We are attempting to develop an analytical/numerical procedure which will provide, at an appropriate station downstream of the body, physically realistic profiles of not only the mean flow quantities (for which perhaps the use of a simpler model might suffice), but also the turbulence quantities. However, two-equation models have been developed, in general, in order to model the effects of turbulent transport on the mean flow--not to model the properties of the turbulence itself, and thus, we do not expect them to be sufficient for our purposes.

In terms of rectangular cartesian tensors (and assuming the usual summation convention), the Hanjalic and Launder/Launder, Reece and Rodi equation for the R_{ij} turbulent correlation is

$$\frac{DR_{ij}}{Dt} = -\left(R_{jk}\frac{\partial U_i}{\partial x_k} + R_{ik}\frac{\partial U_j}{\partial x_k}\right) - \frac{2}{3}\delta_{ij}\varepsilon - C_1\frac{\varepsilon}{k}\left(R_{ij} - \frac{2}{3}\delta_{ij}k\right)$$

$$+ \tilde{\phi}_{ij,2} + C_s\frac{\partial}{\partial x_k}\left[\frac{k}{\varepsilon}\left(R_{k\ell}\frac{\partial R_{ij}}{\partial x_k} + \underline{R_{i\ell}\frac{\partial R_{jk}}{\partial x_\ell}} + \underline{R_{jk}\frac{\partial R_{ki}}{\partial x_\ell}}\right)\right]. \qquad (3.7)$$

Where the terms balancing advection of the correlation represent, in order: production resulting from the interaction of the fluctuating and mean flows, isotropic (high Reynolds number) dissipation, the so-called "tendency toward isotropy" component of the pressure-strain correlation ($\tilde{\phi}_{ij,1}$), the mean strain component of the pressure-strain correlation, and finally turbulent diffusion. The mean-strain component of the pressure-strain correlation (as developed by Launder, et al.) is defined as

$$\tilde{\phi}_{ij,2} = -\frac{(C_2 + 8)}{11}(P_{ij} - \frac{2}{3}P_k\delta_{ij}) - \frac{(30C_2 - 2)}{55}k\left(\frac{\partial U_i}{\partial x_j} + \frac{\partial U_j}{\partial x_i}\right)$$

$$- \frac{(8C_2 - 2)}{11}(D_{ij} - \frac{2}{3}P_k\delta_{ij})$$

where

$$P_{ij} = -\left(R_{i\ell}\frac{\partial U_j}{\partial x_\ell} + R_{j\ell}\frac{\partial U_i}{\partial x_\ell}\right) \quad , \text{ and } \quad D_{ij} = -\left(R_{i\ell}\frac{\partial U_\ell}{\partial x_j} + R_{j\ell}\frac{\partial U_\ell}{\partial x_i}\right)$$

and P_k represents the rate of turbulent energy production, $\frac{1}{2}P_{ii}$. The two underlined turbulent diffusion terms are neglected in the often-used diffusion expression of Daly and Harlow (1970). The quantity k is the turbulent kinetic energy which is equal to $\frac{1}{2}R_{ii}$, and ε is the turbulent energy "dissipation rate", determined from the model equation,

$$\frac{D\varepsilon}{Dt} = -C_{\varepsilon_1}\frac{\varepsilon}{k}R_{i\ell}\frac{\partial U_i}{\partial x_\ell} - C_{\varepsilon_2}\frac{\varepsilon^2}{k} + C_\varepsilon\frac{\partial}{\partial x_k}\left(\frac{k}{\varepsilon}R_{k\ell}\frac{\partial \varepsilon}{\partial x_\ell}\right). \tag{3.8}$$

Here, the terms balancing advection of dissipation rate represent its production, dissipation and turbulent diffusion.

The correlation and dissipation rate equations are presented in terms of the cylindrical coordinate system of this study in Appendix B. The model constants are also defined in that appendix. As a check of the equations, we note that for non-swirling flows, $V = 0$ and, as a result, $R_{r\theta} = R_{\theta z} = 0$; with the simplified Daly-Harlow expression for diffusion, the model equations in cylindrical coordinates then reduce identically to those used by Pope and Whitelaw (1976).

As an inspection of the equations in Appendix B will verify, the model equations are exceedingly lengthy. This is due, in part, to the modeling assumed by Hanjalic and Launder for the turbulent diffusion terms. A rather demanding constraint on the time period of this research effort suggested the application of a simplifying hypothesis—we assume that derivatives with respect to z in the turbulent diffusion terms may be neglected. This is a boundary-layer-like assumption which we expect will have a minimal effect on the prediction of the non-recirculating wake flows of interest here. The inclusion of these terms should be carefully considered, of course, if a model such as this were to be applied to such recirculating flows as highly swirling jets. With this simplifying assumption, the model equations become first-order in z ; they are second-order in r only. The simplified model diffusion terms are included in Appendix B.

3.1.3 Boundary Conditions

The system of equations presented in the previous section is elliptic and boundary conditions are required on all boundaries of the

solution domain (see Figure 3.1). In what follows (and in the computer code itself), boundaries and orientations are given in terms of the directions North, South, East and West. The North boundary is located at radial position, $r = R_{max}$, and the South boundary is at the axis of symmetry ($r = 0$). The West Boundary, at $z = Z_i$, is a plane transverse to the axis, located just aft of the body tail, and the East boundary is a transverse plane, at some distance, Z_{max}, downstream. Thus the domain in which the solution is to be obtained is defined by $0 \leq r \leq R_{max}$, $Z_i \leq z \leq Z_{max}$.

At the axis of symmetry (South boundary), continuity requires that $U = 0$. Then from symmetry conditions along with an examination of the mean flow equations (keeping in mind that shear stress must vanish at the axis), we find that V, $\partial W/\partial r$, $\partial P/\partial r$, $\partial R_{rr}/\partial r$, $R_{\theta\theta}/\partial r$, $\partial R_{zz}/\partial r$, $\partial \varepsilon/\partial r$, $R_{r\theta}$, R_{rz}, and $R_{\theta z}$ must all vanish. Under these conditions, the turbulence model, as it should, will predict $R_{rr} = R_{\theta\theta}$ at the axis (Pope, 1976).

We assume that the radial (North) boundary is located sufficiently far removed from the axis of symmetry (and body track) and that all turbulence quantities, as well as the propeller induced swirl velocity, vanish. We assume also that the axial velocity is uniform and equal to its free-stream value; then, since $\partial W/\partial z = 0$, we allow a radial flux into the domain with the condition that $\partial(Ur)/\partial r = 0$, which is obtained from the continuity equation. We obtain the radial pressure gradient, $\partial P/\partial r$, at R_{max} from the mean-flow radial momentum equation, and apply it as a boundary condition on P.

At the West (inflow) boundary, we assume that the mean velocity, turbulent correlations, and dissipation rate are all specified. Those quantities which are not experimentally or theoretically known must be estimated. We compute the axial pressure gradient, $\partial P/\partial z$, from the axial mean-flow momentum equations, and apply it as the boundary condition on P.

As a result of the simplifying approximation discussed in the previous section, no conditions are required for the turbulence quantities at the East boundary; however, we must supply conditions on the mean velocity components and the pressure. The conditions applied in this study are given below:

$$\frac{\partial P}{\partial r} = \frac{V^2}{r} - \left[\frac{\partial R_{rr}}{\partial r} + \frac{R_{rr} - R_{\theta\theta}}{r} \right] , \tag{3.9}$$

$$U \frac{\partial V}{\partial r} + W \frac{\partial V}{\partial z} + \frac{UV}{r} = \frac{1}{Re} \left[\frac{\partial^2 V}{\partial r^2} + \frac{1}{r} \frac{\partial V}{\partial r} - \frac{V}{r^2} \right] - \left[\frac{\partial R_{r\theta}}{\partial r} + 2 \frac{R_{r\theta}}{r} \right] , \tag{3.10}$$

$$U \frac{\partial W}{\partial r} + W \frac{\partial W}{\partial z} = - \frac{\partial P}{\partial z} + \frac{1}{Re} \left[\frac{\partial^2 W}{\partial r^2} + \frac{1}{r} \frac{\partial W}{\partial r} \right] - \left[\frac{\partial R_{rz}}{\partial r} + \frac{R_{rz}}{r} \right] , \tag{3.11}$$

and

$$\frac{\partial (Ur)}{\partial r} = - r \frac{\partial W}{\partial z} . \tag{3.12}$$

This system of equation is valid for slender, swirling shear flows in which radial gradients are in general much larger than axial gradients, and it is sometimes known as the "quasi-cylindrical approximation" (Hall, 1966). It is simply a boundary-layer approximation in which P, instead of being uniform across the flow, varies to balance centrifugal acceleration and turbulent transport. This system has been applied by many investigators (e.g., Hall, 1965; Mager, 1972) although it has not previously been applied as a boundary condition. By using it as a boundary condition, we avoid the necessity of applying much cruder approximations (such as the often-used requirement that axial derivatives of flow quantities vanish), and our solutions will automatically match with the nonstratified far-wake solution which satisfies these equations.

3.1.4 Coordinate Transformation

In order that we may choose the boundary locations R_{max} and Z_{max} sufficiently large that the above boundary conditions may be accurately applied, while at the same time maintaining sufficient radial mesh resolution within the wake ($r < 1$), and axial mesh resolution, particularly in the upstream portion of the wake where axial gradients are expected to be greatest, we perform logarithmic coordinate transformations. We introduce the independent variables y and x where

$$y = \frac{1}{a_y} \ln(1 + r/b_y) , \text{ and } x = \frac{1}{a_x} \ln(1 + (z - z_i)/b_x) .$$

These have been applied in conjunction with numerical solutions to a number of flow problems (e.g., Pao and Daugherty, 1969, and Grabowski

and Berger, 1976), and are used here to map the region $0 \le r \le R_{max}$, $Z_i \le z \le Z_{max}$, in which we wish to obtain a solution, onto the region $0 \le y \le \frac{1}{2}$, $0 \le x \le 1$ in transformed space. The values of the four transformation parameters a_y, a_x, b_y, and b_x are determined from the specified values of R_{max} and Z_{max}, and the desired number and distribution of grid points in each of the coordinate directions. Details are presented in Appendix C. Derivatives of dependent variables transform into the new coordinate system as follows:

$$\frac{1}{r}\frac{\partial U}{\partial r} = fh\frac{\partial U}{\partial y}\ , \quad \frac{\partial^2 U}{\partial r^2} = f^2\frac{\partial^2 U}{\partial y^2} + g\frac{\partial U}{\partial y}\ ,$$

$$\frac{\partial U}{\partial z} = s\frac{\partial U}{\partial x}\ , \quad \text{and} \quad \frac{\partial^2 U}{\partial z^2} = s^2\frac{\partial^2 U}{\partial x^2} + t\frac{\partial U}{\partial x}\ ,$$

where

$$f(y) = \exp(-a_y y)/(a_y b_y)\ ,$$

$$g(y) = -\exp(-2a_y y)/(a_y b_y^2)\ ,$$

$$h(y) = 1/r(y)\ ,$$

$$s(x) = \exp(-a_x x)/(a_x b_x)\ ,$$

and

$$t(x) = -\exp(-2a_x x)/(a_x b_x^2)\ .$$

In terms of the independent variables x and y, the transformed mean-flow momentum equations are

$$fU\frac{\partial U}{\partial y} + sW\frac{\partial U}{\partial x} - hV^2 = -f\frac{\partial P}{\partial y} + \frac{1}{Re}\left[f^2\frac{\partial^2 U}{\partial y^2} + (g + fh)\frac{\partial U}{\partial y} + s^2\frac{\partial^2 U}{\partial x^2} + t\frac{\partial U}{\partial x} - h^2 U\right]$$

$$-\left[s\frac{\partial R_{rz}}{\partial x} + f\frac{\partial R_{rr}}{\partial y} + h(R_{rr} - R_{\theta\theta})\right]\ , \qquad (3.13)$$

$$fU\frac{\partial V}{\partial y} + sW\frac{\partial V}{\partial x} + hUV = \frac{1}{Re}\left[f^2\frac{\partial^2 V}{\partial y^2} + (g + fh)\frac{\partial V}{\partial y} + s^2\frac{\partial^2 V}{\partial x^2} + t\frac{\partial V}{\partial x} - h^2 V\right]$$

$$-\left[s\frac{\partial R_{\theta z}}{\partial x} + f\frac{\partial R_{r\theta}}{\partial y} + 2hR_{r\theta}\right]\ , \qquad (3.14)$$

$$fU\frac{\partial W}{\partial y} + sW\frac{\partial W}{\partial x} = -s\frac{\partial P}{\partial x} + \frac{1}{Re}\left[f^2\frac{\partial^2 W}{\partial y^2} + (g + fh)\frac{\partial W}{\partial y} + s^2\frac{\partial^2 W}{\partial x^2} + t\frac{\partial W}{\partial x}\right]$$

$$-\left[s\frac{\partial R_{zz}}{\partial x} + f\frac{\partial R_{rz}}{\partial y} + hR_{rz}\right] \quad . \qquad (3.15)$$

The equations for the turbulent correlations, the dissipation rate, and the boundary conditions transform similarly and are not shown here.

3.2 Numerical Procedure

3.2.1 Introduction of τ

In order to obtain a solution of Equations (3.13) through (3.15), along with the transformed turbulence model equations and the boundary conditions, we introduce a time-like independent variable, τ, and add the "time derivative" terms $\partial U/\partial\tau$, $\partial V/\partial\tau$, $\partial W/\partial\tau$, $\partial\varepsilon/\partial\tau$, $\partial R_{rr}/\partial\tau$, $\partial R_{\theta\theta}/\partial\tau$, etc., to Equations (3.13) through (3.15) and the model equations for ε, R_{rr}, $R_{\theta\theta}$, etc., respectively. We also modify the East boundary conditions with the addition of $\partial V/\partial\tau$ and $\partial W/\partial\tau$ to the transformed version of Equations (3.10) and (3.11), respectively. The East boundary condition thus becomes what might be termed an "unsteady quasi-cylindrical" approximation.* The introduction of a time-like dependence to the system has two important advantages. First, it allows the system to be solved to the steady state, in which the "time derivatives" vanish, by any one of the many numerical schemes developed for initial value problems. The steady state solution is obviously the solution we desire. The conversion of a boundary-value problem to an initial/boundary-value problem in order to facilitate numerical solution is a standard procedure. We also gain a second related benefit from the introduction of a τ-dependence in that the application of the East boundary condition is significantly facilitated. The equations at the East boundary and those in the interior of the domain are marched forward in τ in unison in straightforward fashion. We thus have the not unusual situation of an initial/boundary-value problem with a boundary condition which varies in "time."

*Note that $\partial U/\partial\tau$ is not added to Equation (3.9). For the purposes of this study we may assume that $\partial U/\partial\tau \ll \partial P/\partial r$ at the East boundary.

3.2.2 The Pressure Equation

As noted in an earlier section, we obtain a Poisson equation for P by taking the divergence of the momentum equations. In terms of the transformed variables, we write the equation as

$$f^2 \frac{\partial^2 P}{\partial y^2} + (g + fh) \frac{\partial P}{\partial y} + s^2 \frac{\partial^2 P}{\partial x^2} + t \frac{\partial P}{\partial x} = F(U, V, W, R_{rr}, \text{etc.}) \quad , \quad (3.16)$$

where

$$F = f^2 \frac{\partial C_y}{\partial y} + (g + fh)C_y + s^2 \frac{\partial C_x}{\partial x} + tC_x + \partial D/\partial \tau \quad ,$$

$$C_y = -f^{-1} \left[-fU \frac{\partial U}{\partial y} - sW \frac{\partial U}{\partial x} + hV^2 + s \frac{\partial R_{rz}}{\partial x} + f \frac{\partial R_{rr}}{\partial y} + h(r_{rr} - R_{\theta\theta}) \right] ,$$

$$C_x = -s^{-1} \left[-fU \frac{\partial W}{\partial y} - sW \frac{\partial W}{\partial x} + s \frac{\partial R_{zz}}{\partial x} + f \frac{\partial R_{rz}}{\partial y} + hR_{rz} \right] ,$$

and

$$D = hf \frac{\partial}{\partial y} (h^{-1}U) + s \frac{\partial W}{\partial x} \quad .$$

The quantity D is the divergence of the velocity field in terms of the transformed variables. Although continuity (that is, the condition D should equal zero) has been applied to eliminate the viscous terms, the "time" derivative of D must be retained in order to assure stable solution. The necessity of retaining $\partial D/\partial \tau$ when the Poisson equation for pressure is solved numerically was first noted by Harlow and Welch (1965). The motivation for the retention of this term is that in the finite-difference computation truncation and round-off error which exist at any time level, $n-\frac{1}{2}$ (we use half-time steps in the finite-difference procedure), result in a non-zero divergence which, unless properly treated, grows and gives rise to a computational instability. However, since at time-level n, D ought to equal zero, we approximate $\partial D/\partial \tau$ at any grid point by finite-difference at time level n as $(0 - D^{n-\frac{1}{2}})/(1/2\Delta\tau)$. This stratagem, which prevents the growth of D, was originally suggested by Harlow and Welch.

There are many possible mathematically consistent forms in which the remaining terms in F may be expressed. The formulation used here was arrived at after some experimentation and consideration. In essence, each term in F corresponds to a term on the left-hand side of

the equation and, in fact, is arrived at by using the appropriate equation to evaluate the derivatives of P. For example, the term tC_x is obtained by using the x-momentum equation to express $\partial P/\partial x$ in terms of velocity components and turbulent correlations. This expression is included in F to correspond to the $t\partial P/\partial x$ term on the left. The other terms in F are obtained similarly. We note that we have combined all of the "time derivatives" into $\partial D/\partial \tau$ and, since the Reynolds number is assumed large so that the error arising from the finite-difference representation of the viscous terms is negligible, we have used continuity (that is, the assumption that D is identically zero) to combine and eliminate them.

3.2.3 Finite-Difference Formulation and Numerical Procedure

To generate a numerical procedure for the solution of Equations (3.13), (3.14), (3.15), (3.16), and the seven transformed turbulence model equations, we first overlay the region $0 \leq x \leq 1$, $0 \leq y \leq \frac{1}{2}$, in which the solution is to be obtained, with a finite-difference grid system of N points in the x-direction and M points in the y-direction. The location (x,y) of any grid point is given by the indices i,j as $x = (i-1)\Delta x$, $y = (j-1)\Delta y$, where Δx and Δy are uniform (but not equal) mesh widths in the x and y directions, respectively (Figure 3.2). The "unsteady" solution functions $U(x,y,\tau)$, $V(x,y,\tau)$, $W(x,y,\tau)$, $R_{rr}(x,y,\tau)$, etc., are represented by the discrete functions U^n_{ij}, V^n_{ij}, W^n_{ij}, $R^n_{rr_{ij}}$, etc., which are defined at each grid point i,j. The superscript n refers to the number of discrete time steps of length $\Delta\tau$ equivalent to τ, i.e. $\tau = n\Delta\tau$. The pressure $P(x,y,\tau)$ is represented by the discrete function $P^n_{i+\frac{1}{2},j+\frac{1}{2}}$ which is defined on a second grid system staggered with respect to the first by half of a mesh width in both coordinate directions.

The finite-difference formulation of the transformed mean flow equations (Equations 3.13 through 3.15) is based on the well-known ADI (Alternating-Direction-Implicit) procedure of Peaceman and Rachford (1955), and the finite-difference equations are presented in detail in Appendix D. We approximate all derivatives in the viscous diffusion, Reynolds stress, pressure gradient and radial convection terms with the usual centered second-order finite-difference approximations, while

we approximate axial advection terms such as $W\partial U/\partial x$ with a weighted centered-upwind formula of the form

$$\left[U_{i+1,j}(W_{ij} - \alpha_i|W_{ij}|) + 2\alpha_i U_{ij}|W_{ij}| - U_{i-1,j}(W_{ij} + \alpha_i|W_{ij}|)\right]/2\Delta x \quad .$$

The values permitted for the variable weighting factor α_i are bounded by zero and unity in which cases the formula yields, respectively, second-order centered and first-order upwind differencing.

The ADI procedure introduces two halftime-steps of length $\frac{1}{2}(\Delta\tau)$, during which y and x derivatives of the mean-flow velocities U, V, and W, including the derivatives in the convection terms, are alternately differenced implicitly (in time). As a result of this procedure, three tridiagonal matrix equations for $U_{ij}^{n+\frac{1}{2}}$, $V_{ij}^{n+\frac{1}{2}}$, $W_{ij}^{n+\frac{1}{2}}$, are defined at each value of i for $2 \leq j \leq M$ during the first halftime-step. When modified to incorporate the appropriate boundary conditions, these equations yield the solution at the grid points i, $1 \leq j \leq M$. During the second half-step, three tridiagonal equations are defined at each value of j, and these, after incorporation of the appropriate boundary conditions, yield the solution U_{ij}^{n+1}, V_{ij}^{n+1}, and W_{ij}^{n+1} at the grid points j, $2 \leq i \leq N$ (recall that the solution is specified at $i = 1$). The tridiagonal matrix equations are solved using the simple Thomas variant (Roache, 1972) of Gaussian elimination with a modification which allows the incorporation of Neumann boundary conditions to second-order.

Since the seven equations which determine the turbulence quantities contain second-order derivatives in y only, implicit differencing is applied only in the y direction. Centered spatial differences are used to approximate all derivatives except those appearing in axial advection terms. As described above, we approximate these with weighted centered-upwind differences.* During every half time-step, seven tridiagonal matrix equations, into which the North, South and West boundary conditions are incorporated, are inverted for each value of i (except $i = 1$) to yield the turbulence quantities at the grid points i, $1 \leq j \leq M$.

---

*The finite-difference representation of the equation for R_{rr} is included in Appendix D.

The discretized pressure, P , is defined on the staggered grid system denoted by $i+\frac{1}{2}$, $j+\frac{1}{2}$ in order to simplify the application of the Neumann pressure boundary conditions at the North, South and West boundaries and to increase the accuracy of the scheme. Centered second-order differences are used to approximate all of the derivatives of P in Equation 3.16. Centered differences are also used to approximate all of the derivatives appearing in the expression F except for the terms $sW\partial U/\partial x$ and $sW\partial W/\partial x$ which appear, respectively, in C_y and C_x. These advection terms are approximated with the weighted centered-upwind formula described above. The finite-difference approximation to the pressure equation is included in Appendix D.

To obtain the solution of the discretized pressure equation at each halftime-step, we employ the direct (that is, noniterative) technique of Swartztrauber (1974). The method is based on the cyclic reduction technique and is fully described in Swartztrauber's paper. It was developed for the numerical solution of general second-order separable elliptic partial differential equations in which the coefficients or differential terms vary with the particular variable of differentiation.* The transformed pressure equation derived in this study is an excellent example of such an equation, and application of the method is straightforward. We were fortunate to obtain a copy of the computer code BLKTRI, which is based on the method, from the National Center for Atmospheric Research. The routine BLKTRI is incorporated into the ICWAKE code. Each solution of the $(N - 1)(M - 1)$ interior values of P requires only $(M - 1)(N - 1)\log_2 (M - 1)$ operations excluding the operations required to compute F . The procedure is thus quite efficient.

The transformed counterparts of Equations (3.10) and (3.11) which apply at the East boundary are approximated with central differences for all derivatives except those in the axial convection terms which are approximated with first-order backward differences. During the alternating halftime-steps, the y and x derivatives are treated implicitly. Two tridiagonal matrix equations result during the first half step for $V_{Nj}^{n+\frac{1}{2}}$ and $W_{Nj}^{n+\frac{1}{2}}$. These may be inverted, and the solution

*We note that the procedure may also be applied to the matrix problem generated by the discretization of a separable elliptic equation over a non-uniform finite-difference grid with mesh spacing which varies independently in the two coordinate directions. We also note that by separable we mean that the differential operator is separable. The inhomogeneous terms need not be separable.

along with the appropriate turbulence quantities are used to integrate Equation (3.9) for $P^{n+\frac{1}{2}}_{Nj+\frac{1}{2}}$ and Equation (3.12) for $U^{n+\frac{1}{2}}_{Nj}$. These values of $P^{n+\frac{1}{2}}_{Nj+\frac{1}{2}}$ are used as boundary conditions for the calculation of P^{n+1} in the interior of the domain. During the second half-time step, Equations (3.10), (3.11), and (3.12) are incorporated directly into the matrix equations for each j. After these equations are inverted, Equation (3.9) is used to obtain $P^{n+1}_{Nj+\frac{1}{2}}$ which is used as a boundary condition for the calculation of P^{n+1}.

As implied in the above discussion, a calculation through a complete time step proceeds as follows. Based on the known values of all the flow variables at time step n, the values $U^{n+\frac{1}{2}}_{ij}$, $V^{n+\frac{1}{2}}_{ij}$, and $W^{n+\frac{1}{2}}_{ij}$ are first obtained for all i,j from the momentum equations with y derivatives treated implicitly. With these values, the seven turbulence quantities are then obtained at $n + \frac{1}{2}$. To complete the half-step, the pressure $P^{n+\frac{1}{2}}$ is calculated using the function F evaluated at $n+\frac{1}{2}$ with the known values of the other variables. The second time-step essentially repeats the first and yields the solution at time level $n + 1$. The difference between the first and second time half-steps is in the treatment of the mean-flow momentum equations only.

It should be obvious that this finite-difference procedure can be used for the calculation of laminar flows. For such a calculation, the computation of the turbulent correlations is simply not performed.

4. Sample Calculations

In this section, we present results from four near-wake calculations. The first calculation is initialized by and compared with the laboratory data of Schetz (reported by Swanson, et al. (1974) and Chieng, et al. (1974)). The second calculation is initialized by and compared with the data of Chevray (1968), and is also compared with a calculation of Pope and Whitelaw (1976). The third and fourth calculations are initialized with profiles obtained from the boundary layer/propeller model described in Section 2. The third is for $Re = 1.5 \times 10^4$ and is compared with the data of Lin, et al. (1974) at $z/R_b = 12$. The fourth is for $Re = 1.5 \times 10^7$. Comparative plots of wake width versus z for the third and fourth calculations are shown.

4.1 Calculation Initialized By the Data of Schetz

The data of Schetz were obtained in the wake behind a blunt-nosed, parallel-sided, sharp-sterned, axisymmetric body with a maximum diameter of 6 inches and a length of 60 inches. The flow Reynolds number, based on free-stream velocity and body radius, was 3.1×10^5. The body was fitted with a three-bladed 6-inch-diameter aft-mounted propeller and the experiments were conducted under approximately drag-free conditions. Hot wire data at axial positions 4, 10, 20, 40 and 80 body radii downstream of the body tail were obtained. These data include the turbulence correlations R_{zz}, $R_{\theta\theta}$, R_{rr}, $R_{\theta z}$, and R_{rz}, as well as W and V, the axial and swirl mean velocity components.

In the ICWAKE calculation presented here, the West boundary was set at the first data station, 4 body radii behind the body, and the East boundary was set at the third data station, 20 body radii downstream. The North boundary was 2 body radii from the axis of symmetry.

The code was initialized at the West boundary by the seven measured profiles and the following estimates for the unmeasured quantities U, $R_{r\theta}$, and ε. The mean radial velocity component, U, was set to zero; the turbulence correlation $R_{r\theta}$ was obtained from the eddy viscosity approximation

$$R_{r\theta} = \nu_e \left(\frac{\partial V}{\partial r} - \frac{V}{r} \right)$$

where $\nu_e = R_{rz} \left(\frac{\partial W}{\partial r}\right)^{-1}$

and the dissipation rate ε was set equal to $K_\varepsilon k^3/\ell$, where $k^2 = \frac{1}{2}(R_{rr} + R_{\theta\theta} + R_{zz})$, K_ε is a constant, and ℓ is the integral length scale of high turbulent Reynold's number theory. The values of K_ε and ℓ were chosen to be 0.53 and 0.2 (i.e., 0.2 body radii), as suggested from the experimental data obtained by Gran (1973).

The grid system for the calculation consisted of 40 points in the axial direction with 10 of the points between $z/R_b = 4$ and $z/R_b = 5$, and 32 points in the radial direction with 16 of the points between $r/R_b = 0$ and $r/R_b = 0.8$. Convergence was assumed when the rate of change of the RMS mean velocity divergence, calculated over the computational grid, became less than 10^{-9}. The time-step used was 0.1; about six minutes of CDC 7600 central processor time was required to do the calculation.

Comparisions of measured and computed cross-wake profiles at $z/R_b = 10$ are presented in Figures 4.1 through 4.6. Figure 4.1 displays the axial and swirl mean velocity components. The predictions are in excellent agreement with the experimental data. Figures 4.2, 4.3, and 4.4 present the three normal correlations R_{zz}, $R_{\theta\theta}$, and R_{rr}, respectively. The predicted values of R_{zz} are in reasonable agreement with the experimental data although the secondary peak in the data at about $r/R_b = 1$, which is presumably due to the vortex system shed from the propeller tips, does not appear in the prediction. The peaks in $R_{\theta\theta}$ and R_{rr} measured near the wake edge also do not appear in the predictions of these quantities, and in the case of R_{rr}, the difference between the predicted and measured values is quite large, although the value of R_{rr} predicted at the axis is in good agreement with the data. Figures 4.5 and 4.6 display the radial and tangential shear stresses, R_{rz} and $R_{\theta z}$, across the wake. The agreement between the predictions and the data for R_{rz} is quite good throughout the wake, and for $R_{\theta z}$ is reasonable in the interior of the wake. Near the edge of the wake, however, the large negative measured values of $R_{\theta z}$ are not predicted.

4.2 Calculation Initialized By the Data of Chevray

The data of Chevray were obtained in the wake behind a five foot long, six-to-one prolate spheroid. The flow Reynolds number, based

on free-stream velocity and body radius, was 2.3×10^5 , and the drag coefficient was 0.06. Hot wire data at axial positions of -0.5, 0, 0.5, 1., 2., 4., 6., 12., 18., 24., 30., and 36 body radii downstream of the body tail were obtained. These data include the turbulence correlations R_{zz} , $R_{\theta\theta}$, R_{rr} , and R_{rz} ($R_{\theta z} = R_{\theta r} = 0$) , and the mean axial and radial velocity components W and U ($V = 0$) .

In the ICWAKE calculations presented here, the West boundary was set at $z/R_b = 0.5$ and the East boundary was set at $z/R_b = 20$. The North boundary was 4 body radii from the axis of symmetry.

The calculation was initialized at the West boundary by the six measured profiles, the knowledge that $R_{\theta z} = R_{\theta r} = V = 0$, and the following assumptions about the dissipation rate ε . From the North boundary to $r/R_b = r^*$, where the production of turbulent energy, P , assumes its maximum value, P_o , ε was set equal to P . From $r/R_b = r^*$ to the axis of symmetry, ε was set equal to P_o .

The grid system for the calculation consisted of 40 points in the axial direction with 10 of the points between $z/R_b = 0.5$ and $z/R_b = 1.5$, and 32 points in the radial direction with 18 of the points between $r/R_b = 0$ and $r/R_b = 1$. The convergence criterion was the same as in the Schetz case. A time-step of 0.05 was required for convergence, and about 10.5 minutes of CDC 7600 central processor time was needed to perform the computation.

Comparisons of measured and computed cross-wake profiles of W , R_{rz} , and R_{zz} at $z/R_b = 6$, 12 , and 18 are presented in Figures 4.7 through 4.9. For W and R_{rz} , the ICWAKE results are also compared to the published computational results of Pope and Whitelaw (1976). Figures 4.7a, b, c present the comparisons for the axial mean velocity, W . The ICWAKE calculation is in excellent agreement with the Pope and Whitelaw calculation, and both calculations give good predictions of Chevray's data. The predictions are slightly less reliable at the axis of symmetry than near the wake boundary, but this discrepancy is eye-catching only at the downstream station, $z/R_b = 6$. Figures 4.8a, b, c display the results for the radial shear stress. Again the ICWAKE results agree very closely with those of Pope and Whitelaw. Although both calculations overestimate the peak magnitudes of the shear stress, they give reasonable predictions of the data. Lastly, Figures

4.9a, b, c show comparisons between ICWAKE results and Chevray's data for the axial turbulence correlation. Results for this variable were not presented by Pope and Whitelaw. The ICWAKE results overestimate the data values, but show the basic trends. The largest overpredictions are at the axis of symmetry, and the best predictions are near the wake edge.

4.3 Calculation Initialized By the Boundary-Layer/Propeller Model, $Re = 1.5 \times 10^4$

The previously described boundary-layer/propeller model was used to simulate a Flow Research laboratory experiment described by Lin, et al. (1974). In this experiment, data were obtained in the wake behind a body/propeller configuration similar to that of Schetz. The maximum body diameter was 10.16 cm, the body length was 119 cm, the propeller diameter was 4.3 cm, and the Reynold's number, $Re = 1.5 \times 10^4$. Hot film data at axial positions 12, 30, 48, and 144 body radii downstream of the body tail were obtained. These data included the turbulence correlations R_{zz}, R_{rr}, and R_{rz}, and the axial mean velocity component W.

In the ICWAKE calculation, the West boundary was set at $z/R_b = 0$ where all initial conditions were specified by the boundary-layer/propeller model. The propeller parameters required by the model were obtained from measurements of the propeller on the laboratory vehicle. The East boundary was set at 20 body radii downstream and the North boundary was set at 2 body radii from the axis of symmetry.

Because of numerical problems which were encountered, special treatment of the initial turbulence intensity and dissipation rate profiles was required. The predicted profiles of these variables at the initial station, $z/R_b = 0$, were such that the variable values dropped to zero roughly halfway between the axis of symmetry and the edge of the wake. As experience showed, the code would fail catastrophically unless these profiles were non-zero throughout the wake. So from the point at which these variables became sufficiently small to be dynamically insignificant, say less than 10^{-6}, to the edge of the wake where they were constrained by the North boundary conditions to be zero, a linear approximation was used. In addition, it was found necessary to assign an upper bound to $\varepsilon/\sqrt{(R_{zz}^2 + R_{\theta\theta}^2 + R_{rr}^2)}$, in the outer wake region. This

bound was chosen from examination of previous successful calculations to be 10^{-4}.

The grid system for the calculation consisted of 60 points in the axial direction with 20 of the points between $z/R_b = 0$ and $z/R_b = 1$, and 32 points in the radial direction with 24 of the points between $r/R_b = 0$ and $r/R_b = 1.2$. The convergence criterion was again as in the Schetz case. A time-step of 0.05 was used, and about eleven minutes of CDC 7600 central processor time was required to do the calculations.

Comparisons of measured and computed cross-wake profiles at $r/R_b = 12$ are presented in Figures 4.10 and 4.11. The quantities displayed are W and R_{zz}, respectively. The agreement between predictions and measurements is quite reasonable in both cases except for the axial mean velocity component near the axis of symmetry.

Figure 4.12 shows a plot of the width of the simulated wake versus downstream distance. Wake width at a given downstream station is defined as the distance from the axis of symmetry at which the cross-wake profile of axial turbulent intensity, $\sqrt{R_{zz}}$, falls to half of its peak value. The predicted wake width at $z/R_b = 12$ differs by only about 5% from the value presented by Lin, et al. (1974).

4.4 Calculation Initialized By Boundary-Layer/Propeller Model, $Re = 1.5 \times 10^7$

The Reynolds number for the calculation described in this section was achieved by multiplying all lengths in the calculation for $Re = 1.5 \times 10^4$ by 100, and all velocities by 10. The grid was again 60 x 32, but since high resolution near the body was required, the East boundary was set to $z/R_b = 12$ and the North boundary to $z/R_b = 1.2$. There were 20 points between $z/R_b = 0.$ and 0.6, 24 points between $r/R_b = 0.$ and 0.72. Because of the higher space resolution, the time step required for convergence was one-fifth of that used in the calculation for $Re = 1.5 \times 10^4$. All other aspects of the calculation for $Re = 1.5 \times 10^7$ were the same as for $Re = 1.5 \times 10^4$. The calculation required about 55 minutes of CDC 7600 central processor time.

A plot of the calculated wake width for $Re = 1.5 \times 10^7$ is presented in Figure 4.12, alongside the wake width plot for $Re = 1.5 \times 10^4$. As one might expect, the wake is narrower for the high Re case.

5. Conclusions

A two-part procedure for modeling the turbulent flow in the near-wake of a submerged, axisymmetric, self-propelled vehicle has been presented. Only gross parameters such as the body speed, the body dimensions, and the propeller geometry are required to initialize the model. The first part of the procedure establishes conditions at the tail of the vehicle, just aft of the propeller, which can be used to initialize the second part of the procedure, a finite difference simulation of the turbulent near-wake. Laboratory data can also be used to initialize the wake simulation.

A computer code based on the procedure has been used to generate four sets of predictions, three of which have been compared to laboratory measurements. Two sets of these predictions were also initialized by the laboratory data. As can be seen from Sections 4.1, 4.2, and 4.3, the comparisions suggest that the model holds substantial promise of being able to successfully describe turbulent near-wakes.

In spite of these good results, several aspects of the model clearly require further consideration. For example, the analysis used to construct the first part of the modeling procedure is relatively simplified and is only justified if it turns out that the flow in the turbulent wake does not depend too strongly on the details of the flow at the tail of the vehicle. The degree of this dependence has to be determined by systematically evaluating the sensitivity of the downstream flow to the conditions at the vehicle's tail. If it turns out that certain upstream variables are critical for the wake's evolution, then these quantities must be more accurately determined. It is our conjecture that the mean flow quantities are far more critical than the turbulence variables for the wake's evolution, and thus, that our model would benefit from a more accurate determination of the mean flow just aft of the propeller.

A related question is how critical are the methods used to complete an incomplete set of laboratory data which is used to initialize the calculation of the turbulent near-wake. For example, in the simulation of Schetz's flow we have used an eddy viscosity assumption to determine the initial $R_{r\theta}$ profile, even though we know that for complex turbulent flows, eddy viscosity assumptions often fail. Also, in

Schetz's case, to determine the initial dissipation rate profile, we have used the high Reynold's number assumption that $\varepsilon = k^{3/2}/\ell$, where k is the turbulent kinetic energy and ℓ is a turbulence integral scale, whereas in the case of Chevray's flow, we have followed Pope and Whitelaw (1976) and assumed that the dissipation rate is equal to the production rate of turbulent kinetic energy. It is not clear which approach for estimating ε is better. A final example is that we have set the initial mean radial velocity profile to zero for Schetz's flow, even though Pope and Whitelaw (1976) show that the downstream evolution of Chevray's flow is fairly sensitive to this quantity. Our hope is that the downstream character of the wake does not depend strongly on crudely estimated quantities such as $R_{r\theta}$, ε, and U in the above examples. Sensitivity studies are again called for.

In the near-wake calculation, we assumed that axial gradients of turbulence quantities which appear in turbulence diffusion terms may be neglected. Although the good agreement between our calculation and Pope and Whitelaw's for the Chevray case, suggests that this approximation is a good one, it should be more carefully evaluated. Further numerical studies should provide some insight into the applicability of and the error resulting from this assumption.

Finally, we come to the seven-equation turbulence model that is used in the near-wake calculation. Although the model we have used here is derived from a large number of flow simulations, it would be overly optimistic for us to expect that it is necessarily applicable to the flows of interest here. We should expect that the model would benefit from at least some modification or "tuning" of constants. Because of the short time span of this effort, none was attempted. Perhaps after applying the model to other flow situations similar to those of interest here (with the <u>expectation</u> of encountering difficulty), we will acquire the necessary insight and experience required to make rational and helpful model improvements.

References

Abramowitz, M. and Stegun, I. A. (1970) "Handbook of Mathematical Functions," Dover Publications, N.Y.

Bradshaw, P. (1967) "The Turbulence Structure of Equilibrium Boundary Layers," J. Fl. Mech., 29, pp. 625.

Chevray, R. (1968) "The Turbulent Wake of a Body of Revolution," A.S.M.E. J. Basic Eng., 90, pp. 275.

Chieng, C. C., Jokubowski, A. K. and Schetz, J. A. (1974), "Investigation of the Turbulent Properties of the Wake Behind Self-Propelled, Axisymmetric Bodies," Virginia Polytechnic Institute and State University Report Aero-025.

Coles, D. E. and Hirst, E. A. (1969) "Proceedings-Computation of Turbulent Boundary Layers - 1968 AFOSR-IFP-Stanford Conference; Volume II Compiled Data," Stanford University Press.

Daly, B. J. and Harlow, F. H. (1970) "Transport Equations in Turbulence," The Physics of Fluids, Vol. 13, No. 11, pp. 2634.

Grabowski, W. J. and Berger, S. A. (1976) "Solutions of the Navier-Stokes Equations for Vortex Breakdown," JFM, Vol. 75, Part 3, pp. 525.

Grabowski, W. J. and Robins, R. E. (1976) "Turbulent Flow Past a Self-Propelled Vehicle, Vol. II: Computation," Flow Research Note No. 95, December, in revision.

Gran, R. L. (1973) "An Experiment on the Wake of a Slender Propeller-Driven Body," TRW Report No. 20086-6006-RO-00.

Hall, M. G. (1965) "A Numerical Method for Solving the Equation for a Vortex Core," Aero. Res. Council R&M 3467.

Hall, M. G. (1966) "The Structure of Concentrated Vortex Cores," Progress in Aeronautical Science (ed. D. Kucheman), Vol. 7, pp. 53, Pergamon Press.

Hanjalic, K. and Launder, B. E. (1972) "A Reynolds Stress Model of Turbulence and its Application to Thin Shear Flow," JFM, Vol. 52, Part 4, pp. 609.

Harlow, F. H. and Welch, J. E. (1965) "Numerical Calculation of Time-Dependent Viscous Incompressible Flow of Fluid With Free Surface," Physics of Fluids, Vol. 8, No. 12, pp. 2189.

Klebanoff, P. S. (1955) "Characteristics of Turbulence in a Boundary Layer with Zero Pressure Gradient," NACA Tech. Report No. 1247.

Launder, B. E., Reece, G. J. and Rodi, W. (1975) "Progress in the Development of a Reynolds Stress Turbulence Closure," JFM, Vol. 68, Part 3, pp. 537.

References (Cont.)

Lilley, D. G. (1973) "Prediction of Inert Turbulent Swirl Flows," AIAA Journal, Vol. 11, No. 7, pp. 995.

Lin, J. T., Pao, Y. H. and Veenhuizen, S. D. (1974) "Turbulent Wake of a Propeller-Driven Slender Body in Stratified and Non-Stratified Fluids," Presented at the 27th Annual Meeting of the Fluid Dynamics Division of the American Physical Society, November 25-27, 1974, California Institute of Technology, Pasadena, California. Abstract in Bull. Amer. Phys. Soc., 19, pp. 1165.

McLemore, H. C. (1962) "Wind-Tunnel Tests of a 1/20-Scale Airship Model with Stern Propellers," NASA Tech. Note D-1026.

Mager, A. (1972) "Dissipation and Breakdown of a Wing-Tip Vortex," JFM, Vol. 55, Part 4, pp. 609.

Pao, Y.-H. and Daugherty, R. J. (1969) "Time-Dependent Viscous Incompressible Flow Past a Finite Flat Plate," Boeing Scientific Research Laboratories, D1-82-0822.

Patel, V. C. (1973a) "On the Equations of a Thick Axisymmetric Turbulent Boundary Layer," Iowa Inst. of Hyd. Res. Report No. 143.

Patel, V. C. (1973b) "A Simple Integral Method for the Calculation of Thick Axisymmetric Turbulent Boundary Layers," Iowa Inst. of Hyd. Res. Report No. 150.

Patel, V. C., Nakayama, A. and Damian, R. (1974) "Measurements in the Thick Axisymmetric Turbulent Boundary Layer Near the Tail of a Body in Revolution," J. Fl. Mech., 63, pp. 345-367. (Also, Patel, V. C., "An Experimental Study of the Thick Turbulent Boundary Layer Near the Tail of a Body of Revolution," Iowa Inst. of Hyd. Res. Report No. 142.)

Peaceman, D. W. and Rachford, H. H., Jr. (1955) "The Numerical Solution of Parabolic and Elliptic Differential Equations," SIAM Journal, Vol. 3, No. 1, pp. 280.

Pope, S. B. and Whitelaw, J. H. (1976) "The Calculation of Near-Wake Flows," JFM, Vol. 73, Part 1, pp. 9.

Roache, P. J. (1972) Computational Fluid Dynamics, Hermosa Publishers, Albuquerque, New Mexico.

Rotta, J. (1951) "Statisticle Theorie Nichthomogener Turbulenz," Z. Phys., Vol. 129, pp. 547.

References (Cont.)

Schwartz, L. W. and Bernstein, S. (1975) "Documentation of a Propeller Analysis Computer Program," Flow Research Note No. 67.

Swanson, R. C., Jr., Schetz, J. A. and Jakubowski, A. K. (1974) "Turbulent Wake Behind Slender Bodies Including Self-Propelled Configurations," Virginia Polytechnic Institute and State University Report Aero-024.

Swartzrauber, P. N. (1974) "A Direct Method for the Discrete Solution of Separable Elliptic Equations," SIAM J. Numer. Anal., Vol. 11, No. 6.

Tennekes, H. and Lumley, J. L. (1973) "A First Course in Turbulence," the M.I.T. Press, Cambridge, Mass.

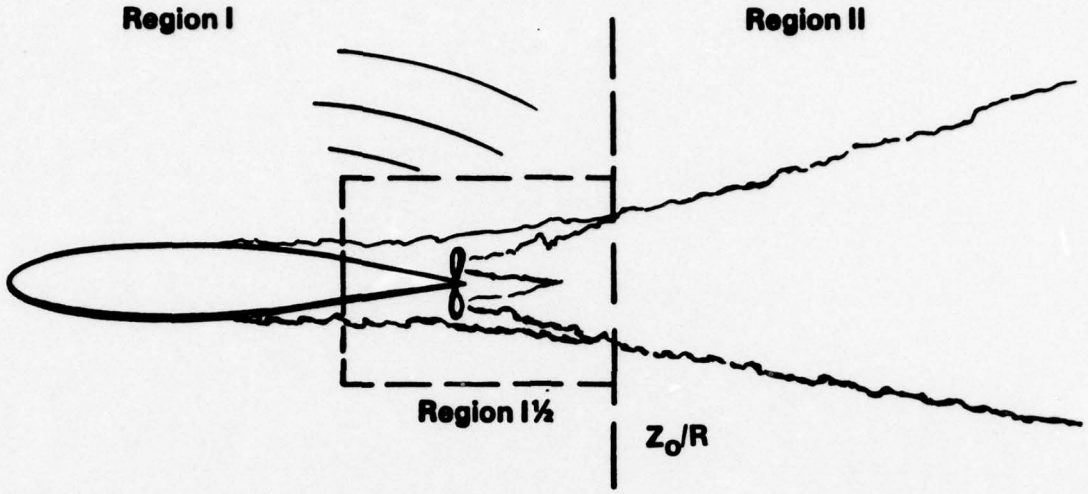

Figure 1-1. Submerged Self-Propelled Body

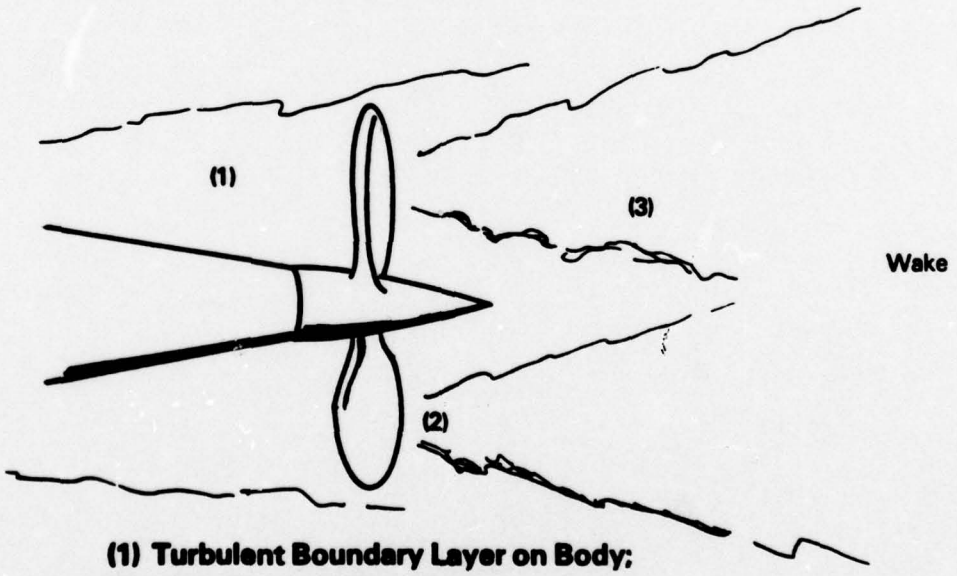

(1) Turbulent Boundary Layer on Body;
(2) Flow Through Propeller;
(3) Rapidly Varying Near Wake.

Figure 1-2. Region I½ - Key Elements.

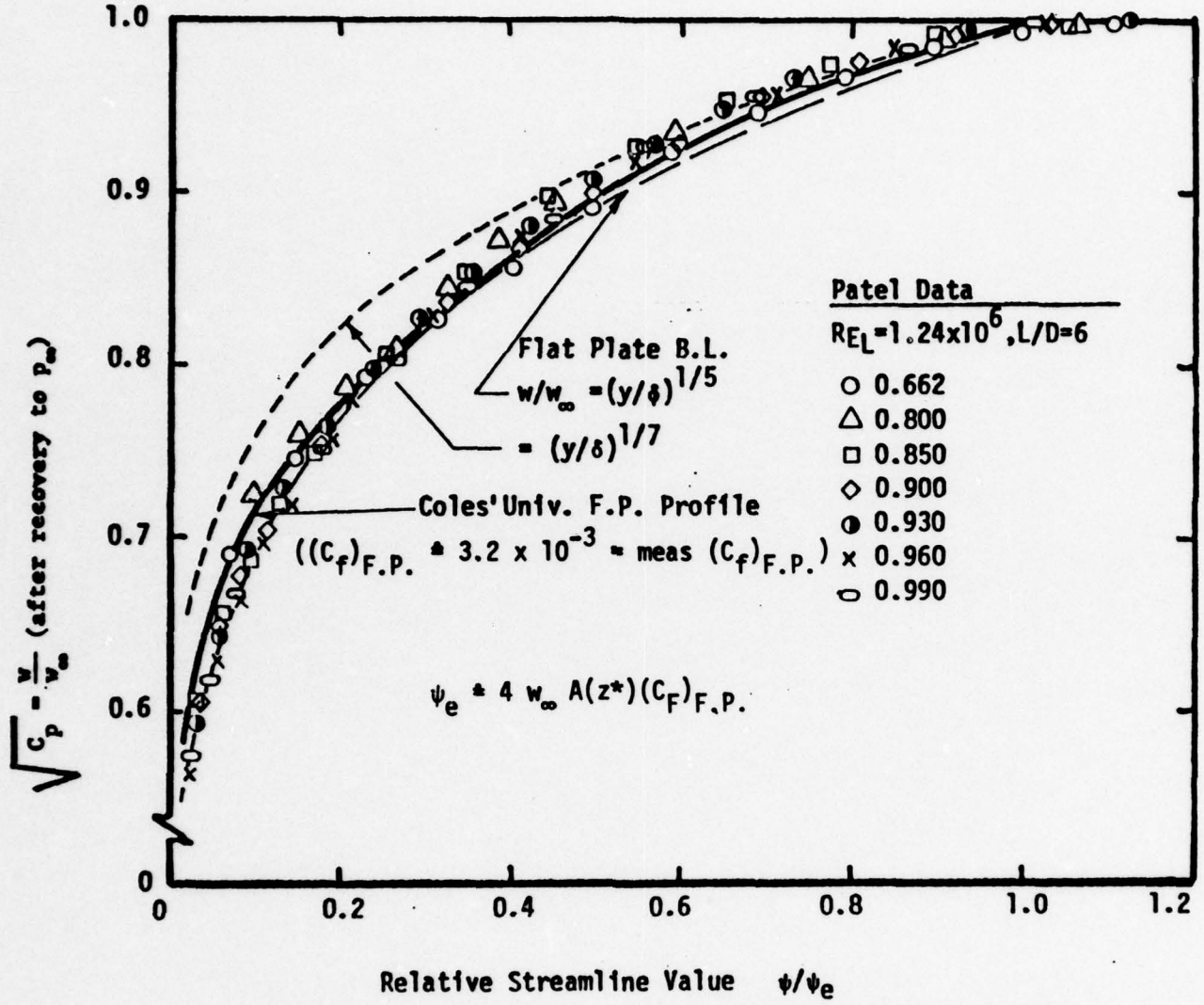

Fig. 2.1 Correlation of Aft-body Boundary Layer Data with Flat-Plate Boundary Layer Approximations.

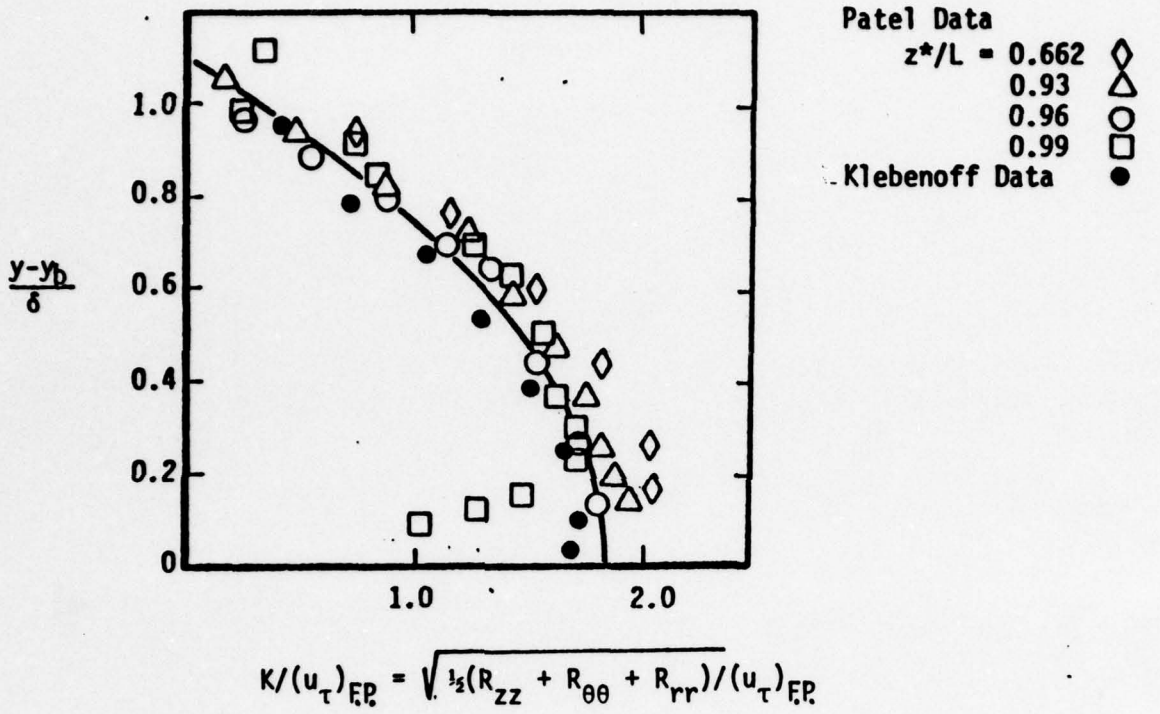

Figure 2.2 Distribution of Turbulent Intensity across Aft-Body Boundary Layer

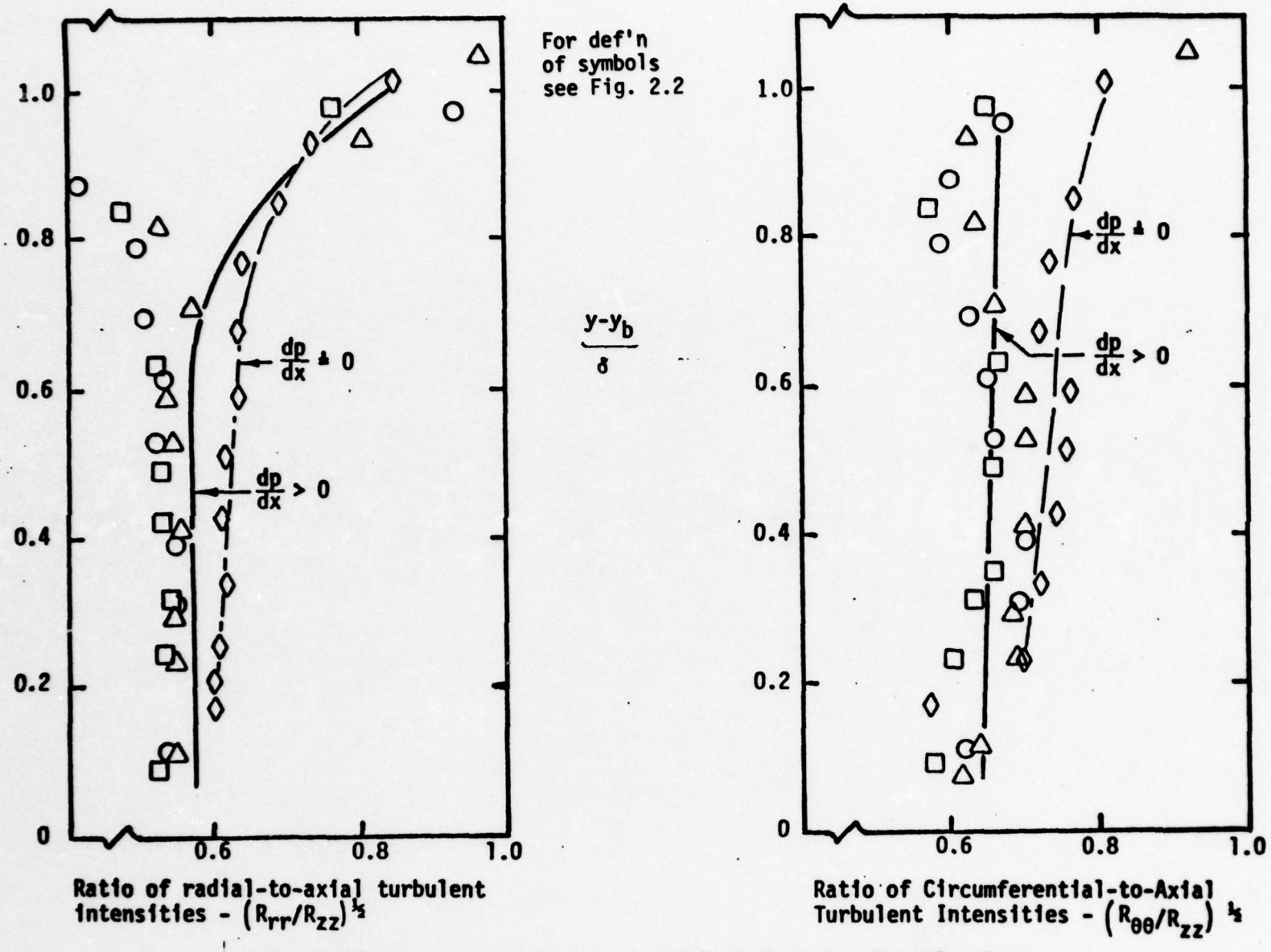

Figure 2.3 Degree of Anisotropy in Aft-Body Turbulent Boundary Layer

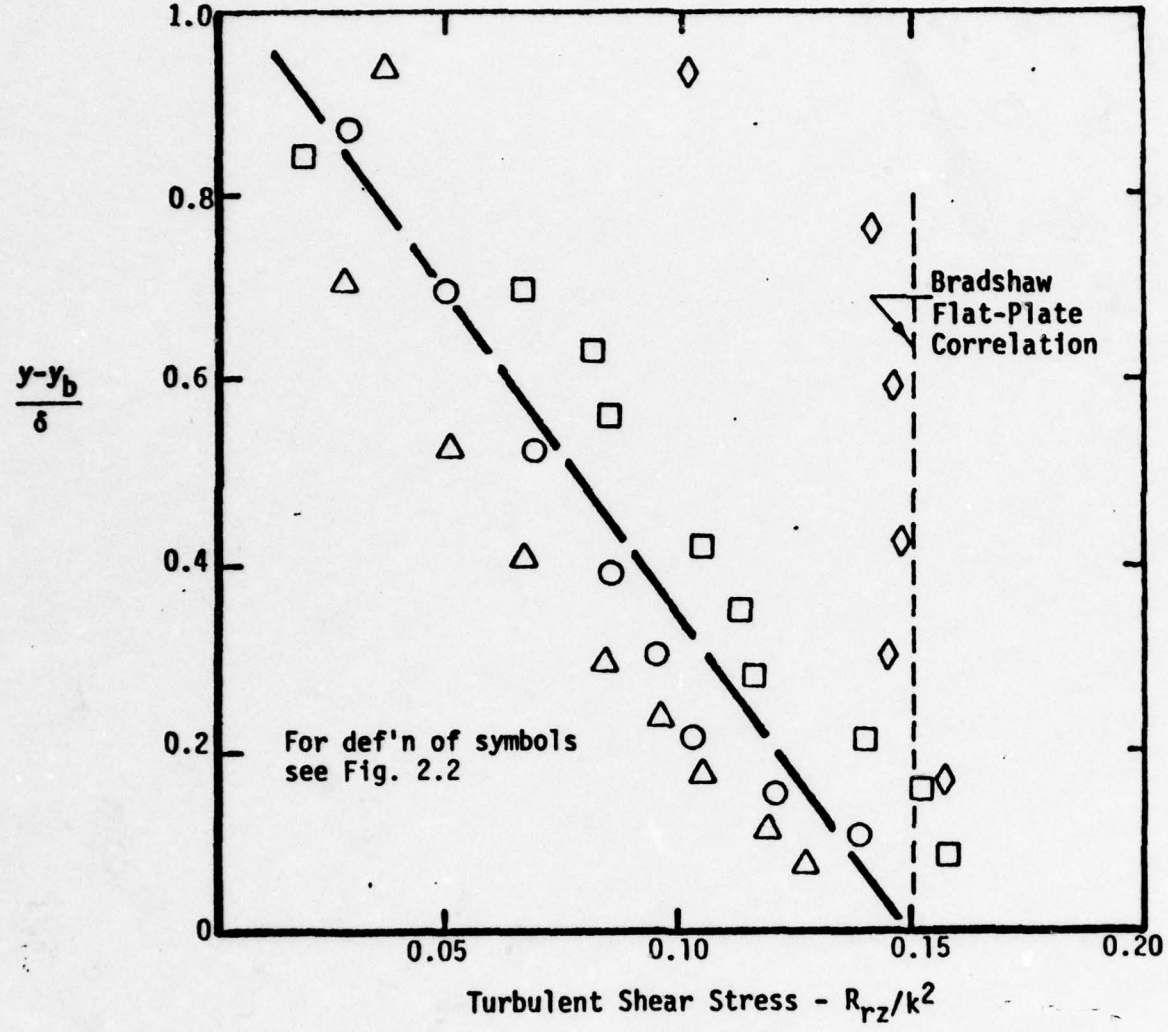

Figure 2.4 Distribution of Turbulent Shear Stress across Aft-Body Boundary Layer.

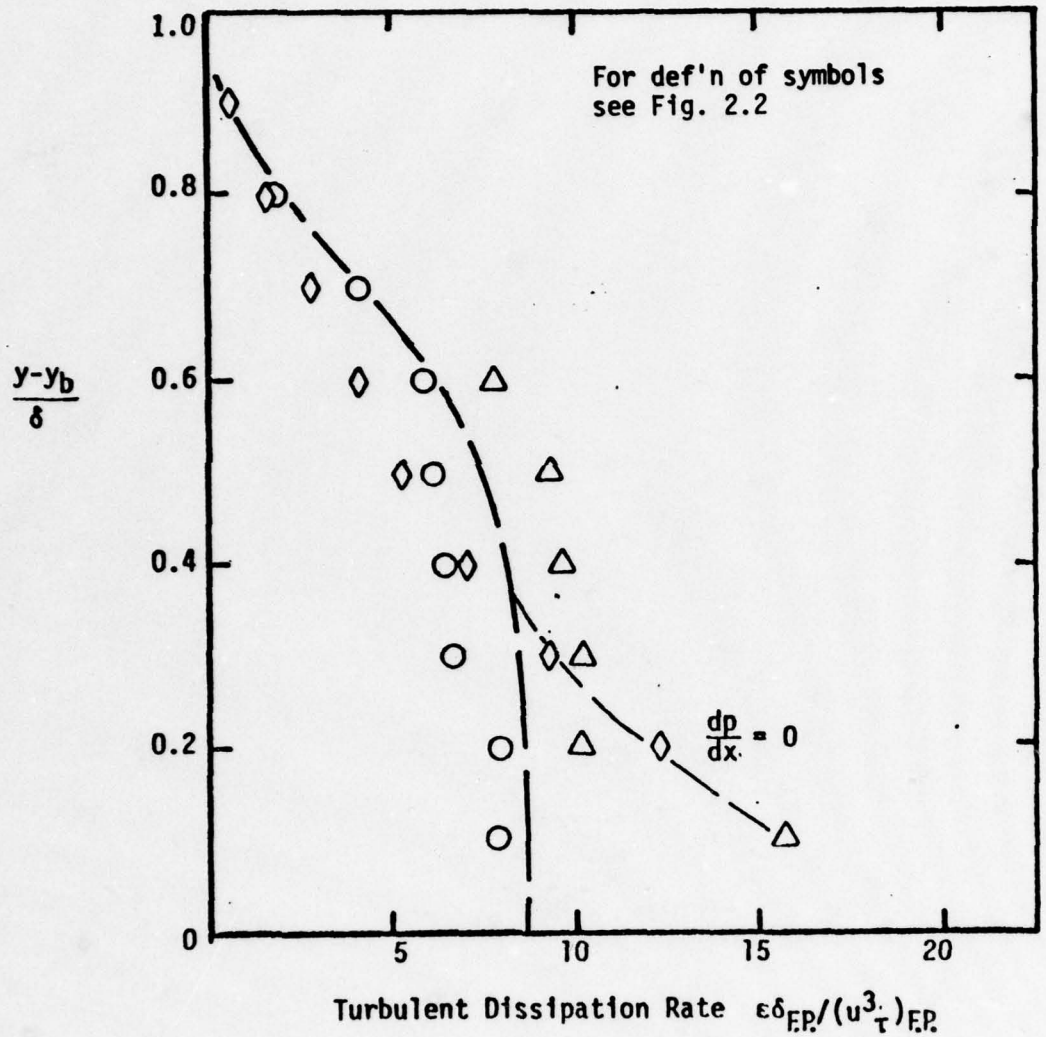

Figure 2.5 Distribution of Turbulent Dissipation Rate across Aft-Body Boundary Layer.

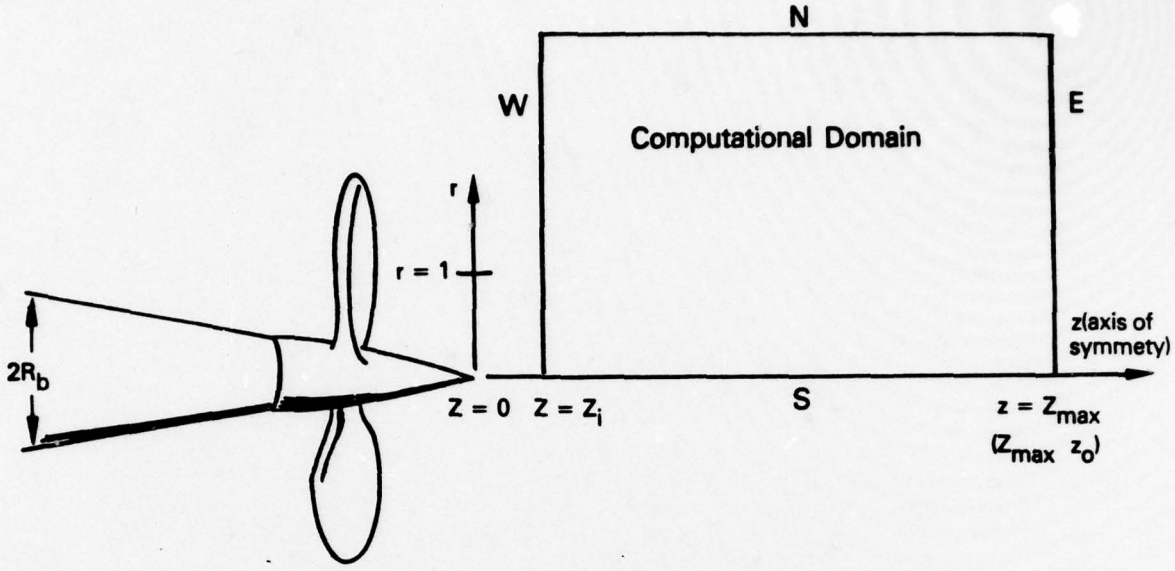

Figure 3-1. Coordinate system and Computational Domain.

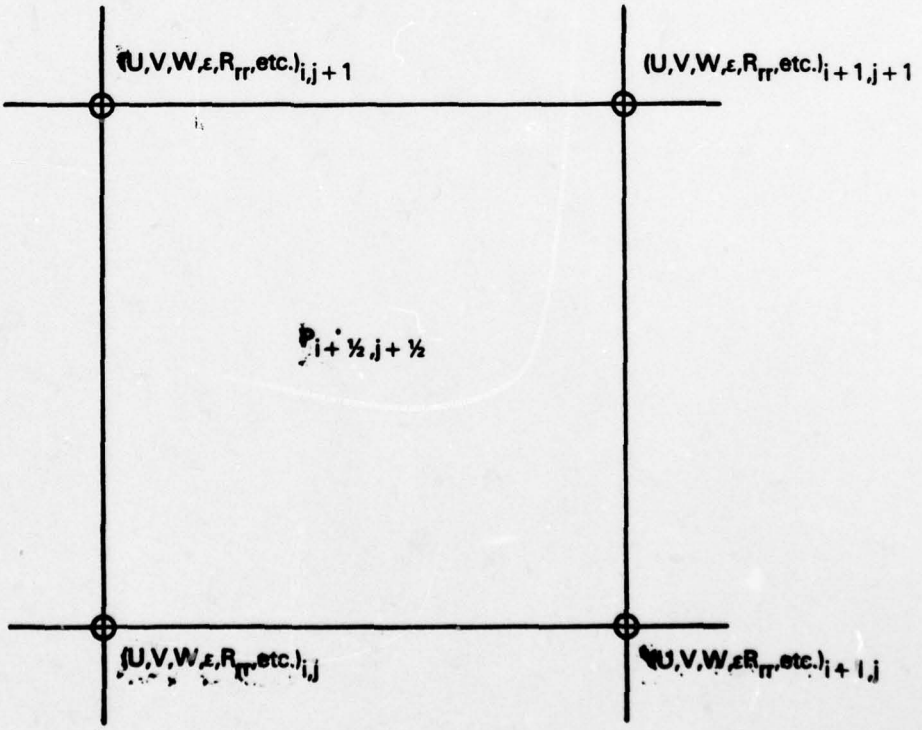

Figure 3-2. Finite-Difference Grid system.

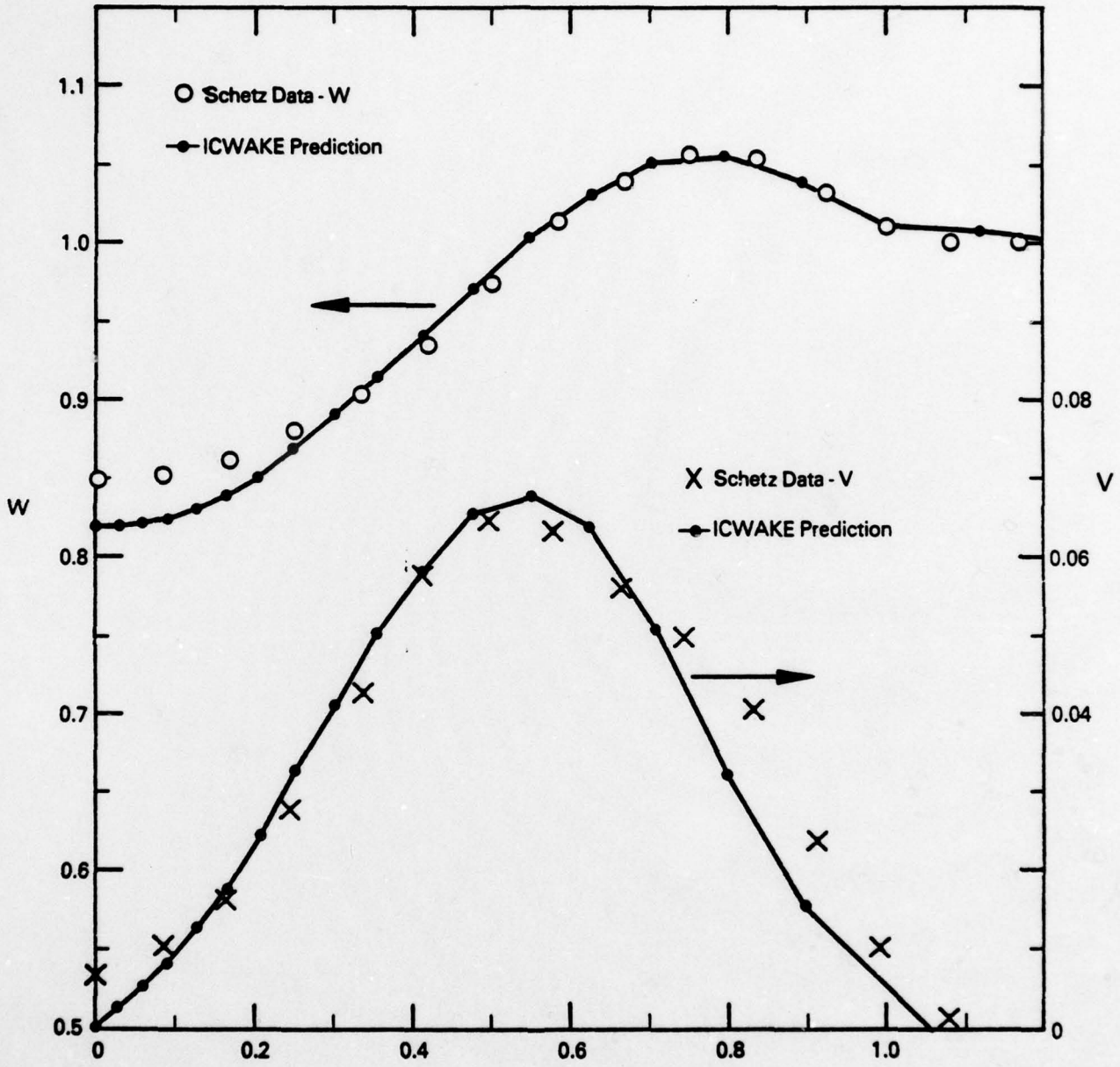

Figure 4-1. Axial and Swirl Mean Velocity Components Across Self-Propelled Body Wake at $z/R_b = 10$.

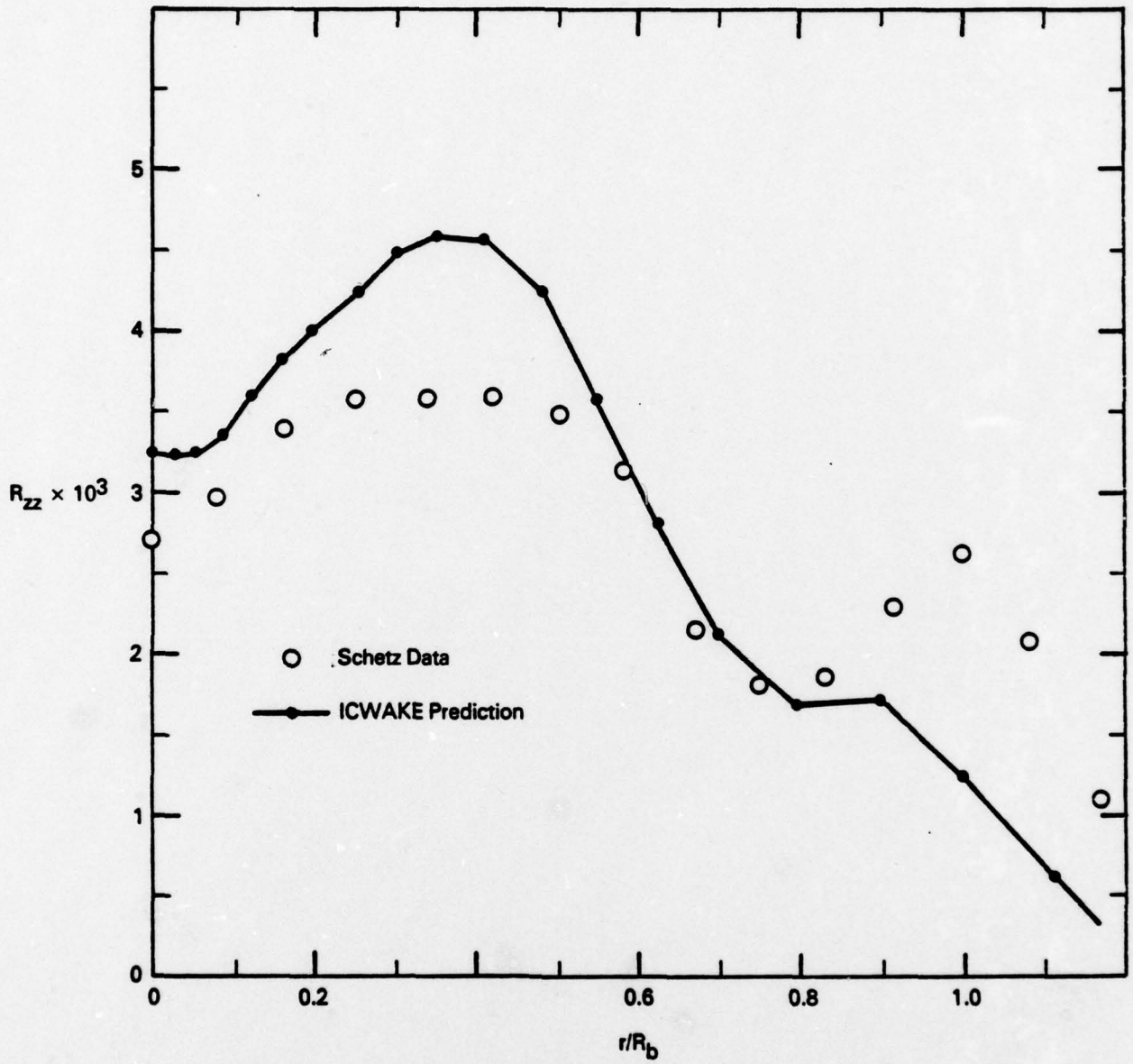

Figure 4-2. Axial Turbulence Intensity Across Self-Propelled Body Wake at $z/R_b = 10$.

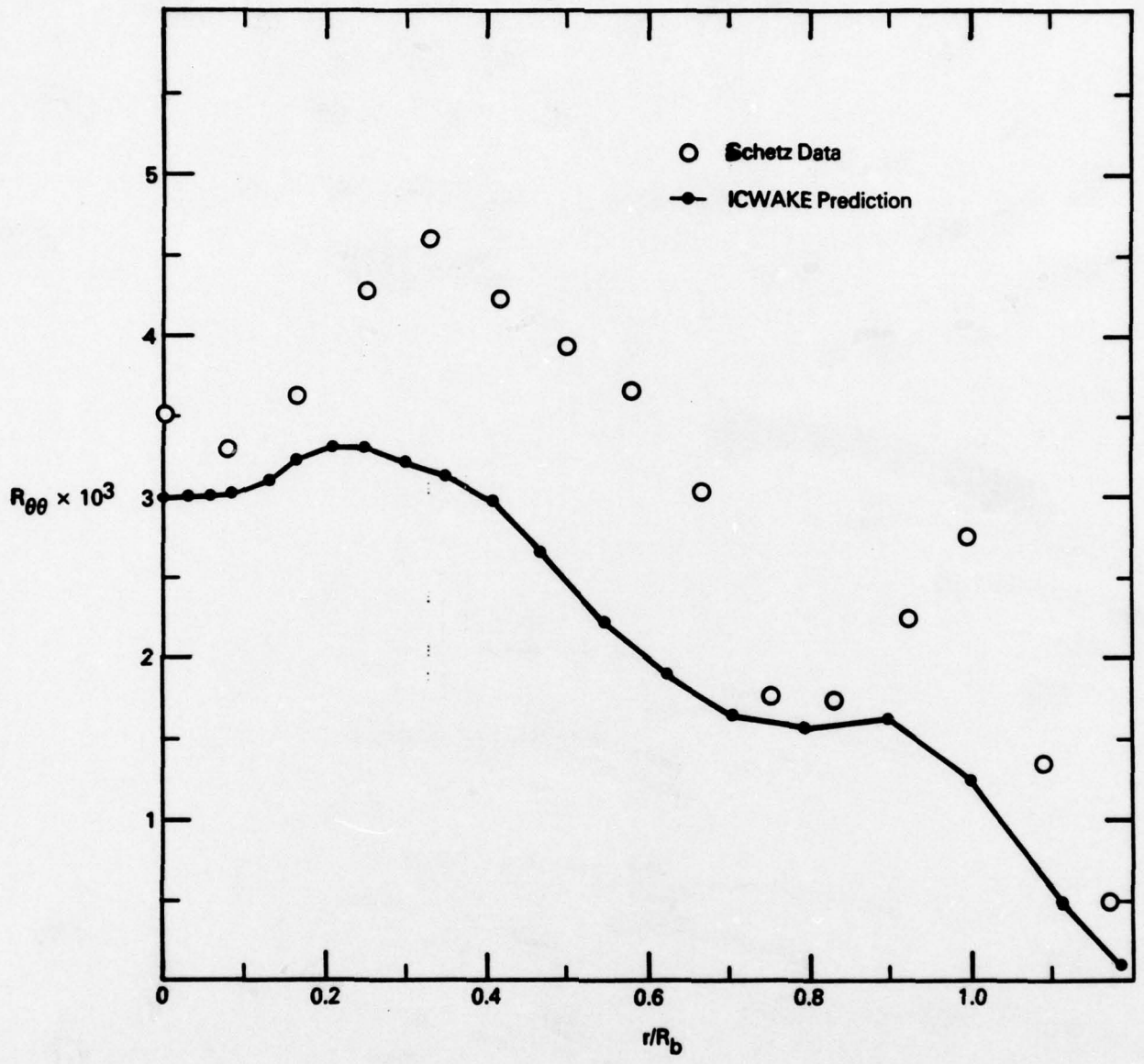

Figure 4-3. Circumferential Turbulence Correlation Across Self-Propelled Body Wake at $z/R_b = 10$.

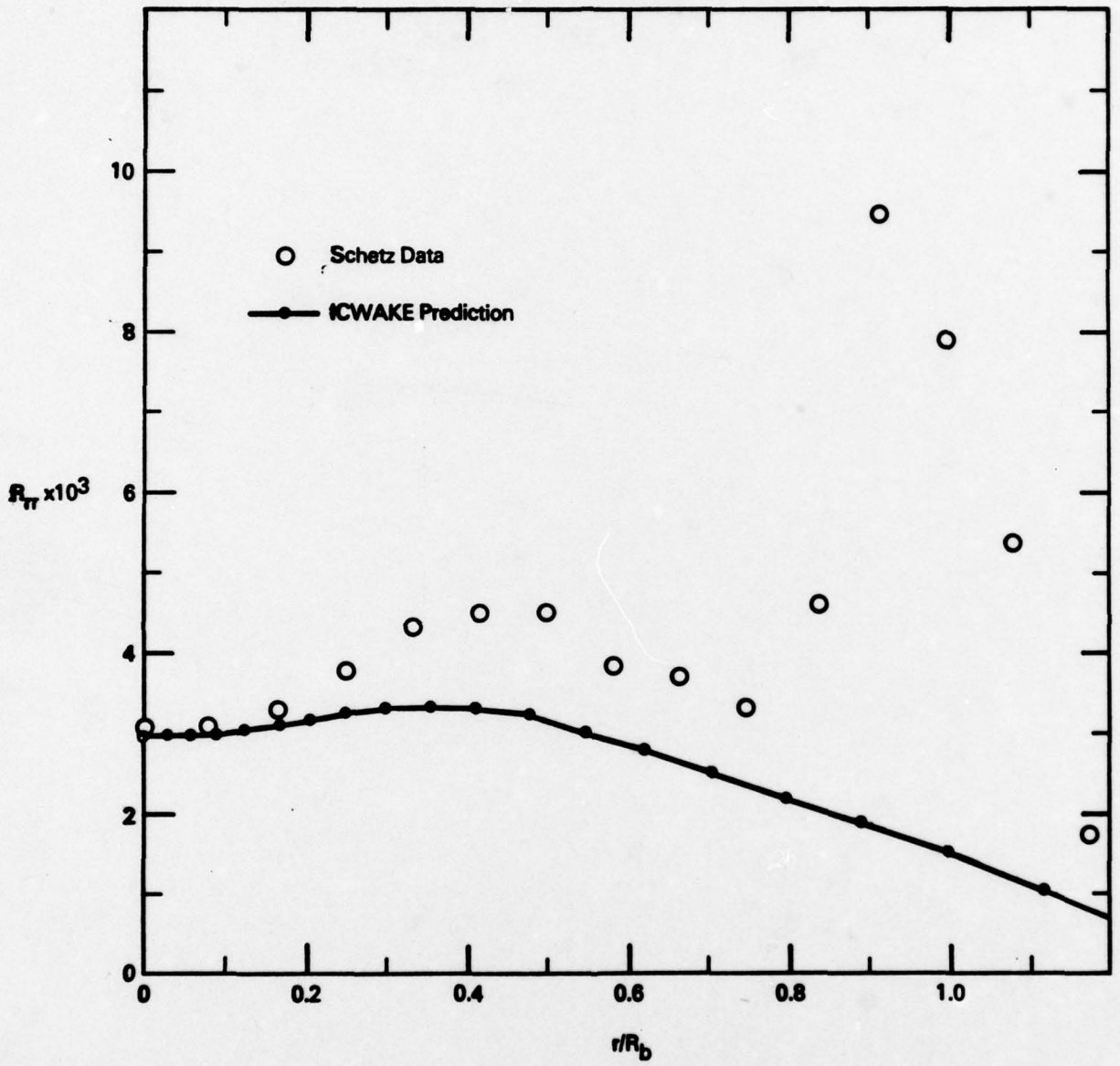

Figure 4-4. Radial Turbulence Correlation Across Self-Propelled Body Wake at $z/R_b = 10$.

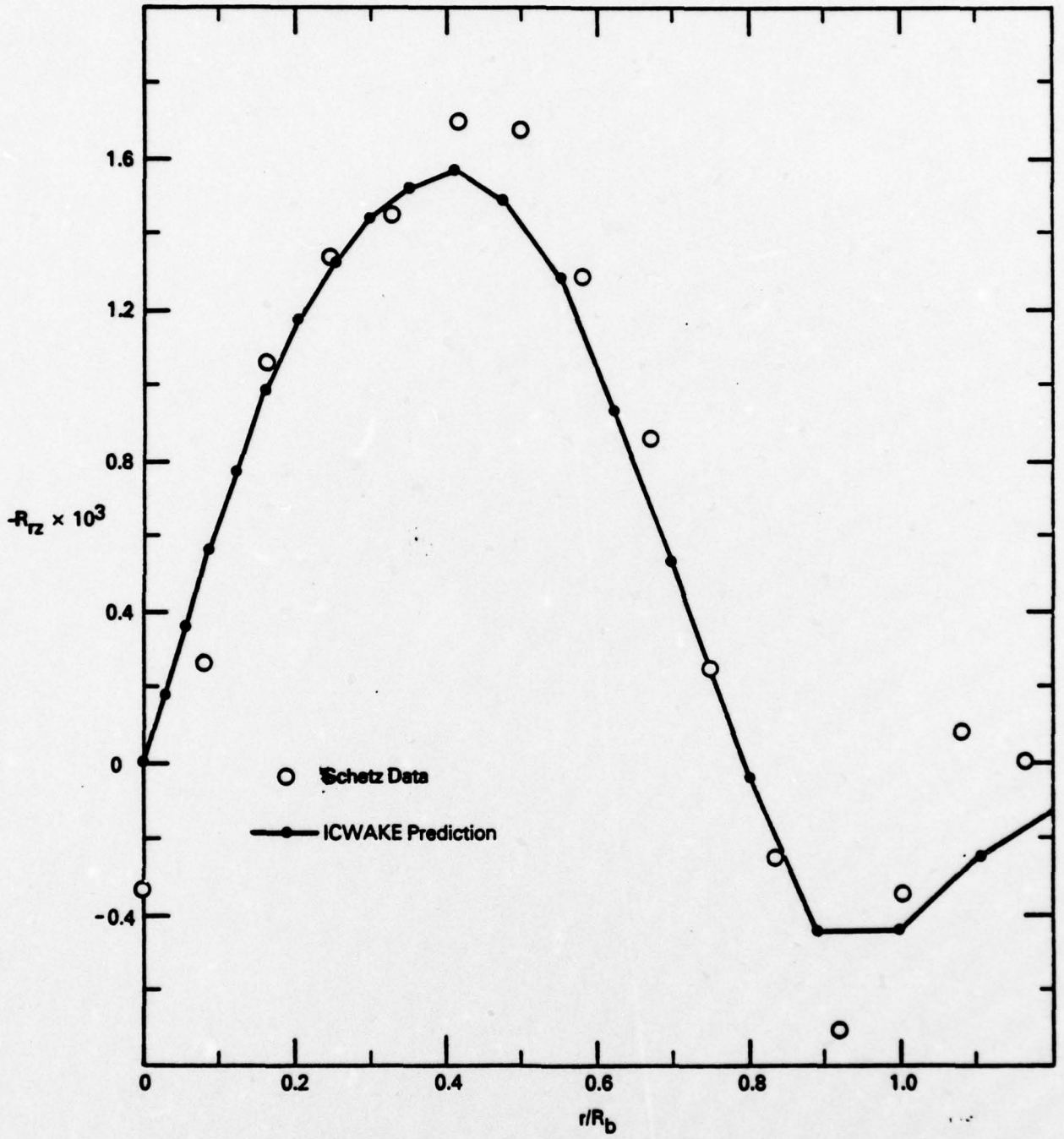

Figure 4-5. Radial Shear Stress R_{rz} Across Self-Propelled Body Wake at $z/R_b = 10$.

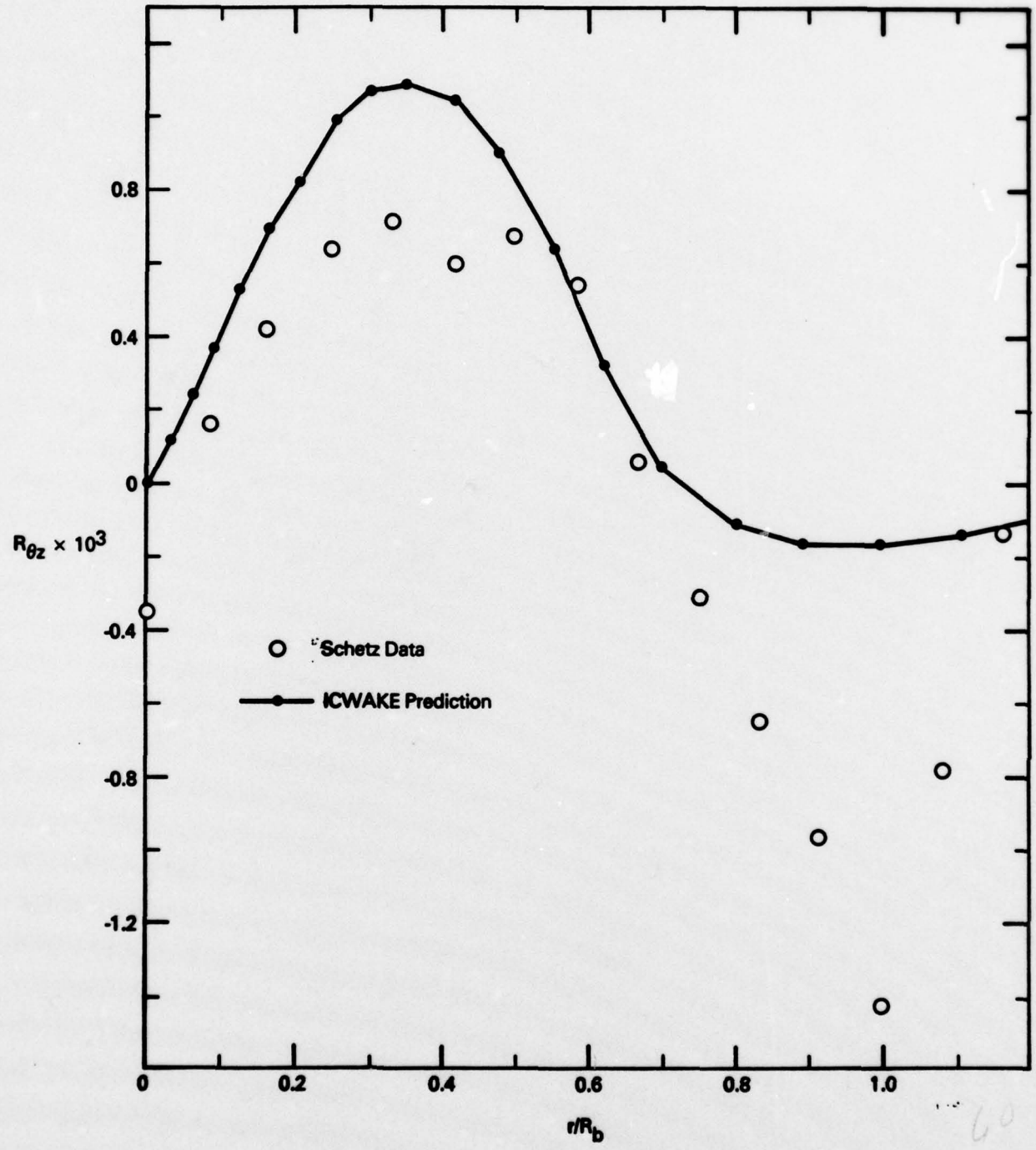

Figure 4-6. Tangential Shear Stress Across Self-Propelled Body Wake at $z/R_b = 10$.

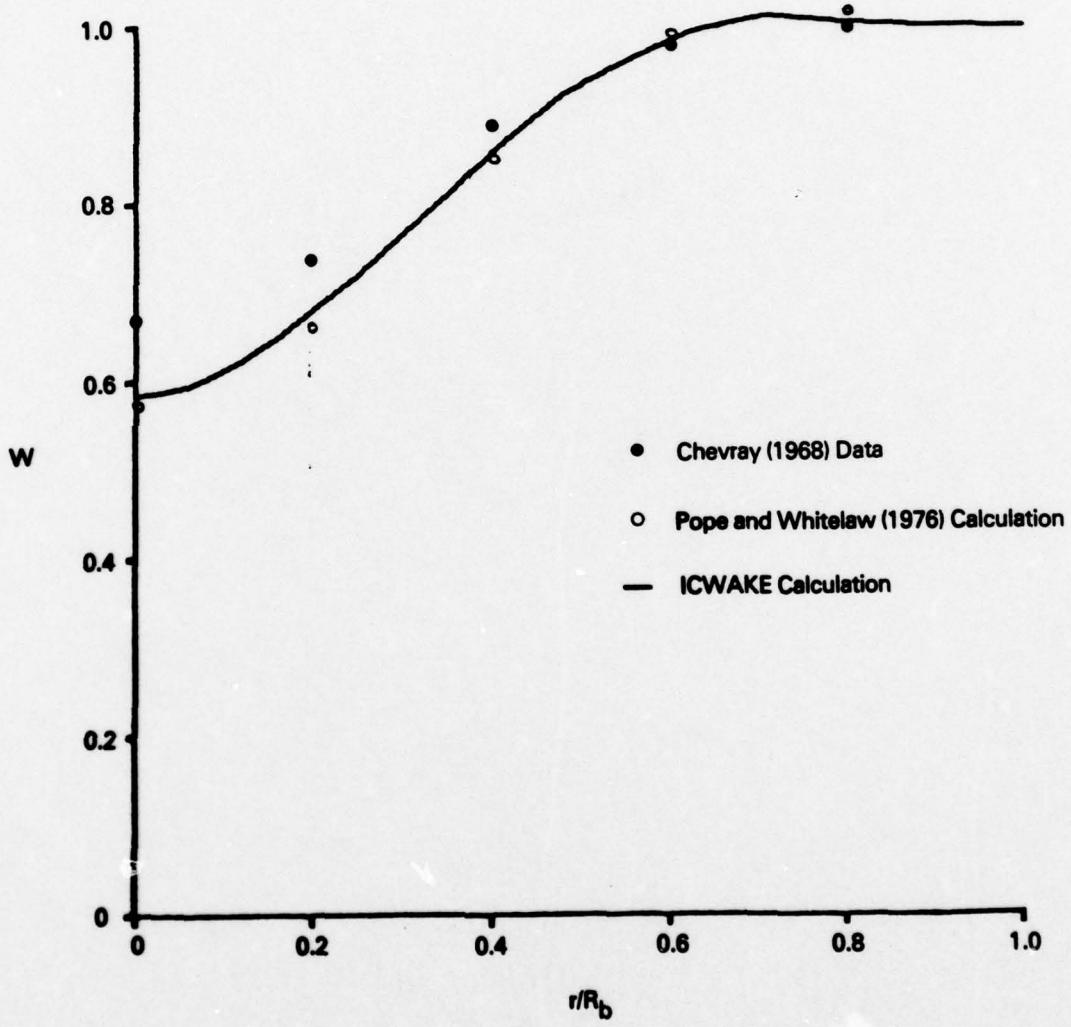

Figure 4-7a. Axial Mean Velocity Component Across Prolate Spheroid Wake at $z/R_b = 6$.

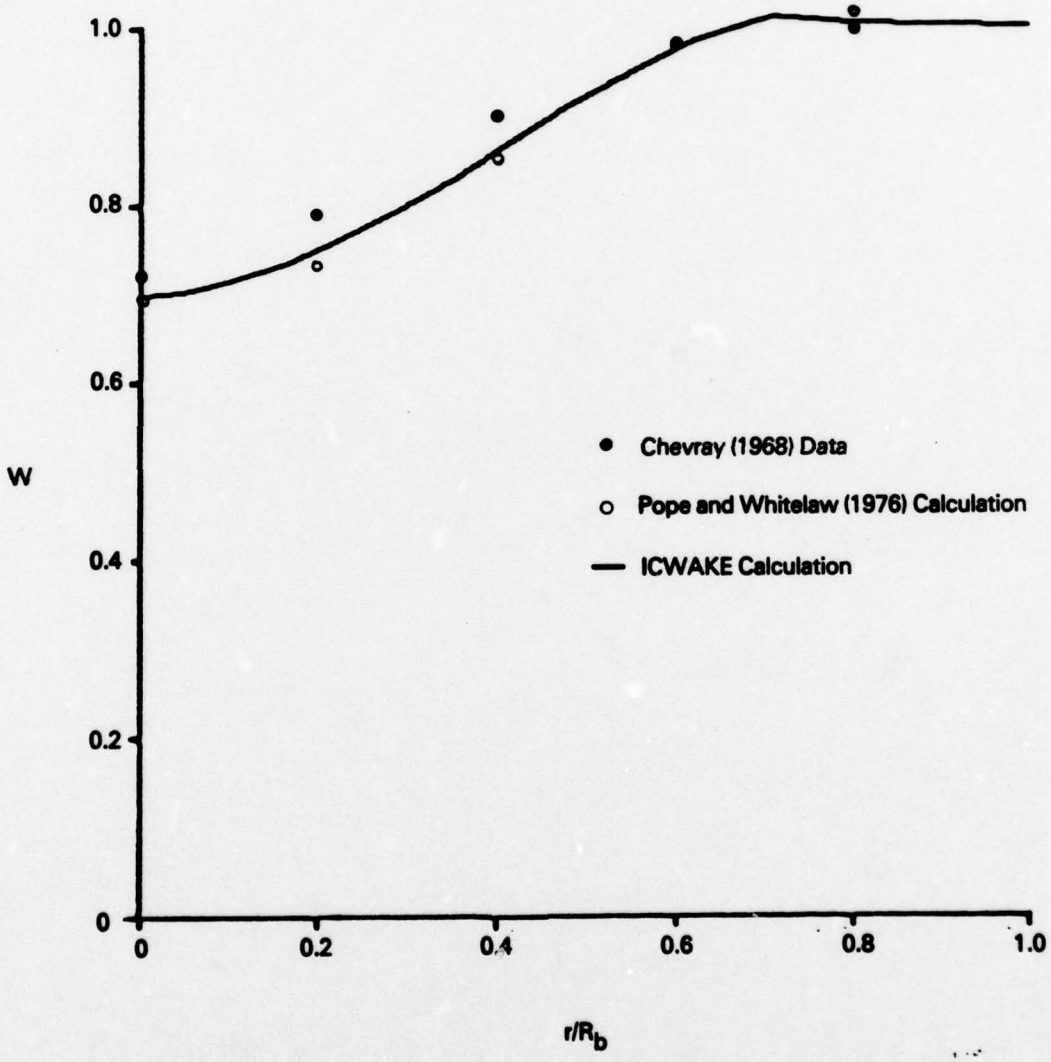

Figure 4-7b. Axial Mean Velocity Component Across Prolate Spheroid Wake at $z/R_b = 12$.

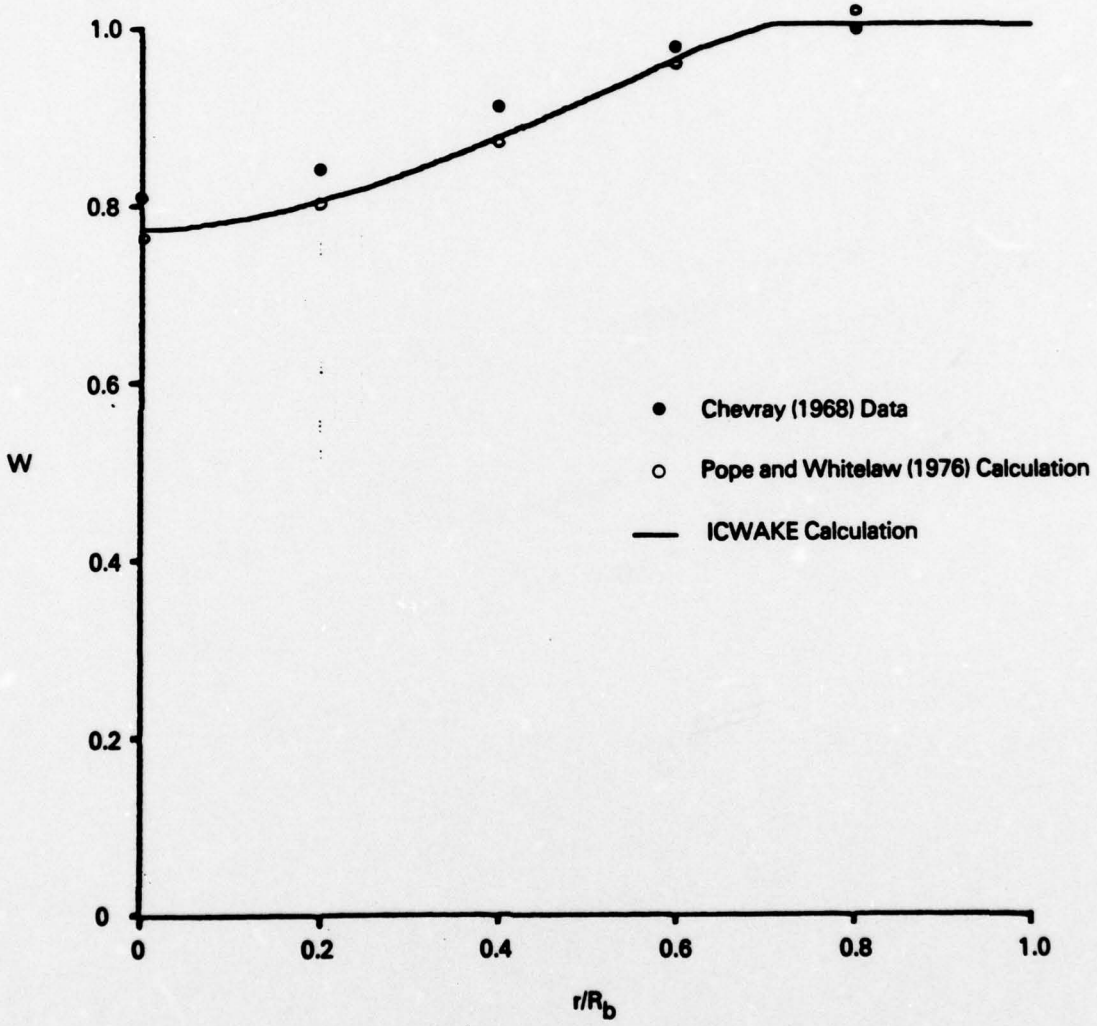

Figure 4-7c. Axial Mean Velocity Component Across Prolate Spheroid Wake at $z/R_b = 18$.

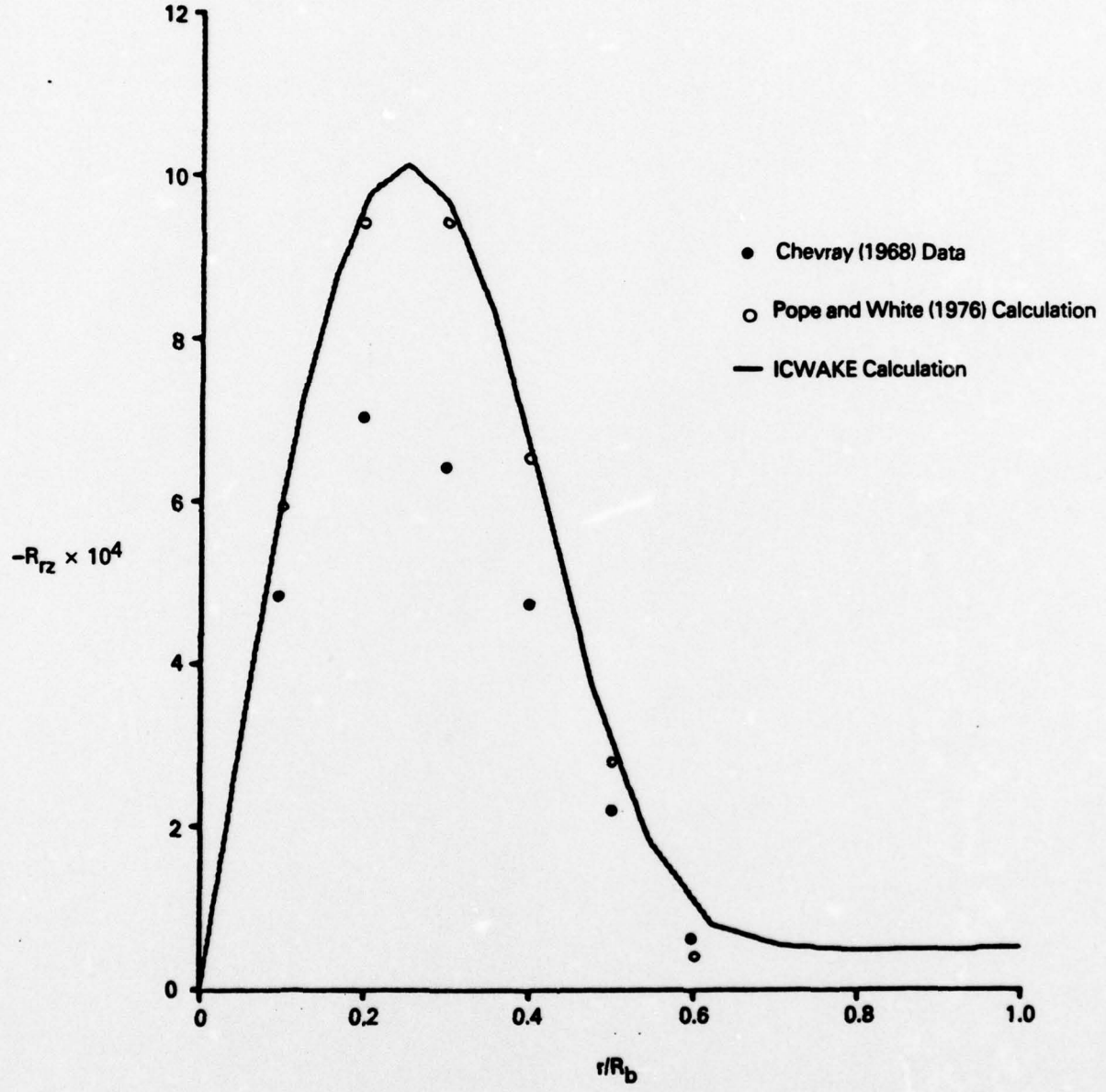

Figure 4-8a. Radial Shear Stress Across Prolate Spheroid Wake at $z/R_b = 6$.

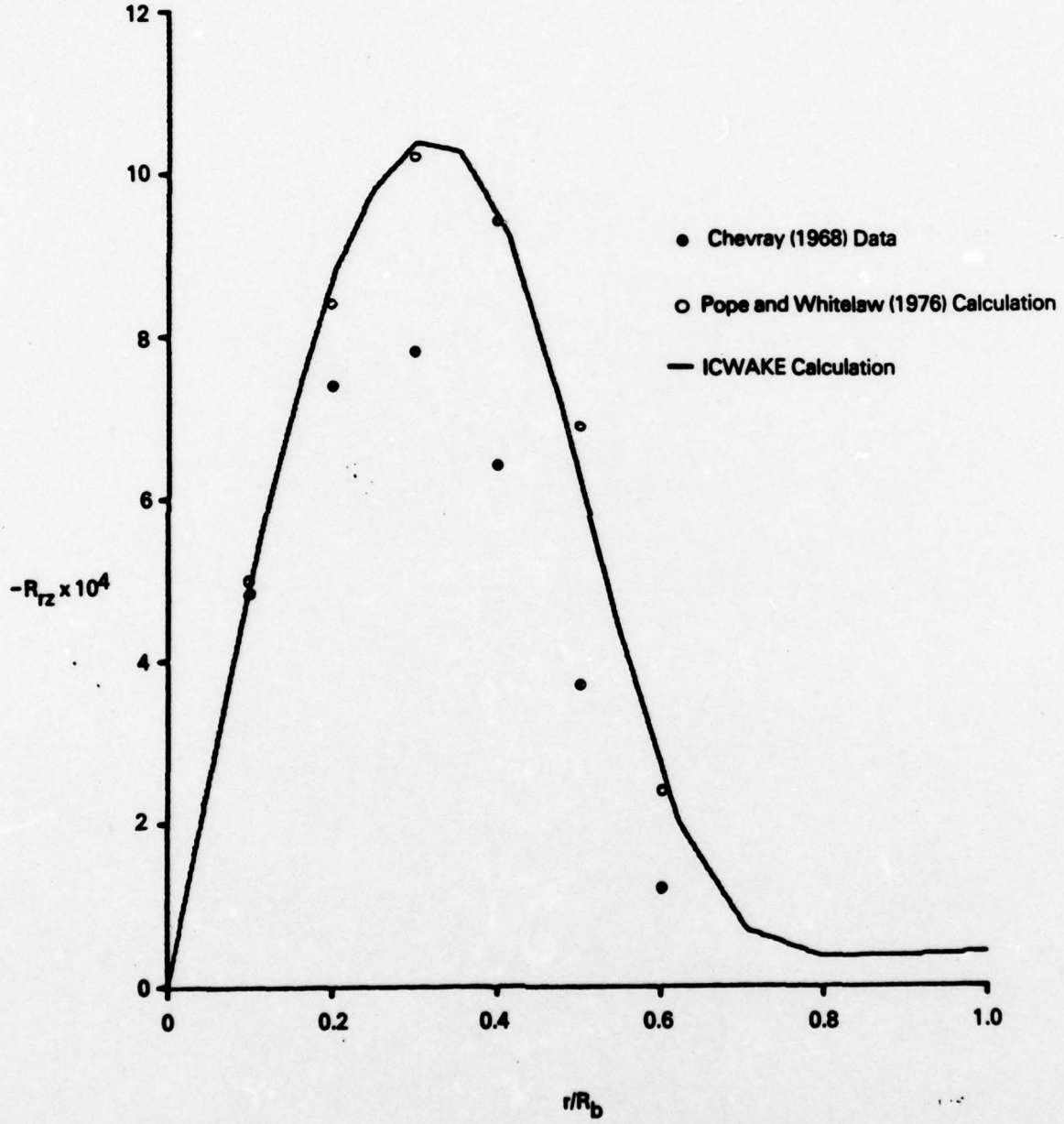

Figure 4-8b. Radial Shear Stress Across Prolate Spheroid Wake at $z/R_b = 12$.

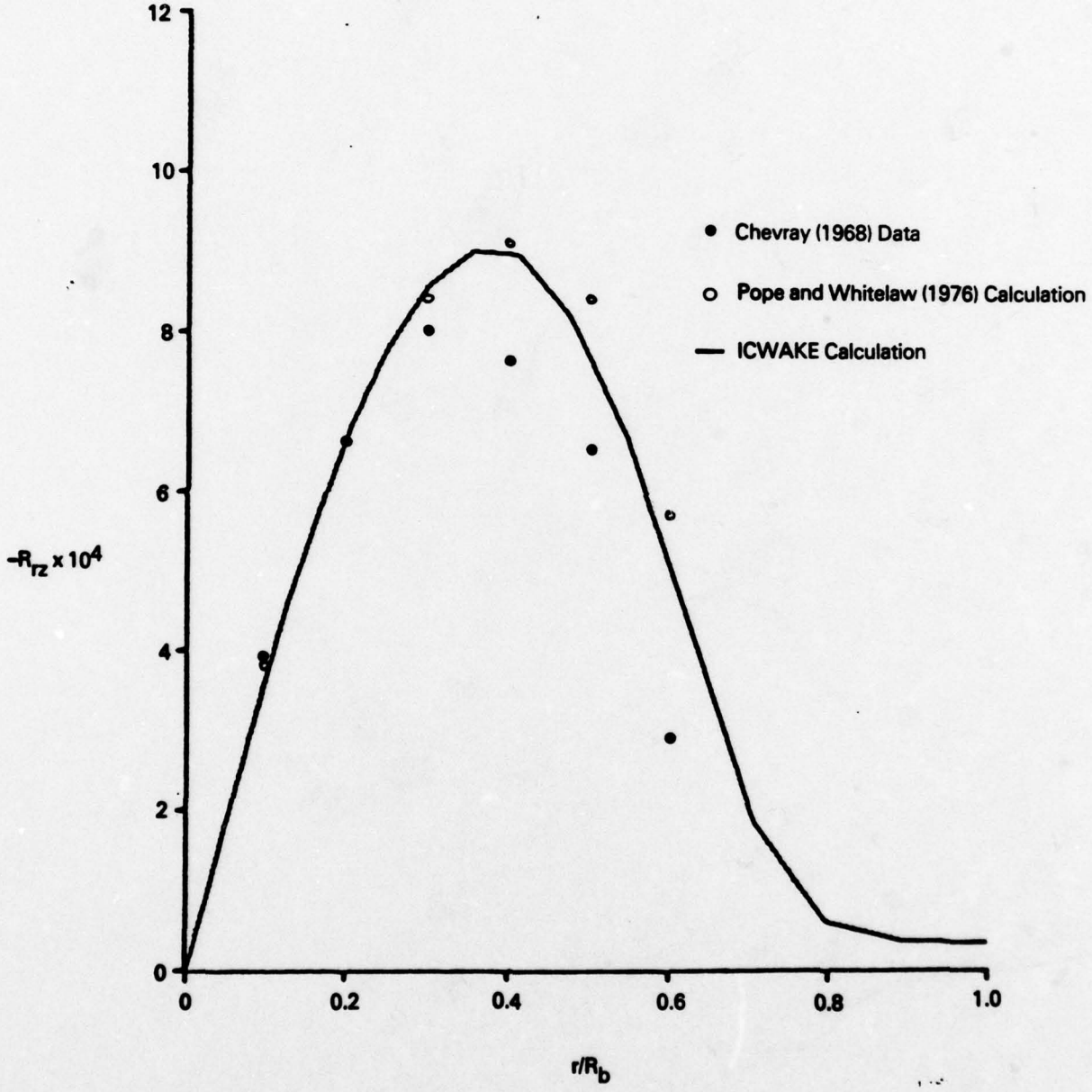

Figure 4-8c. Radial Shear Stress Across Prolate Spheroid Wake at $z/R_b = 18$.

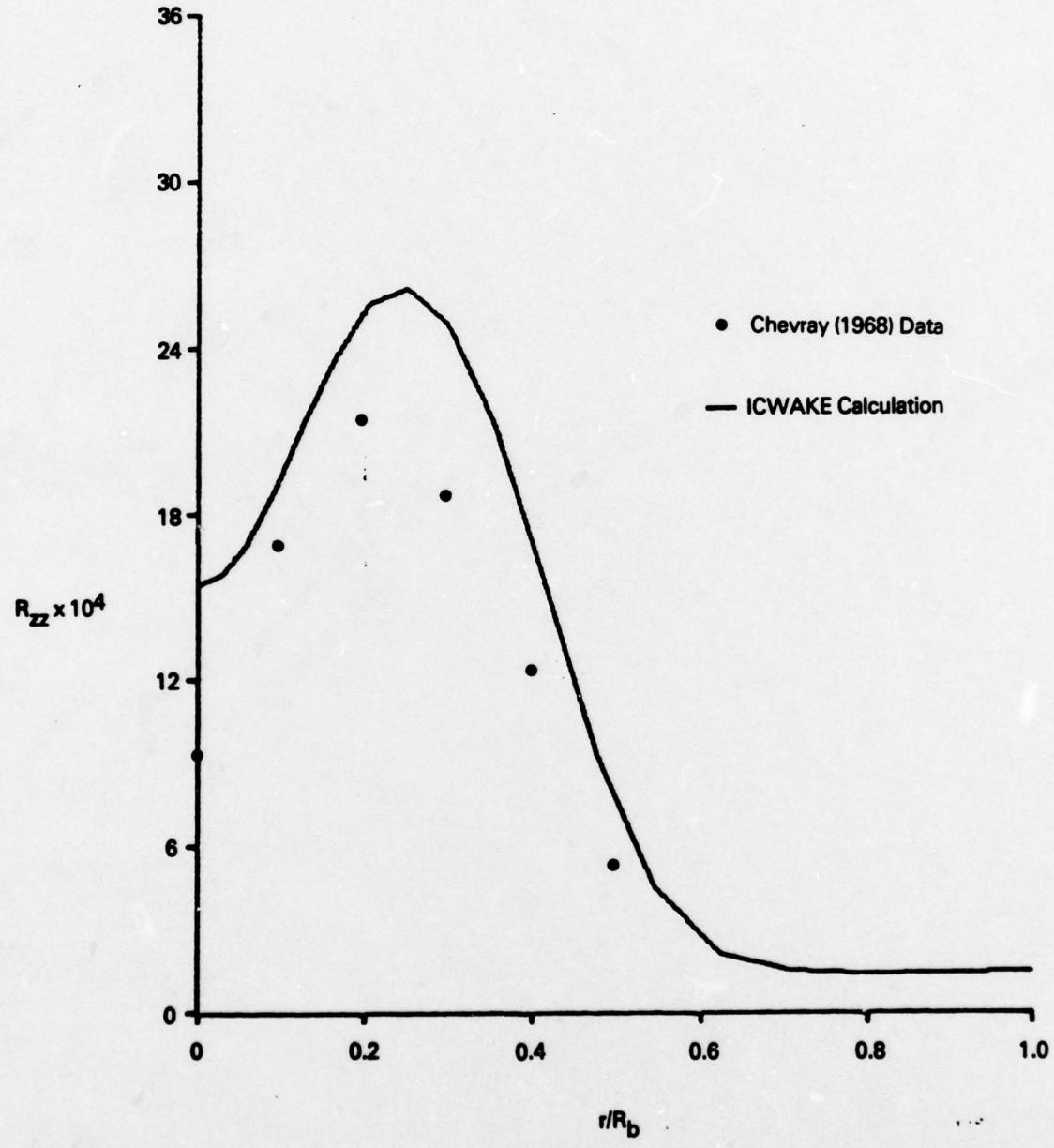

Figure 4-9a. Axial Turbulence Correlation Across Prolate Spheroid Wake at $z/R_b = 6$.

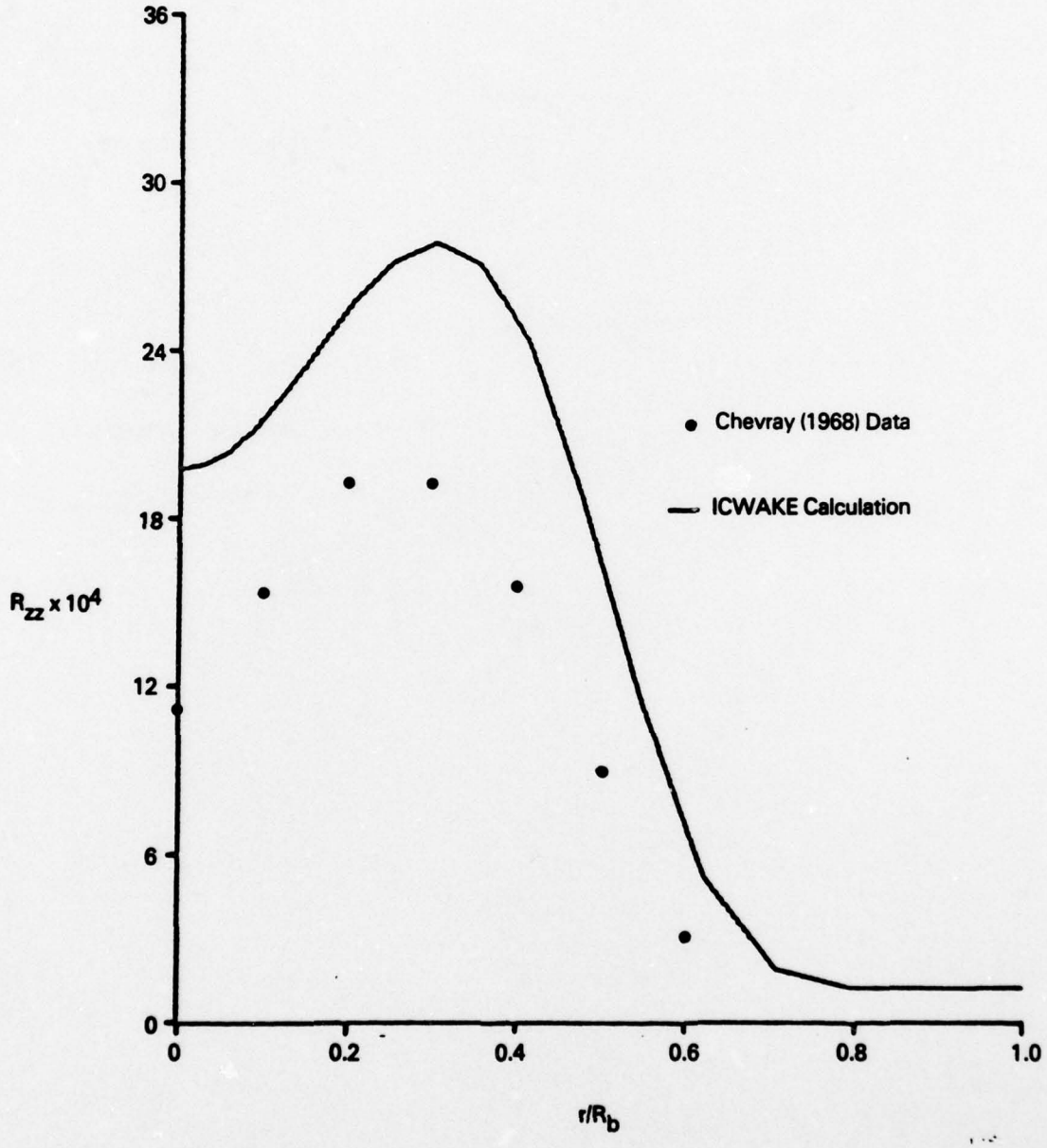

Figure 4-9b. Axial Turbulence Correlation Across Prolate Spheroid Wake at $z/R_b = 12$.

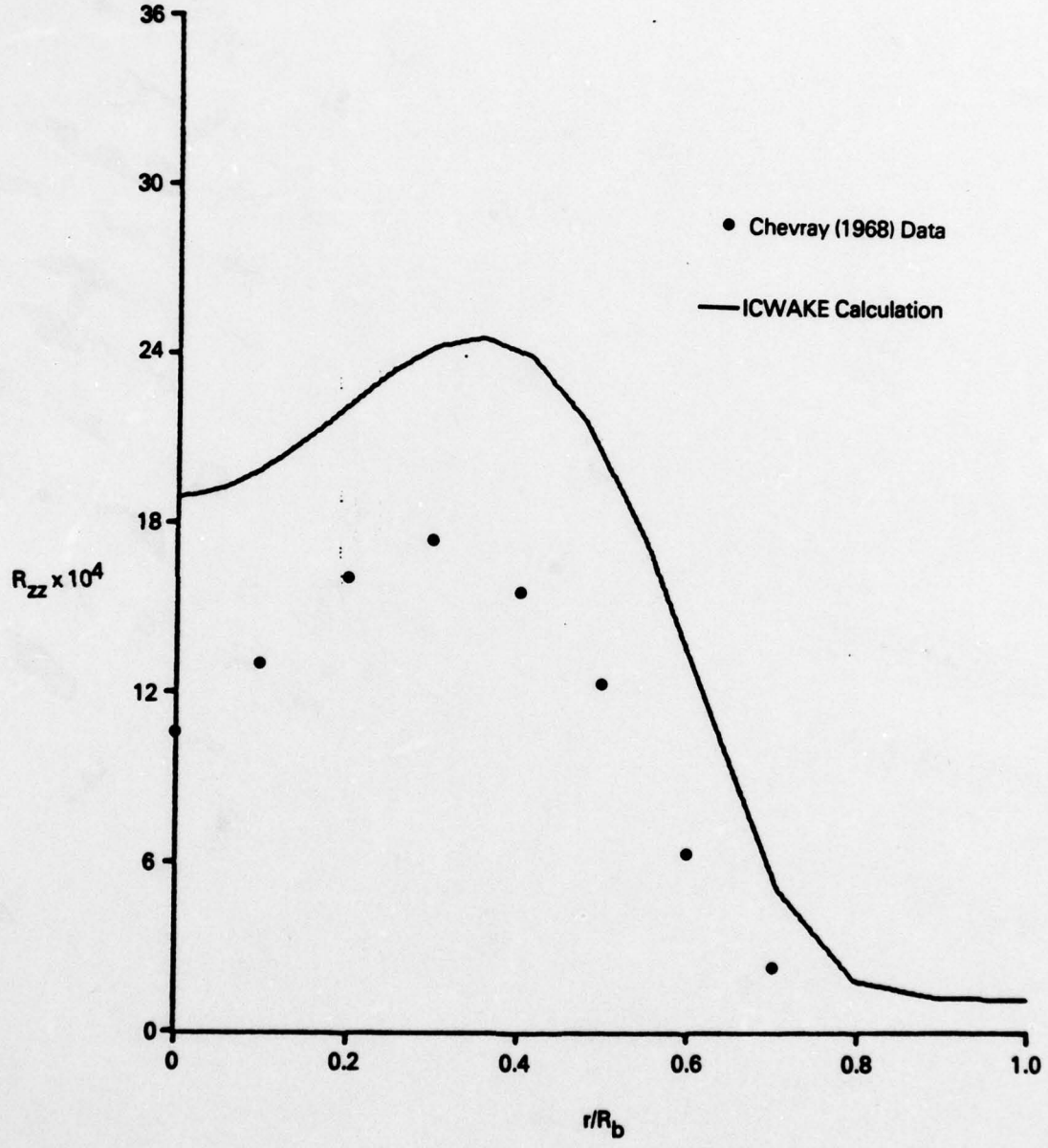

Figure 4-9c. Axial Turbulence Correlation Across Prolate Sheroid Wake at $z/R_b = 18$.

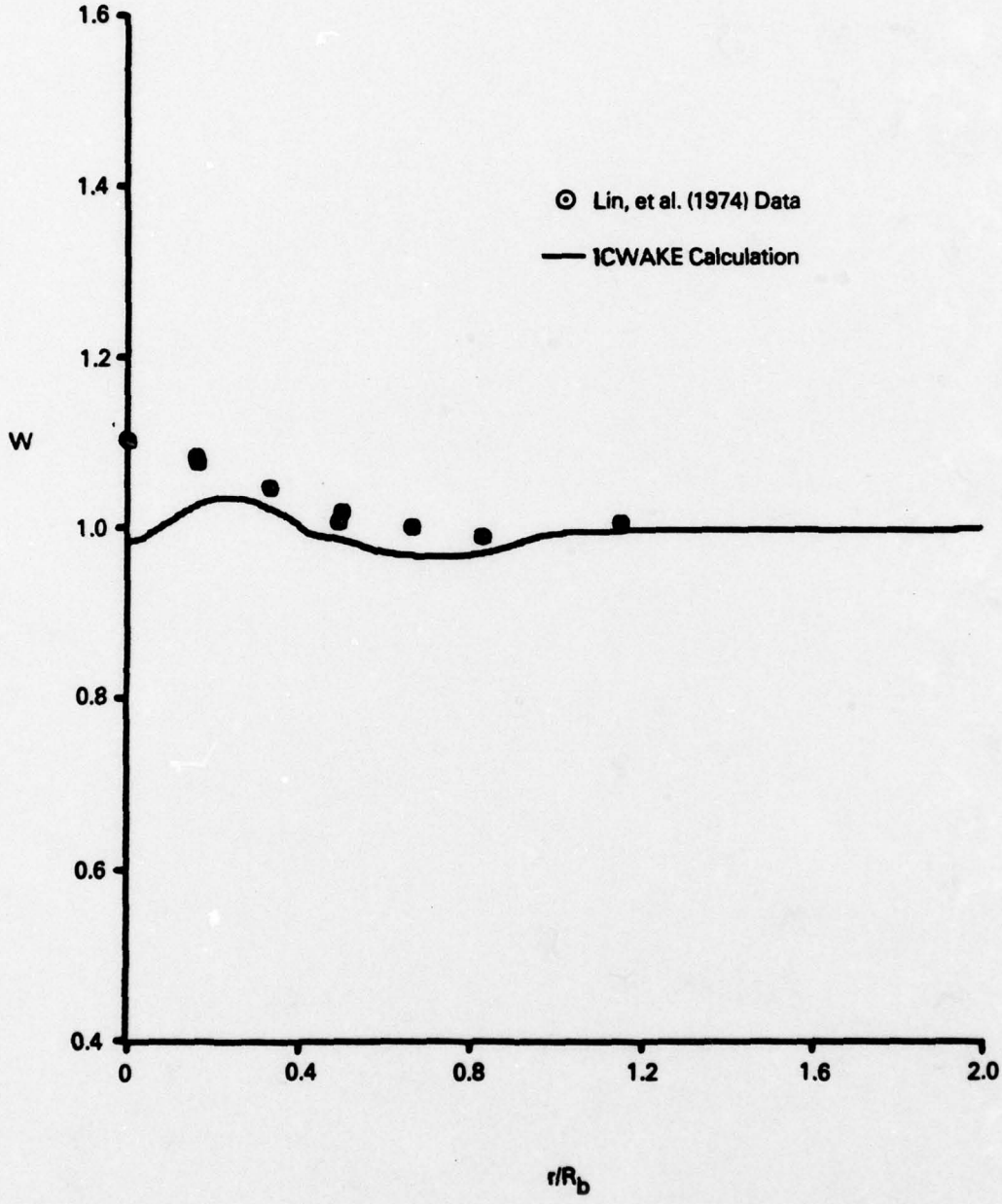

Figure 4-10. Axial Mean Velocity Component Across Self-Propelled Body Wake at $z/R_b = 12$.

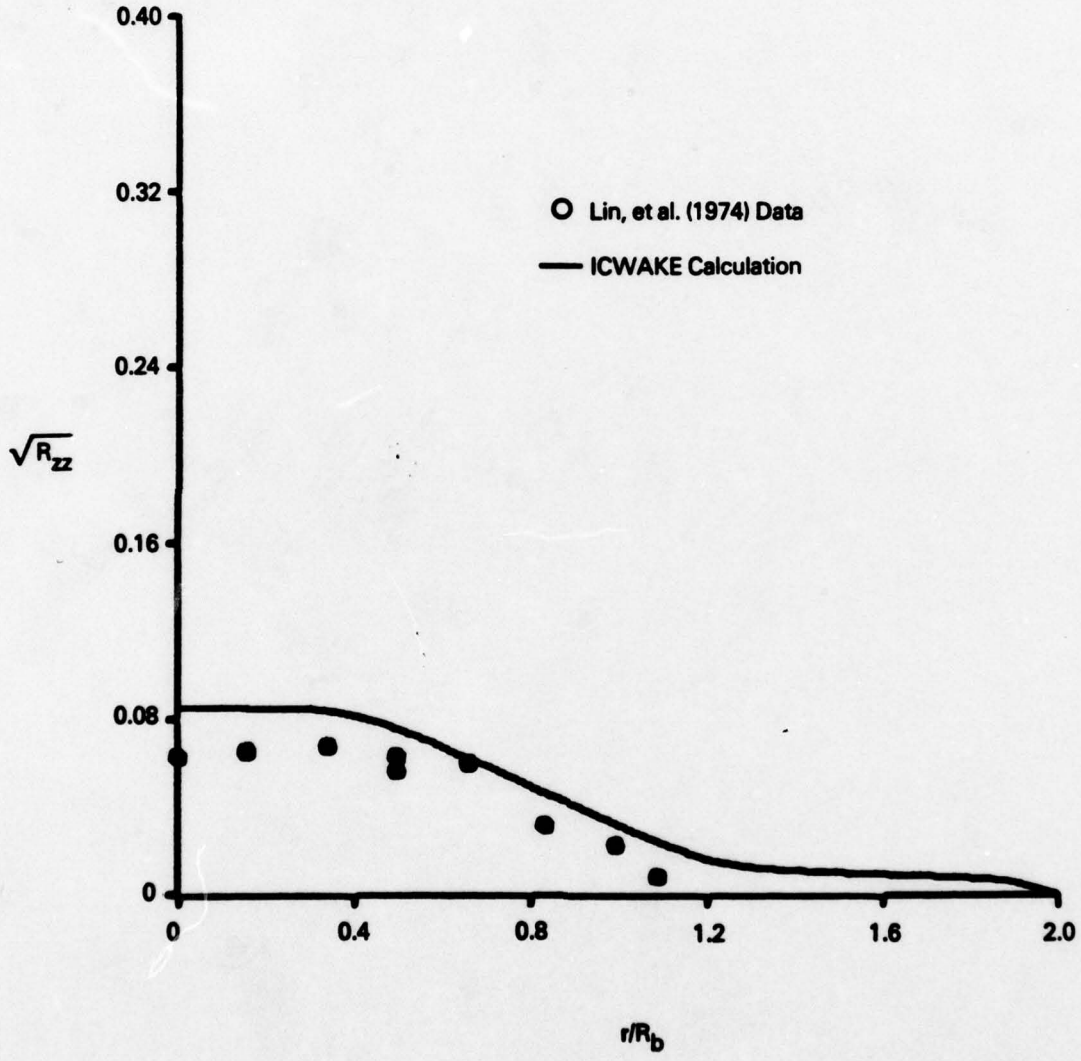

Figure 4-11 Axial Turbulence Intensity Across Self-Propelled Body Wake at $z/R_b = 12$.

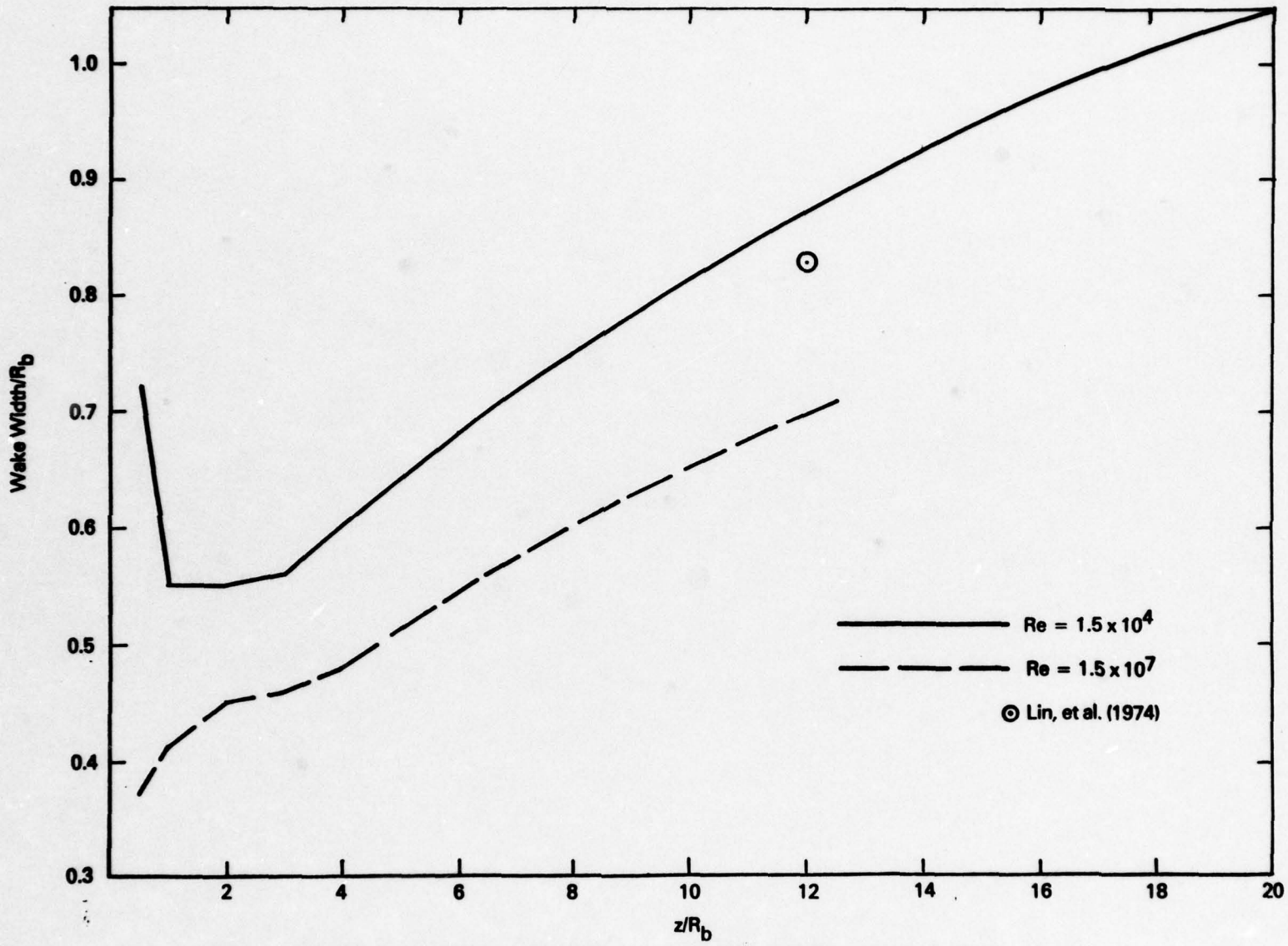

Figure 4-12. Calculated Self-Propelled Body Wake Width Versus Downstream Distance for Re = 1.5×10^4 and Re = 1.5×10^7. An Experimentally Obtained Value for Wake Width at $z/R_b = 12$, for Re = 1.5×10^4, is Also Presented.

Appendix A.1. Estimate of Turbulent Boundary Layer Entrainment

Even the most simple turbulent boundary analysis (see H. Schlichting's Boundary-Layer Theory, McGraw-Hill, 1968, p. 599) results in an expression for the boundary layer growth $d\delta/dz^*$ (where z^* is the streamwise distance from the leading edge),

$$\frac{d\delta}{dz^*} = \frac{36}{7} C_f(z^*) ,$$

with $C_f = \frac{\tau_w}{\frac{1}{2}\rho w_\infty^2}$ ($= C_f'$ in Schlichting's notation). For a non-flat surface we have that the rate of change of the boundary layer's volume flux, ψ_e, is

$$\frac{d\psi_e}{dA} = \frac{w_e d\delta dy}{dz^* dy} = w_e \frac{d\delta}{dz^*} ,$$

where dA is a differential surface area. Thus

$$\psi_e(z^*) = \frac{36}{7} \int_0^{z^*} w_e(\xi)\, C_f(\xi) \frac{dA}{d\xi}\, d\xi .$$

Now, let's assume that $w_e(\xi) = w_\infty(1 + \varepsilon f(\xi))$ $\varepsilon \ll 1$ and that $dA/d\xi = K_A(1 + \varepsilon g(\xi))$ (for example, on a flat plate or an aligned cylinder $\varepsilon \equiv 0$), then

$$\psi_e(z^*) = \frac{36}{7} w_e K_A \int_0^{z^*} C_f(\xi) d\xi$$

$$= \frac{36}{7} w_e A(z^*) \left\{ \frac{1}{z^*} \int_0^{z^*} C_f(\xi) d\xi \right\}$$

since $A(z^*) = K_A z^*$. Note that the factor in the brackets is the definition of the total friction drag acting over the length z^* (denoted C_F here and C_f in Schlichting, to distinguish it from our C_f or Schlichting's C_f'.

Therefore

$$\psi_e \doteq 5.15\, w_e(z^*)A(z^*)C_F(z^*)$$

Because of the crudeness of Schlichting's analysis, let's discount the accuracy of the constant 5.15 but still retain the dependence on w_e, A and C_F.

To test this hypothesis, we will use Patel's axisymmetric 6-to-1 ellipsoid data. For this data, $\psi_e(z^*)$ was determined from integrating his boundary-layer velocity profile data from the wall location to where the measured stagnation pressure $C_p = \left[(p-p_\infty) + \frac{1}{2}\rho w^2\right] / \frac{1}{2}\rho w_\infty^2$ is $(0.995)^2$ (i.e., the velocity ratio is 0.995 if the flow were on a flat plate). That is,

$$\frac{\psi_e(z^*)}{w_\infty} = \int_0^{z^*} 2\pi(r^* + y)\,\frac{w(y)}{w_\infty}\,dy$$

and where r^* is the body radius measured normal to the local surface.

To estimate $C_F(z^*)$ utilize Patel's survey station amidship (where the boundary-layer thickness is very small compared to the local wall radius) and

$$C_F = 2\,\frac{\theta(z^*)}{z^*}$$

where θ is the measured momentum thickness of the boundary layer,

$$\theta = \int_0^{y^*} \frac{w}{w_\infty}\left(1 - \frac{w}{w_\infty}\right)dy$$

In doing this for the survey station at z^*/L, $C_F = 4.50 \times 10^{-3}$, which according to Schlichting's Figure 21.2, which shows friction drag measured as a function of Reynolds number based on flat-plate length, gives a value of $w_\infty z^*/\nu = 1.2 \times 10^6$ which is 50 percent greater than the actual value of $w_\infty z^*/\nu$. This difference is presumably due to

Patel's boundary layer trip. To compute the value of C_F at other stations, use

$$(R_{z^*})_{effective} = 1.2 \times 10^6 \left(\frac{1.71 + z^*}{L}\right)$$

and then look up on the figure what $(C_F)_{F.P.}$ should be at that station.

With the preceeding description, the following table of values was computed for Patel's axisymmetric boundary layer.

Survey Station (z*/L)	Upstream Surface Area (ft^2)	ψ_e/w_∞ (ft^2)	$(C_F)_{F.P.}$ --	$\psi_e/w_\infty AC_F$ --
0.662	7.51	0.116	4.50×10^{-3}	3.43
0.80	9.11	0.153	4.35	3.86
0.85	9.58	0.158	4.31	3.83
0.90	9.98	0.181	4.28	4.24
0.93	10.16	0.204	4.25	4.72
0.96	10.32	0.205	4.23	4.50
0.99	10.75	0.206	4.22	4.55

The average of the values shown in the most right-hand column is 4.16 with a standard deviation of 11 percent of the average. To see how this value, 4.16, compares to flat-plate turbulent boundary-layer data, use Cole's "universal" turbulent boundary layer profile

$$\frac{w(y)}{u_\tau} = \frac{1}{\kappa} \ln \frac{y u_\tau}{\nu} + 5 + \frac{2\pi}{\kappa} \sin^2\left(\frac{\pi y}{2\delta}\right)$$

where

$\kappa = 0.41$ (Karman's constant)

$\pi = 0.55$ (Cole's pressure grad. parameter for a flat-plate B.L.)

$u_\tau = \tau_N/\rho$ (The "Friction Velocity")

Note: $C_f = 2(u_\tau/w_e)^2$. The quantity $\psi_e/w_e LC_F$ has been evaluated using this equation in a manner quite similar to that used for Patel's data. The results of this calculation are

C_f	Re_L	$\theta/\delta = \frac{1}{2}(\frac{LC_F}{\delta})$	$\psi_e/w_e\delta$	$\psi_e/LC_F w_e$
3.2×10^{-3}	1.5×10^6	0.106	0.793	3.73
2×10^{-3}	10^7	0.094	0.785	4.19

Again, a value of about 4 is obtained for the ratio $\psi_e/w_e AC_F$

$$\therefore \dot{\psi}_e(z^*) \doteq 4w_\infty \dot{A}(z^*)\left[C_F(z^*)\right]_{F.P.}$$

Appendix A.2. The Flow Field Induced by a Marine Propeller Immersed Within a Rotational and Nearly Inviscid Flow Field

In this appendix, an exact linearized solution for the nearly inviscid flow through a marine propeller is derived. This solution does rely upon certain assumptions in order to make the problem tractable. These assumptions are:

1. The net thrust of the propeller is small enough so that the contraction of the stream tubes passing through the propeller can be neglected.
2. The propeller has a large number of blades so that circumferential derivatives can be deleted from the equations of motion and so that the vortex sheets shed downstream from the blades can be approximated by a continuous vorticity distribution.
3. The fluid flow is inviscid everywhere except at the plane of the propeller where viscosity is needed in order to invoke the Kutta condition at the blade trailing edges so that a net thrust and torque act on the fluid. Also, viscosity has acted upstream of the propeller in order to create the rotational flow approaching the propeller.
4. The flow field is axially symmetric with no forebody present near the propeller plane.

A cylindrical polar coordinate system (z,r,θ) is chosen with its origin at the intersection of the axis and the propeller plane and with positive z measured downstream of the propeller; w,u,v are the fluid velocity components in the three coordinate directions; ξ,η,ζ are the components of the fluid vorticity vector along the coordinate directions. The inviscid, axially-symmetric equations of motion for an incompressible fluid are then;

(Continuity): $$\frac{\partial}{\partial z}(wr) + \frac{\partial}{\partial r}(ur) = 0 \quad ,$$

(Axial Momentum): $$w \frac{\partial w}{\partial z} + u \frac{\partial w}{\partial r} = - \frac{\partial p}{\partial z} \quad ,$$

(Radial Momentum): $$w \frac{\partial u}{\partial z} + u \frac{\partial u}{\partial r} - \frac{v^2}{r} = - \frac{\partial p}{\partial r} \quad ,$$

(Angular Momentum): $$w \frac{\partial v}{\partial z} + u \frac{\partial v}{\partial r} + \frac{uv}{r} = 0 \quad ,$$

(Streamwise Vorticity): $$\xi \equiv \frac{\partial v}{\partial r} + \frac{v}{r} \quad ,$$

(Radial Vorticity): $$\eta \equiv \frac{\partial v}{\partial z} \quad ,$$

(Circumferential Vorticity): $$\zeta \equiv \frac{\partial u}{\partial z} - \frac{\partial w}{\partial r} \quad .$$

In the above, all length scales (z and r) are made dimensionless by dividing by the propeller radius R and all velocities are made dimensionless by dividing by the freestream speed w_∞. The continuity equation is satisfied by introducing the perturbation stream function $\psi(z,r)$ defined by:

$$w(z,r) = w_o(r) + \frac{1}{r} \frac{\partial \psi}{\partial r}$$

$$u(z,r) = - \frac{1}{r} \frac{\partial \psi}{\partial z} \qquad \text{(A-1)}$$

where $w_o(r)$ is the axial velocity profile far upstream of the propeller. Substituting Equation (A1) into the circumferential vorticity equation results in

$$\frac{\partial^2}{\partial z^2} \left(\frac{\psi}{r}\right) + \frac{\partial}{\partial r} \left(\frac{1}{r} \frac{\partial \psi}{\partial r}\right) = -\zeta - \frac{dw_o}{dr} \qquad \text{(A-2)}$$

Cross-differentiating the axial and radial momentum equations in order to eliminate the pressure field results in

$$w \frac{\partial \zeta}{\partial z} + u \frac{\partial \zeta}{\partial r} - \frac{1}{r} \left(\frac{\partial v^2}{\partial z} + u\zeta\right) = 0 \quad , \qquad \text{(A-3)}$$

whereas the angular momentum equation can be rewritten as

$$w \frac{\partial \xi}{\partial z} + u \frac{\partial \xi}{\partial r} + \frac{\xi}{r} \frac{\partial (ur)}{\partial r} = -\eta \frac{\partial w}{\partial r} \doteq 0 \qquad \text{(A-4)}$$

($\eta \frac{\partial w}{\partial r}$ vanishes upstream and is near zero downstream of the propeller). If the propeller thrust is small we expect that everywhere in the fluid $w \sim 0(1)$ $u,v << 0(1)$. Thus, we can approximate ζ and ξ using Equations (A-3) and (A-4) as

$$\zeta(z,r) = \begin{cases} \zeta_o(r) & z < 0 \\ \zeta_o(r) + \zeta_1(r) & z > 0 \end{cases}$$

$$\xi(z,r) = \begin{cases} 0 & z < 0 \\ \xi_1(r) & z > 0 \end{cases} \qquad \text{(A-5)}$$

where ζ_o is the initial circumferential vorticity distribution ($\zeta_o = -\frac{dw_o}{dr}$) and $\zeta_1(r)$ and $\xi_1(r)$ are the changes caused to the circumferential and streamwise vorticity (the latter is related to the swirl velocity) by the propeller. Since the present solution is only intended to be applicable at and upstream of the propeller plane, the parallel flow approximation implicit in Equation (A-4) is not as restrictive as it might first seem. Since the upstream flow only changes because of the downstream vorticity field (i.e., Biot-Savart's law of the induced velocity from a vortex line) Equation (A-4) is tantamount to assuming the induced velocities upstream are nearly the same as they would be for a parallel flow. Strictly speaking, a parallel flow would require that the radial velocity be zero everywhere, whereas a finite radial velocity distribution is still calculable from the present analysis. If Equation (A-5) and (A-2) are now combined we arrive at

$$\frac{\partial^2}{\partial z^2} \left(\frac{\psi}{r}\right) + \frac{\partial}{\partial r} \left(\frac{1}{r} \frac{\partial \psi}{\partial r}\right) = -\zeta_1(r)\, H(z) \quad , \qquad \text{(A-6)}$$

where

$$H(z) = \begin{cases} 0 & z < 0 \\ 1 & z > 0 \end{cases} .$$

The perturbation streamfunction $\psi(z,r)$ can now be separated into the sum of two functions, one of which is independent of z and the other of which is an odd function of z. Far upstream this sum vanishes (i.e., there is no perturbation far upstream) and far downstream the two add up to represent the jet-like flow caused by the propeller. The axially independent portion of this perturbation streamfunction is related to the induced axial velocity at the propeller plane (which is one-half the axial velocity at $z = +\infty$ if the flow were always inviscid) through

$$\psi_1(r) = -\frac{1}{2}\int_r^\infty \Delta w_+(\rho)\rho d\rho \qquad \text{(A-7)}$$

where $\Delta w_+(\rho)$ is the far downstream axial velocity distribution for a completely inviscid flow.

The odd contribution to the perturbation streamfunction may be shown to be given by

$$\psi_2(z,r) = \mp \psi_1(r) \mp r\int_0^\infty f(\lambda)e^{\mp\lambda z}J_1(\lambda r)d\lambda \ , \ z \lessgtr 0 \ , \qquad \text{(A-8)}$$

with

$$f(\lambda) = -\frac{1}{2}\int_0^\infty \Delta w_+(\rho)J_o(\lambda\rho)\rho d\rho \ ,$$

from a separation-of-variables solution to the resulting partial differential equation; J_o and J_1 are Bessel functions of the first kind of order 0 and 1.

The <u>induced</u> velocity field upstream of the propeller can then be determined from the perturbation streamfunction if the (hypothetical) axial velocity profile Δw_+ can be specified. The upstream axial and radial velocities perturbations are:

$$\Delta w(z,r) = \frac{1}{2}\int_0^\infty \Delta w_+(\rho)\rho d\rho \int_0^\infty \lambda e^{\lambda z} J_o(\lambda r) J_o(\lambda\rho) d\lambda \quad ,$$

$$u(z,r) = -\frac{1}{2}\int_0^\infty \Delta w_+(\rho)\rho d\rho \int_0^\infty \lambda e^{\lambda z} J_o(\lambda r) J_1(\lambda\rho) d\lambda \quad . \tag{A-9}$$

With a considerable amount of work, these relations can be shown to be equal to

$$\Delta w(z,r) = \frac{|z|}{\pi}\int_0^\infty \Delta w_+(\rho)\, G_w(z,r;\rho)\rho d\rho$$

$$z < 0 \tag{A-10}$$

$$u(z,r) = -\frac{1}{2\pi r}\int_0^\infty \Delta w_+(\rho)\, G_u(z,r;\rho)\rho d\rho$$

where

$$G_w(z,r;\rho) = \frac{E(m)}{\left[z^2 + (r-\rho)^2\right]\sqrt{z^2 + (r+\rho)^2}}$$

$$G_u(z,r;\rho) = (r^2 + \rho^2 - z^2)G_u(z,r;\rho) + \frac{K(m)}{\sqrt{z^2 + (r+\rho)^2}}$$

and where $K(m)$ and $E(m)$ are complete elliptic integrals of the first and second kinds with modulus $m = 4r\rho/(z^2 + (r+\rho)^2)$. (See, for example, "Handbook of Mathematical Functions" by Abramowitz and Stegun.) At the propeller plane, $z = 0$, these simplify somewhat to

$$\Delta w(o,r) = \frac{1}{2}\Delta w_+(r) \quad ,$$

$$u(o,r) = -\frac{1}{\pi r}\int_0^\infty \Delta w(o,\rho)\left[\frac{E(m)}{r-\rho} + \frac{K(m)}{r+\rho}\right]\rho d\rho \quad , \tag{A-11}$$

$$m = 4r\rho/(r+\rho)^2 \quad .$$

In other words, the induced axial velocity at the plane of the propeller is one-half the (hypothetical) far downstream axial velocity and the induced radial velocity is directly related to the induced axial velocity at the propeller plane. Note also that nothing has as yet been said about the swirl velocity distribution $v(z,r)$. From Equation (A-5) along with the definition of the streamwise vorticity it follows

that

$$v(z,r) = v_+(r)\, H(z) \ . \qquad \text{(A-12)}$$

In other words, once generated, the swirl velocity profile is independent of z (again, subject to the approximation that the flow is always inviscid). There are no net induced velocities upstream of the propeller caused by the swirl velocity vortex lines.

Note, however, that the swirl velocity distribution is related to the axial velocity perturbation through the parameters which characterize the propeller and its blades. In fact, if these characteristics are specified, it is possible to utilize the present formulae to compute the axial, radial and swirl velocity fields as well as the total thrust and torque acting on the fluid by a procedure quite similar to that described by Schwartz and Bernstein (1975). They addressed the propeller flow field utilizing two-dimensional airfoil theory, and developed a computer code based on their analysis. As mentioned in the text, the above analysis is in some ways more complete than the previous work, and a modification or a rewrite of the Schwartz-Bernstein code was considered. It was concluded, however, that such an effort would result in only a slight improvement over the axial and swirl velocities currently computed. On the other hand, the existing code does not compute the radial velocity field at the plane of the propeller, but assumes it to be identically zero. A better estimate of this profile is available from Equation (A-11).

To illustrate the magnitude and shape of the radial velocity distribution an exact evaluation of Equation (A-11) is possible for certain choices of $\Delta w(o,r)$. For example, if $\Delta w(o,r) = \Delta w_{max}\sqrt{1 - r^2}$, the radial velocity distribution can be shown to be:

$$\frac{u(o,r)}{\Delta w_{max}} = \begin{cases} -\pi r/8 & , \quad 0 < r < 1 \\ -\dfrac{1}{6r^2}\, F\left(\dfrac{3}{2}, \dfrac{1}{2}; \dfrac{5}{2}; \dfrac{1}{r^2}\right) & , \quad r > 1 \end{cases}$$

where F is a hypergeometric function. Thus, the radial velocity is inward and varies linearly over the face of the propeller. At a large distance from the axis the radial velocity approaches zero like r^{-2}. It is noteworthy that the maximum radial inflow velocity, which occurs for r slightly greater than 1, is slightly in excess of $\pi/8$ times the change in the axial velocity which illustrates that the changes in either the radial or axial velocity are of the same order. A numerical calculation of the upstream induced velocities (from which the pressure field can be computed) has been obtained which verifies that the upstream influence is only appreciable for one propeller diameter (i.e., $|C_p| < 0.01$ for $z < -2$).

Appendix A.3. Derivation of Jump Equations Across Propeller Plane for Grabowski's Turbulence Equations

Assume that the axial flow speed, $W(z,r)$, and the radial flow speed, $U(z,r)$, are continuous functions across the propeller plane located at $z=0$ whereas the swirl flow component $V(z,r)$ goes from zero ahead of the propeller to $V(r)$ at $z = 0^+$. Now, assume that each of the turbulent velocity correlations on any streamline $R_{\theta\theta}$, R_{zz}, R_{rr}, $R_{\theta z}$, $R_{\theta r}$, and R_{zr} can experience a step change as the streamline passes through or near the propeller plane and similarly for the dissipation ε.

Consider now the P.D.E.'s for the seven turbulent quantities mentioned above which are shown on page 76 of the ICWAKE report. Note the left-hand-side (LHS) of these equations all involve the material derivative operator $U \frac{\partial}{\partial r} + W \frac{\partial}{\partial z}$. Using the continuity equation, this operator can be written (using the equation for R_{rr} as an example) as

$$\frac{\partial}{\partial r}(UR_{rr}) + \frac{\partial}{\partial z}(WR_{rr}) - \frac{UR_{rr}}{r} \quad .$$

If this operator is integrated from $z = -\Delta$ to $z = +\Delta$ we have

$$\frac{d}{dr} \int_{-\Delta}^{\Delta} UR_{rr}\,dz + \left[WR_{rr}\right] - \frac{1}{r} \int_{-\Delta}^{\Delta} UR_{rr}\,dz$$

where $\left[\ \right]$ denotes the jump in the enclosed quantity across the propeller plane. This, in turn, can be written as

$$r \frac{d}{dr}\left\{\frac{1}{r} \int_{-\Delta}^{\Delta} UR_{rr}\,dz\right\} + \left[WR_{rr}\right] \doteq$$

$$W(0,r)\left[R_{rr}\right] + r \frac{d}{dr}\left\{\frac{1}{r} U(0,r)(\bar{R}_{rr} + R_{rr})\Delta + \frac{1}{r} U(0,r)\bar{R}_{rr}\Delta\right\}$$

$$\doteq W(0,r)\left[R_{rr}\right] + r \frac{d}{dr}\left\{\frac{1}{r} U(0,r)\left[R_{rr}\right]\right\}\Delta \quad .$$

Thus, by allowing Δ to approach zero, the second term in the last relation will vanish whereas the first term remains finite. In this manner, the LHS of each of the seven P.D.E.'s when integrated across the propeller plane reduces to $W(0,r)$ times the jump in the quantity being operated on by $U \frac{\partial}{\partial r} + W \frac{\partial}{\partial z}$.

Now, consider the right-hand-sides of the seven P.D.E.'s when integrated across the propeller. The analysis for a typical production term is

$$\int_{-\Delta}^{\Delta} P_{rr}(z,r)dz = -2 \int_{-\Delta}^{\Delta} (R_{rr} \frac{\partial U}{\partial r} + R_{rz} \frac{\partial U}{\partial z} - R_{r\theta} \frac{V}{r})dz$$

$$= -2(\bar{R}_{rr} + \left[R_{rr} \right]) \frac{\partial U}{\partial r}\Big|_{z=+\Delta} \Delta + 2\bar{R}_{rr} \frac{\partial U}{\partial r}\Big|_{z=-\Delta} \Delta$$

$$- 2(\bar{R}_{rz} + \left[R_{rz} \right]) \frac{\partial U}{\partial z}\Big|_{z=+\Delta} \Delta + 2\bar{R}_{rr} \frac{\partial U}{\partial z}\Big|_{z=-\Delta} \Delta$$

$$+ 2(\bar{R}_{r\theta} + \left[R_{r\theta} \right]) \frac{\left[V(r) \right]}{r} \Delta$$

$$\doteq O(\Delta) \quad .$$

Here, even if $\partial U/\partial r$ is not continuous, <u>all</u> terms are still multiplied by Δ which can be made as small as necessary. On the other hand, the analysis for another typical production term is

$$\int_{-\Delta}^{\Delta} P_{\theta\theta}dz = -2 \int_{-\Delta}^{\Delta} \left\{ R_{r\theta} \frac{\partial V}{\partial r} + R_{\theta z} \frac{\partial V}{\partial z} + R_{\theta\theta} \frac{U}{r} \right\} dz$$

$$\doteq -2(\bar{R}_{r\theta} + \left[R_{r\theta}\right] \frac{dV}{dr} \Delta - 2(\bar{R}_{\theta z} + \left[R_{\theta z}\right])\left[V\right]$$

$$- 2 \frac{U(0,r)}{r} \left\{ (\bar{R}_{\theta\theta} + \left[R_{\theta\theta}\right])\Delta - \bar{R}_{\theta\theta}\Delta \right\}$$

$$= - 2 (\bar{R}_{\theta z} + \left[R_{\theta z}\right]) \left[V\right] + O(\Delta)$$

$$= -2 \left[R_{\theta z}\right]\left[V\right] \qquad \text{since } \bar{R}_{\theta z} = 0 \text{ for } z < 0 .$$

Results for other production terms, after analysis similar to the above is as follows:

$$\int_{-\Delta}^{\Delta} P_{zz} dz = 0$$

$$\int_{-\Delta}^{\Delta} P_{r\theta} dz = -(\bar{R}_{rz} + \left[R_{rz}\right])\left[V\right]$$

$$\int_{-\Delta}^{\Delta} P_{rz} dz = 0$$

$$\int_{-\Delta}^{\Delta} P_{\theta z} dz = -(\bar{R}_{zz} + \left[R_{zz}\right]\left[V\right]$$

$$\int_{-\Delta}^{\Delta} P_{\varepsilon} dz = -C_{\varepsilon 1} \frac{\bar{\varepsilon} + \left[\varepsilon\right]}{(\bar{k})^2 + \left[k^2\right]} (\bar{R}_{\theta z} + \left[R_{\theta z}\right]) \left[V\right] \doteq -C_{\varepsilon 1} \frac{\bar{\varepsilon} + \left[\varepsilon\right]}{(\bar{k})^2 + \left[k^2\right]} \left[R_{\theta z}\right]\left[V\right]$$

(since $\bar{R}_{\theta z} = 0$)

where $k^2 = \frac{1}{2}(R_{rr} + R_{\theta\theta} + R_{zz})$.

For the first part of the modeled pressure-strain correlations, we have

$$\int_{-\Delta}^{\Delta} \tilde{\phi}_{ij,1} dz \doteq 0 \quad \text{to order } \Delta ,$$

and for the second part of the modeled pressure-strain correlations, the following results hold:

$$\int_{-\Delta}^{\Delta} \tilde{\phi}_{rr,2} dz = \frac{2C_3}{3} \int_{-\Delta}^{\Delta} \frac{1}{2} P_{\theta\theta} dz + \frac{2C_5}{3} \int_{-\Delta}^{\Delta} \frac{1}{2} P_{\theta\theta} dz$$

$$\text{(since } P_k = \frac{1}{2}(P_{rr} + P_{\theta\theta} + P_{zz}) \text{ and } \int_{-\Delta}^{\Delta} D_{rr} dz = 0(\Delta))$$

$$= -2 \frac{C_3 + C_5}{3} \left[R_{\theta z}\right] \left[V\right] + 0(\Delta)$$

$$\int_{-\Delta}^{\Delta} \tilde{\phi}_{\theta\theta,2} dz = -\frac{2C_3}{3} \int_{-\Delta}^{\Delta} P_{\theta\theta} dz + \frac{2C_5}{3} \int_{-\Delta}^{\Delta} \frac{P_{\theta\theta}}{2} dz$$

$$= \frac{4C_3}{3} \left[R_{\theta z}\right] \left[V\right] - \frac{2C_5}{3} \left[R_{\theta z}\right] \left[V\right]$$

$$= \frac{4C_3 - 2C_5}{3} \left[R_{\theta z}\right] \left[V\right]$$

$$\int_{-\Delta}^{\Delta} \tilde{\phi}_{zz,2} dz = \frac{2C_3}{3} \int_{-\Delta}^{\Delta} \frac{P_{\theta\theta}}{2} dz + 2C_5 \left[R_{\theta z}\right] \left[V\right] + \frac{2C_5}{3} \int_{-\Delta}^{\Delta} \frac{P_{\theta\theta}}{2} dz$$

$$= -\frac{2C_3}{3} \left[R_{\theta z}\right] \left[V\right] + 2C_5 \left[R_{\theta z}\right] \left[V\right] - \frac{2C_5}{3} \left[R_{\theta z}\right] \left[V\right]$$

$$= \frac{2}{3} (2C_5 - C_3) \left[R_{\theta z}\right] \left[V\right]$$

$$\int_{-\Delta}^{\Delta} \tilde{\phi}_{r\theta,2} dz = C_3 (\bar{R}_{rz} + \left[R_{rz}\right]) \left[V\right]$$

$$\int_{-\Delta}^{\Delta} \tilde{\phi}_{rz,2}\,dz = C_5 \left[R_{r\theta}\right]\left[V\right]$$

$$\int_{-\Delta}^{\Delta} \tilde{\phi}_{\theta z,2}\,dz = C_3(\bar{R}_{zz} + \left[R_{zz}\right])\left[V\right] - C_4((\bar{k})^2 + \left[k^2\right])\left[V\right]$$

$$+ C_5(\bar{R}_{\theta\theta} + \left[R_{\theta\theta}\right])\left[V\right]$$

$$\doteq (C_3\bar{R}_{zz} - C_4(\bar{k})^2 + C_5\bar{R}_{\theta\theta})\left[V\right] .$$

Using the above results, ignoring $\left[R_{rr}\right]$, $\left[R_{\theta\theta}\right]$, $\left[R_{zz}\right]$, $\left[\varepsilon\right]$, $\left[R_{rz}\right]$ relative to $\bar{R}_{rr}$, $\bar{R}_{\theta\theta}$, $\bar{R}_{zz}$, $\bar{\varepsilon}$, $\bar{R}_{rz}$, and ignoring the diffusive terms (i.e., the $\int_{-\Delta}^{\Delta} Df_{rr}\,dz$ etc.), we have the following new forms for the seven turbulence equations after they are integrated across the propeller plane.

$$W\left[R_{rr}\right] = -\frac{2}{3}(C_3 + C_5)\left[R_{\theta z}\right]\left[V\right]$$

$$W\left[R_{\theta\theta}\right] = -2\left[R_{\theta z}\right]\left[V\right] + \frac{4C_3 - 2C_5}{3}\left[(R_{\theta z}\right]\left[V\right] = \frac{4C_3 - 2C_5 - 6}{3}\left[R_{\theta z}\right]\left[V\right]$$

$$W\left[R_{zz}\right] = \frac{2}{3}(2C_5 - C_3)\left[R_{\theta z}\right]\left[V\right]$$

$$W\left[R_{r\theta}\right] = -\bar{R}_{rz}\left[V\right] + C_3\bar{R}_{rz}\left[V\right] = (C_3 - 1)\bar{R}_{rz}\left[V\right]$$

$$W\left[R_{rz}\right] = C_5\left[R_{r\theta}\right]\left[V\right]$$

$$W\left[R_{\theta z}\right] = -\bar{R}_{zz}\left[V\right] + (C_3\bar{R}_{zz} - C_4(\bar{k})^2 + C_5\bar{R}_{\theta\theta})\left[V\right]$$

$$= \left\{(C_3 - \frac{C_4}{2} - 1)\bar{R}_{zz} + (C_5 - \frac{C_4}{2})\bar{R}_{\theta\theta} - \frac{C_4}{2}\bar{R}_{rr}\right\}\left[V\right]$$

$$= F(\tilde{r})\left[V\right], \quad \text{where } \tilde{r} = \frac{r}{r_p} \quad (r_p \text{ is the propeller radius}),$$

and lastly,

$$W\left[\varepsilon\right] = -C_{\varepsilon 1}\frac{\bar{\varepsilon}}{(\bar{k})^2}\left[R_{\theta z}\right]\left[V\right]$$

From the previous equations, and the constants given in Appendix B (p. 90), the following conditions, presented in Section 2 (p. 16), may be obtained.

$$\left[R_{r\theta}\right] = (C_3-1)\bar{R}_{rz}\frac{[V]}{W} = -0.236\,\bar{R}_{rz}\frac{[V]}{W}$$

$$\left[R_{rz}\right] = C_5(C_3-1)\bar{R}_{rz}\left(\frac{[V]}{W}\right)^2 = -0.026\,\bar{R}_{rz}\left(\frac{[V]}{W}\right)^2$$

$$\left[R_{\theta z}\right] = F(\tilde{r})\frac{[V]}{W}$$

$$\left[R_{rr}\right] = -\frac{2}{3}(C_3 + C_5)F(\tilde{r})\left(\frac{[V]}{W}\right)^2 = -0.582\,F(\tilde{r})\left(\frac{[V]}{W}\right)^2$$

$$\left[R_{\theta\theta}\right] = \frac{4C_3 - 2C_5 - 6}{3}F(\tilde{r})\left(\frac{[V]}{W}\right)^2 = -1.055\,F(\tilde{r})\left(\frac{[V]}{W}\right)^2$$

$$\left[R_{zz}\right] = \frac{2}{3}(2C_5 - C_3)F(\tilde{r})\left(\frac{[V]}{W}\right)^2 = -0.364\,F(\tilde{r})\left(\frac{[V]}{W}\right)^2$$

$$\left[\varepsilon\right] = -C_{1\varepsilon}\frac{\bar{\varepsilon}}{k^2}F(\tilde{r})\left(\frac{[V]}{W}\right)^2 = -1.44\frac{\bar{\varepsilon}}{(\bar{k})^2}F(\tilde{r})\left(\frac{[V]}{W}\right)^2$$

where $F(\tilde{r}) = -0.327\,\bar{R}_{zz} + 0.018\,\bar{R}_{\theta\theta} - 0.091\,\bar{R}_{rr}$.

Appendix B: Turbulence Model Equations For Axisymmetric, Incompressible Flow With Swirl

The turbulence model equations presented in this Appendix are based on the model of Hanjalic and Launder (1972) and its extension by Launder, Reece and Rodi (1975). The equations are presented in the general form

Advection = Production + Dissipation + Pressure-Strain (where applicable) + Diffusion

Dissipation Rate Equation

$$U \frac{\partial \varepsilon}{\partial r} + W \frac{\partial \varepsilon}{\partial z} = P_\varepsilon - C_{\varepsilon 2} \frac{\varepsilon^2}{k} + Df_\varepsilon$$

Turbulent Correlation Equations

$$U \frac{\partial R_{rr}}{\partial r} + W \frac{\partial R_{rr}}{\partial z} - 2 \frac{V}{r} R_{r\theta} = P_{rr} - \frac{2}{3} \varepsilon + \tilde{\phi}_{rr,1} + \tilde{\phi}_{rr,2} + Df_{rr}$$

$$U \frac{\partial R_{\theta\theta}}{\partial r} + W \frac{\partial R_{\theta\theta}}{\partial z} + 2 \frac{V}{r} R_{r\theta} = P_{\theta\theta} - \frac{2}{3} \varepsilon + \tilde{\phi}_{\theta\theta,1} + \tilde{\phi}_{\theta\theta,2} + Df_{\theta\theta}$$

$$U \frac{\partial R_{zz}}{\partial r} + W \frac{\partial R_{zz}}{\partial z} = P_{zz} - \frac{2}{3} \varepsilon + \tilde{\phi}_{zz,1} + \tilde{\phi}_{zz,2} + Df_{zz}$$

$$U \frac{\partial R_{r\theta}}{\partial r} + W \frac{\partial R_{r\theta}}{\partial z} + \frac{V}{r} \left(R_{rr} - R_{\theta\theta} \right) = P_{r\theta} + \tilde{\phi}_{r\theta,1} + \tilde{\phi}_{r\theta,2} + Df_{r\theta}$$

$$U \frac{\partial R_{rz}}{\partial r} + W \frac{\partial R_{rz}}{\partial z} - \frac{V}{r} R_{\theta z} = P_{rz} + \tilde{\phi}_{rz,1} + \tilde{\phi}_{rz,2} + Df_{rz}$$

$$U \frac{\partial R_{\theta z}}{\partial r} + W \frac{\partial R_{\theta z}}{\partial z} + \frac{V}{r} R_{rz} = P_{\theta z} + \tilde{\phi}_{\theta z,1} + \tilde{\phi}_{\theta z,2} + Df_{\theta z}$$

The production terms in the above equations are defined as

$$P_\varepsilon = - C_{\varepsilon 1} \frac{\varepsilon}{k} \left[R_{rr} \frac{\partial U}{\partial r} + R_{\theta\theta} \frac{U}{r} + R_{zz} \frac{\partial W}{\partial z} + R_{r\theta} \left(\frac{\partial V}{\partial r} - \frac{V}{r} \right) \right.$$

$$\left. + R_{rz} \left(\frac{\partial U}{\partial z} + \frac{\partial W}{\partial r} \right) + R_{\theta z} \frac{\partial V}{\partial z} \right]$$

$$P_{rr} = -2\left\{R_{rr}\frac{\partial U}{\partial r} + R_{rz}\frac{\partial U}{\partial z} - R_{r\theta}\frac{V}{r}\right\},$$

$$P_{\theta\theta} = -2\left\{R_{r\theta}\frac{\partial V}{\partial r} + R_{\theta z}\frac{\partial V}{\partial z} + R_{\theta\theta}\frac{U}{r}\right\},$$

$$P_{zz} = -2\left\{R_{zz}\frac{\partial W}{\partial z} + R_{rz}\frac{\partial W}{\partial r}\right\},$$

$$P_{r\theta} = -\left\{R_{rr}\frac{\partial V}{\partial r} - R_{\theta\theta}\frac{V}{r} + R_{r\theta}\left(\frac{\partial U}{\partial r} + \frac{U}{r}\right) + R_{rz}\frac{\partial V}{\partial z} + R_{\theta z}\frac{\partial U}{\partial z}\right\},$$

$$P_{rz} = -\left\{R_{rr}\frac{\partial W}{\partial r} + R_{zz}\frac{\partial U}{\partial z} + R_{rz}\left(\frac{\partial W}{\partial z} + \frac{\partial U}{\partial r}\right) - R_{\theta z}\frac{V}{r}\right\},$$

and $$P_{\theta z} = -\left\{R_{zz}\frac{\partial V}{\partial z} + R_{r\theta}\frac{\partial W}{\partial r} + R_{rz}\frac{\partial V}{\partial r} + R_{\theta z}\left(\frac{\partial W}{\partial z} + \frac{U}{r}\right)\right\}.$$

The first part of the modeled pressure-strain correlations was suggested by Rotta (1951):

$$\tilde{\phi}_{rr,1} = -C_1\frac{\varepsilon}{k}\left(R_{rr} - \frac{2}{3}k\right),$$

$$\tilde{\phi}_{\theta\theta,1} = -C_1\frac{\varepsilon}{k}\left(R_{\theta\theta} - \frac{2}{3}k\right),$$

$$\tilde{\phi}_{zz,1} = -C_1\frac{\varepsilon}{k}\left(R_{zz} - \frac{2}{3}k\right),$$

$$\tilde{\phi}_{r\theta,1} = -C_1\frac{\varepsilon}{k}R_{r\theta},$$

$$\tilde{\phi}_{rz,1} = -C_1\frac{\varepsilon}{k}R_{rz},$$

and $$\tilde{\phi}_{\theta z,1} = -C_1\frac{\varepsilon}{k}R_{\theta z}.$$

The second part of the modeled pressure-strain correlations is due to Launder, Reece and Rodi (1975):

$$\tilde{\phi}_{rr,2} = -C_3\left(P_{rr} - \frac{2}{3}P_k\right) - 2C_4 k\frac{\partial U}{\partial r} - C_5\left(D_{rr} - \frac{2}{3}P_k\right),$$

$$\tilde{\phi}_{\theta\theta,2} = - C_3\left(P_{\theta\theta} - \frac{2}{3} P_k\right) - 2C_4 k \frac{U}{r} - C_5\left(D_{\theta\theta} - \frac{2}{3} P_k\right) ,$$

$$\tilde{\phi}_{zz,2} = - C_3\left(P_{zz} - \frac{2}{3} P_k\right) - 2C_4 k \frac{\partial W}{\partial z} - C_5\left(D_{zz} - \frac{2}{3} P_k\right) ,$$

$$\tilde{\phi}_{r\theta,2} = - C_3 P_{r\theta} - C_4 k\left(\frac{\partial V}{\partial r} - \frac{V}{r}\right) - C_5 D_{r\theta} ,$$

$$\tilde{\phi}_{rz,2} = - C_3 P_{rz} - C_4 k\left(\frac{\partial W}{\partial r} + \frac{\partial U}{\partial z}\right) - C_5 D_{rz} ,$$

and $$\tilde{\phi}_{\theta z,2} = - C_3 P_{\theta z} - C_4 k \frac{\partial V}{\partial z} - C_5 D_{\theta z} ,$$

where P_k is the production rate of turbulent kinetic energy

$$P_k = \frac{1}{2}\left(P_{rr} + P_{\theta\theta} + P_{zz}\right) ,$$

and the D_{ij} terms are defined as follows:

$$D_{rr} = - 2 \left\{R_{rr} \frac{\partial U}{\partial r} + R_{r\theta} \frac{\partial V}{\partial r} + R_{rz} \frac{\partial W}{\partial r}\right\} ,$$

$$D_{\theta\theta} = - 2 \left\{R_{\theta\theta} \frac{U}{r} - R_{r\theta} \frac{V}{r}\right\} ,$$

$$D_{zz} = - 2 \left\{R_{zz} \frac{\partial W}{\partial z} + R_{rz} \frac{\partial U}{\partial z} + R_{\theta z} \frac{\partial V}{\partial z}\right\} ,$$

$$D_{r\theta} = - \left\{R_{\theta\theta} \frac{\partial V}{\partial r} - R_{rr} \frac{V}{r} + R_{r\theta}\left(\frac{\partial U}{\partial r} + \frac{U}{r}\right) + R_{\theta z} \frac{\partial W}{\partial r}\right\} ,$$

$$D_{rz} = - \left\{R_{rr} \frac{\partial U}{\partial z} + R_{zz} \frac{\partial W}{\partial r} + R_{r\theta} \frac{\partial V}{\partial z} + R_{rz}\left(\frac{\partial W}{\partial z} + \frac{\partial U}{\partial r}\right) + R_{\theta z} \frac{\partial V}{\partial r}\right\} ,$$

and $$D_{\theta z} = - \left\{R_{\theta\theta} \frac{\partial V}{\partial z} + R_{r\theta} \frac{\partial U}{\partial z} - R_{rz} \frac{V}{r} + R_{\theta z}\left(\frac{\partial W}{\partial z} + \frac{U}{r}\right)\right\} .$$

The expression for the diffusion of dissipation rate is based on the proposal of Hanjalic and Launder (1972):

$$Df_\varepsilon = \frac{C_\varepsilon}{r} \frac{\partial}{\partial r}\left[r \frac{k}{\varepsilon}\left(R_{rr} \frac{\partial \varepsilon}{\partial r} + R_{rz} \frac{\partial \varepsilon}{\partial z}\right)\right] + C_\varepsilon \frac{\partial}{\partial z}\left[\frac{k}{\varepsilon}\left(R_{rz} \frac{\partial \varepsilon}{\partial r} + R_{zz} \frac{\partial \varepsilon}{\partial z}\right)\right] .$$

When $n = 0$ the turbulent correlation diffusion terms below are based on the proposal of Daly and Harlow (1970); when $n = 1$, they are based on the proposal of Hanjalic and Launder (1972).

$$
\begin{aligned}
Df_{rr} = {} & (2n+1)\frac{C_{sn}}{r}\frac{\partial}{\partial r}\left\{ r\frac{k}{\varepsilon}\left[R_{rr}\frac{\partial R_{rr}}{\partial r} - 2\frac{R_{r\theta}^2}{r} + R_{rz}\frac{\partial R_{rr}}{\partial z}\right]\right\} \\
& - 2\frac{C_{sn}}{r}\frac{k}{\varepsilon}\left\{(n+1)\left[R_{r\theta}\frac{\partial R_{r\theta}}{\partial r} + R_{\theta\theta}\frac{\left(R_{rr} - R_{\theta\theta}\right)}{r} + R_{\theta z}\frac{\partial R_{\theta z}}{\partial z}\right]\right. \\
& \left. + n\left[R_{rr}\frac{\partial R_{\theta\theta}}{\partial r} + 2\frac{R_{r\theta}^2}{r} + R_{rz}\frac{\partial R_{\theta\theta}}{\partial z}\right]\right\} \\
& + C_{sn}\frac{\partial}{\partial z}\left\{\frac{k}{\varepsilon}\left[R_{rz}\frac{\partial R_{rr}}{\partial r} - 2\frac{R_{r\theta}R_{\theta z}}{r} + R_{zz}\frac{\partial R_{rr}}{\partial z}\right.\right. \\
& \left.\left. + 2n\left(R_{rr}\frac{\partial R_{rz}}{\partial r} - \frac{R_{r\theta}R_{\theta z}}{r} + R_{rz}\frac{\partial R_{rz}}{\partial z}\right)\right]\right\} ,
\end{aligned}
$$

$$
\begin{aligned}
Df_{\theta\theta} = {} & \frac{C_{sn}}{r}\frac{\partial}{\partial r}\left\{ r\frac{k}{\varepsilon}\left[R_{rr}\frac{\partial R_{\theta\theta}}{\partial r} + 2\frac{R_{r\theta}^2}{r} + R_{rz}\frac{\partial R_{\theta\theta}}{\partial z}\right.\right. \\
& \left.\left. + 2n\left(R_{r\theta}\frac{\partial R_{r\theta}}{\partial r} + R_{\theta\theta}\frac{\left(R_{rr} - R_{\theta\theta}\right)}{r} + R_{\theta z}\frac{\partial R_{r\theta}}{\partial z}\right)\right]\right\} \\
& + 2\frac{C_{sn}}{r}\frac{k}{\varepsilon}\left\{(n+1)\left[R_{r\theta}\frac{\partial R_{r\theta}}{\partial r} + R_{\theta\theta}\frac{\left(R_{rr} - R_{\theta\theta}\right)}{r} + R_{\theta z}\frac{\partial R_{r\theta}}{\partial z}\right]\right. \\
& \left. + n\left[R_{rr}\frac{\partial R_{\theta\theta}}{\partial r} + 2\frac{R_{r\theta}^2}{r} + R_{rz}\frac{\partial R_{\theta\theta}}{\partial z}\right]\right\} \\
& + C_{sn}\frac{\partial}{\partial z}\left\{\frac{k}{\varepsilon}\left[R_{rz}\frac{\partial R_{\theta\theta}}{\partial r} + 2\frac{R_{\theta z}R_{r\theta}}{r} + R_{zz}\frac{\partial R_{\theta\theta}}{\partial z}\right.\right. \\
& \left.\left. + 2n\left(R_{r\theta}\frac{\partial R_{\theta z}}{\partial r} + \frac{R_{\theta\theta}R_{rz}}{r} + R_{\theta z}\frac{\partial R_{\theta z}}{\partial z}\right)\right]\right\} ,
\end{aligned}
$$

$$Df_{zz} = \frac{C_{sn}}{r}\frac{\partial}{\partial r}\left\{r\frac{k}{\varepsilon}\left[R_{rr}\frac{\partial R_{zz}}{\partial r} + R_{rz}\frac{\partial R_{zz}}{\partial z} + 2n\left(R_{rz}\frac{\partial R_{rz}}{\partial r} - \frac{R_{\theta z}^2}{r} + R_{zz}\frac{\partial R_{rz}}{\partial z}\right)\right]\right\} + (2n+1)\,C_{sn}\frac{\partial}{\partial z}\left\{\frac{k}{\varepsilon}\left(R_{rz}\frac{\partial R_{zz}}{\partial r} + R_{zz}\frac{\partial R_{zz}}{\partial z}\right)\right\} ,$$

$$Df_{r\theta} = \frac{C_{sn}}{r}\frac{\partial}{\partial r}\left\{r\frac{k}{\varepsilon}\left[(n+1)\left(R_{rr}\frac{\partial R_{r\theta}}{\partial r} + R_{r\theta}\frac{(R_{rr}-R_{\theta\theta})}{r} + R_{rz}\frac{\partial R_{r\theta}}{\partial z}\right) + n\left(R_{r\theta}\frac{\partial R_{rr}}{\partial r} - 2\frac{R_{\theta\theta}R_{r\theta}}{r} + R_{\theta z}\frac{\partial R_{rr}}{\partial z}\right)\right]\right\} + \frac{C_{sn}}{r}\frac{k}{\varepsilon}\left\{R_{r\theta}\frac{\partial R_{rr}}{\partial r} - 2\frac{R_{\theta\theta}R_{r\theta}}{r} + R_{\theta z}\frac{\partial R_{rr}}{\partial z} - (2n+1)\left[R_{r\theta}\frac{\partial R_{\theta\theta}}{\partial r} + 2\frac{R_{\theta\theta}R_{r\theta}}{r} + R_{\theta z}\frac{\partial R_{\theta\theta}}{\partial z}\right] + 2n\left[R_{rr}\frac{R_{r\theta}}{\partial r} + R_{r\theta}\frac{\left(R_{rr}-R_{\theta\theta}\right)}{r} + R_{rz}\frac{\partial R_{r\theta}}{\partial z}\right]\right\} + C_{sn}\frac{\partial}{\partial z}\left\{\frac{k}{\varepsilon}\left[R_{rz}\frac{\partial R_{r\theta}}{\partial r} + R_{\theta z}\frac{\left(R_{rr}-R_{\theta\theta}\right)}{r} + R_{zz}\frac{\partial R_{r\theta}}{\partial z} + n\left(R_{rr}\frac{\partial R_{\theta z}}{\partial r} + \frac{R_{r\theta}R_{rz}}{r} + R_{rz}\frac{\partial R_{\theta z}}{\partial z} + R_{r\theta}\frac{\partial R_{rz}}{\partial r} + R_{\theta z}\frac{\partial R_{rz}}{\partial z} - \frac{R_{\theta\theta}R_{\theta z}}{r}\right)\right]\right\} ,$$

$$Df_{rz} = \frac{C_{sn}}{r}\frac{\partial}{\partial r}\left\{r\frac{k}{\varepsilon}\left[(n+1)\left(R_{rr}\frac{\partial R_{rz}}{\partial r} - \frac{R_{\theta z}R_{r\theta}}{r} + R_{rz}\frac{\partial R_{rz}}{\partial z}\right) + n\left(R_{rz}\frac{\partial R_{rr}}{\partial r} - 2\frac{R_{r\theta}R_{\theta z}}{r} + R_{zz}\frac{\partial R_{rr}}{\partial z}\right)\right]\right\}$$

$$- \frac{C_{sn}}{r} \frac{k}{\varepsilon} \left\{ (n+1) \left(R_{r\theta} \frac{\partial R_{\theta z}}{\partial r} + \frac{R_{\theta\theta} R_{rz}}{r} + R_{\theta z} \frac{\partial R_{\theta z}}{\partial z} \right) \right.$$

$$\left. + n \left(R_{rz} \frac{\partial R_{\theta\theta}}{\partial r} + 2 \frac{R_{\theta z} R_{r\theta}}{r} + R_{zz} \frac{\partial R_{\theta\theta}}{\partial z} \right) \right\}$$

$$+ C_{sn} \frac{\partial}{\partial z} \left\{ \frac{k}{\varepsilon} \left[(n+1) \left(R_{rz} \frac{\partial R_{rz}}{\partial r} - \frac{R_{\theta z}^2}{r} + R_{zz} \frac{\partial R_{rz}}{\partial z} \right) \right. \right.$$

$$\left. \left. + n \left(R_{rr} \frac{\partial R_{zz}}{\partial r} + R_{rz} \frac{\partial R_{zz}}{\partial z} \right) \right] \right\} ,$$

$$Df_{\theta z} = \frac{C_{sn}}{r} \frac{\partial}{\partial r} \left\{ r \frac{k}{\varepsilon} \left[R_{rr} \frac{\partial R_{\theta z}}{\partial r} + \frac{R_{r\theta} R_{rz}}{r} + R_{rz} \frac{\partial R_{\theta z}}{\partial z} \right. \right.$$

$$+ n \left(R_{rz} \frac{\partial R_{r\theta}}{\partial r} + R_{\theta z} \frac{\left(R_{rr} - R_{\theta\theta} \right)}{r} + R_{zz} \frac{\partial R_{r\theta}}{\partial z} \right.$$

$$\left. \left. \left. + R_{r\theta} \frac{\partial R_{rz}}{\partial r} - \frac{R_{\theta\theta} R_{\theta z}}{r} + R_{\theta z} \frac{\partial R_{rz}}{\partial z} \right) \right] \right\}$$

$$+ \frac{C_{sn}}{r} \frac{k}{\varepsilon} \left\{ R_{r\theta} \frac{\partial R_{rz}}{\partial r} - \frac{R_{\theta\theta} R_{\theta z}}{r} + R_{\theta z} \frac{\partial R_{rz}}{\partial z} \right.$$

$$+ n \left[R_{rz} \frac{\partial R_{r\theta}}{\partial r} + R_{\theta z} \frac{\left(R_{rr} - R_{\theta\theta} \right)}{r} + R_{zz} \frac{\partial R_{r\theta}}{\partial z} + R_{rr} \frac{\partial R_{\theta z}}{\partial r} \right.$$

$$\left. \left. + \frac{R_{r\theta} R_{rz}}{r} + R_{rz} \frac{\partial R_{\theta z}}{\partial z} \right] \right\}$$

$$+ C_{sn} \frac{\partial}{\partial z} \left\{ \frac{k}{\varepsilon} \left[(n+1) \left(R_{rz} \frac{\partial R_{\theta z}}{\partial r} + \frac{R_{\theta z} R_{rz}}{r} + R_{zz} \frac{\partial R_{\theta z}}{\partial z} \right) \right. \right.$$

$$\left. \left. + n \left(R_{r\theta} \frac{\partial R_{zz}}{\partial r} + R_{\theta z} \frac{\partial R_{zz}}{\partial z} \right) \right] \right\} .$$

There are six model constants which must be specified.

Following Hanjalic and Launder, we let

$$C_\varepsilon = 0.15 ,$$

$$C_{\varepsilon 1} = 1.44 ,$$

and $$C_{\varepsilon 2} = 1.90 ,$$

and following Launder, Reece and Rodi, we let

$$C_1 = 1.5 ,$$

$$C_2 = 0.4 ,$$

and $$C_{sn} = \begin{cases} C_{s0} = 0.25 & \text{when } n = 0 \\ C_{s1} = 0.11 & \text{when } n = 1 . \end{cases}$$

The constants C_3 , C_4 and C_5 are defined as

$$C_3 \equiv (C_2 + 8)/11 ,$$

$$C_4 \equiv (30C_2 - 2)/55 ,$$

and $$C_5 \equiv (8C_2 - 2)/11 .$$

In order to simplify this rather lengthy system of equations, we assume that in the turbulent diffusion terms, axial derivatives of the various turbulent quantities may be neglected compared to their radial derivatives. We emphasize that this assumption is applied only to the turbulent diffusion terms.

The simplified turbulent diffusion terms are as follows:

$$Df_\varepsilon = \frac{C_\varepsilon}{r} \frac{\partial}{\partial r} \left[r \frac{k}{\varepsilon} R_{rr} \frac{\partial \varepsilon}{\partial r} \right] ,$$

$$Df_{rr} = (2n + 1)\frac{C_{sn}}{r}\frac{\partial}{\partial r}\left\{r\frac{k}{\varepsilon}\left[R_{rr}\frac{\partial}{\partial r}R_{rr} - 2\frac{R_{r\theta}^2}{r}\right]\right\}$$

$$- 2\frac{C_{sn}}{r}\frac{k}{\varepsilon}\left\{(n + 1)\left[R_{r\theta}\frac{\partial R_{r\theta}}{\partial r} + R_{\theta\theta}\frac{\left(R_{rr} - R_{\theta\theta}\right)}{r}\right] + n\left[R_{rr}\frac{\partial R_{\theta\theta}}{\partial r} + 2\frac{R_{r\theta}^2}{r}\right]\right\} ,$$

$$Df_{\theta\theta} = \frac{C_{sn}}{r}\frac{\partial}{\partial r}\left\{r\frac{k}{\varepsilon}\left[R_{rr}\frac{\partial R_{\theta\theta}}{\partial r} + 2\frac{R_{r\theta}^2}{r} + 2n\left(R_{r\theta}\frac{\partial R_{r\theta}}{\partial r} + R_{\theta\theta}\frac{\left(R_{rr} - R_{\theta\theta}\right)}{r}\right)\right]\right\}$$

$$+ 2\frac{C_{sn}}{r}\frac{k}{\varepsilon}\left\{(n + 1)\left[R_{r\theta}\frac{\partial R_{r\theta}}{\partial r} + R_{\theta\theta}\frac{\left(R_{rr} - R_{\theta\theta}\right)}{r}\right] + n\left[R_{rr}\frac{\partial R_{\theta\theta}}{\partial r} + \frac{2R_{r\theta}^2}{r}\right]\right\} ,$$

$$Df_{zz} = \frac{C_{sn}}{r}\frac{\partial}{\partial r}\left\{r\frac{k}{\varepsilon}\left[R_{rr}\frac{\partial R_{zz}}{\partial r} + 2n\left(R_{rz}\frac{\partial R_{rz}}{\partial r} - \frac{R_{\theta z}^2}{r}\right)\right]\right\} ,$$

$$Df_{r\theta} = \frac{C_{sn}}{r}\frac{\partial}{\partial r}\left\{r\frac{k}{\varepsilon}\left[(n + 1)\left(R_{rr}\frac{\partial R_{r\theta}}{\partial r} + R_{r\theta}\frac{\left(R_{rr} - R_{\theta\theta}\right)}{r}\right)\right.\right.$$

$$\left.\left. + n\left(R_{r\theta}\frac{\partial R_{rr}}{\partial r} - 2\frac{R_{\theta\theta}R_{r\theta}}{r}\right)\right]\right\}$$

$$+ \frac{C_{sn}}{r}\frac{k}{\varepsilon}\left\{R_{r\theta}\frac{\partial R_{rr}}{\partial r} - 4(n + 1)\frac{R_{\theta\theta}R_{r\theta}}{r} - (2n + 1)R_{r\theta}\frac{\partial R_{\theta\theta}}{\partial r}\right.$$

$$\left. + 2n\left[R_{rr}\frac{\partial R_{r\theta}}{\partial r} + R_{r\theta}\frac{\left(R_{rr} - R_{\theta\theta}\right)}{r}\right]\right\} ,$$

$$Df_{rz} = \frac{C_{sn}}{r}\frac{\partial}{\partial r}\left\{r\frac{k}{\varepsilon}\left[(n + 1)R_{rr}\frac{\partial R_{rz}}{\partial r} + nR_{rz}\frac{\partial R_{rr}}{\partial r} - (3n + 1)\frac{R_{\theta z}R_{r\theta}}{r}\right]\right.$$

$$\left. - \frac{C_{sn}}{r}\frac{k}{\varepsilon}\left\{(n + 1)\left(R_{r\theta}\frac{\partial R_{\theta z}}{\partial r} + \frac{R_{\theta\theta}R_{rz}}{r}\right) + n\left(R_{rz}\frac{\partial R_{\theta\theta}}{\partial r} + 2\frac{R_{r\theta}R_{\theta z}}{r}\right)\right\} ,\right.$$

$$Df_{\theta z} = \frac{C_{sn}}{r}\frac{\partial}{\partial r}\left\{ r\,\frac{k}{\varepsilon}\left[R_{rr}\frac{\partial R_{\theta z}}{\partial r} + \frac{R_{r\theta}R_{rz}}{r} + n\left(R_{rz}\frac{\partial R_{r\theta}}{\partial r} + R_{\theta z}\frac{\left(R_{rr} - R_{\theta\theta}\right)}{r} \right.\right.\right.$$

$$\left.\left.\left. + R_{r\theta}\frac{\partial R_{rz}}{\partial r} - \frac{R_{\theta\theta}R_{\theta z}}{r}\right)\right]\right\}$$

$$+ \frac{C_{sn}}{r}\frac{k}{\varepsilon}\left\{ R_{r\theta}\frac{\partial R_{rz}}{\partial r} - \frac{R_{\theta\theta}R_{\theta z}}{r} + n\left[R_{rz}\frac{\partial R_{r\theta}}{\partial r} + R_{\theta z}\frac{\left(R_{rr} - R_{\theta\theta}\right)}{r} \right.\right.$$

$$\left.\left. + R_{rr}\frac{\partial R_{\theta z}}{\partial r} + \frac{R_{r\theta}R_{rz}}{r}\right]\right\} .$$

Appendix C: Coordinate Transformation Parameters

This Appendix describes the calculation of the four parameters appearing in the logarithmic coordinate transformations used in this study. The transformations are briefly described in Section 2.4 of this report.

We introduce the new independent variables y and x in place of r and z where

$$y \equiv a_y^{-1} \ln(1 + r/b_y)$$

and

$$x \equiv a_x^{-1} \ln(1 + (z - Z_i)/b_x) \ .$$

In order to arrive at appropriate values of the parameters a_y and b_y which appear in the r to y transformation, we first specify R_{max} (the location of the North boundary), and the value desired for y at R_{max}. We will denote this value as y_{max}. We assume that a total of M_c grid points will be distributed radially over the region $0 \leq r \leq R_c$ where R_c is less than R_{max}. Generally, R_c is approximately the wake radius at the West (upstream) boundary, and M_c is the number of grid points across the wake at this station. Then, since $\Delta y = y_{max}/(M_c - 1)$, y_c, which is the y value corresponding to R_c, is given by $y_c = (M_c - 1)\Delta y$. After inverting the transformation we may, therefore, write

$$R_c = b_y(\exp(a_y y_c) - 1)$$

and

$$R_{max} = b_y(\exp(a_y y_{max}) - 1) \ .$$

We rearrange and divide these expressions to yield

$$\frac{(1 - \exp(a_y y_c))}{(1 - \exp(a_y y_{max}))} - \frac{R_c}{R_{max}} = 0 \ .$$

We solve this equation for a_y using a simple Newton-Raphson iterative procedure beginning with an initial estimate (guess) for a_y. With a_y known, we obtain b_y explicitly from either

$$b_y = R_c(\exp(a_y y_c) - 1)^{-1},$$

or

$$b_y = R_{max}(\exp(a_y y_{max}) - 1)^{-1}.$$

The calculation of the parameters a_x and b_x of the z to x transformation follows a procedure identical to that which has been described above.

Appendix D: Finite-Difference Equations

The finite-difference formulations of the transformed version of the mean-flow, pressure, turbulence model, and East boundary condition equations are presented in this Appendix. The finite-difference grid system is shown in Figure 3.2 and has been described in Section 3 of this report.

D.1 Notation

In the difference equations presented below, centered second-order differences are used to approximate most spatial derivatives, and are denoted as follows (where ϕ can represent U, V, W, R_{rr}, etc.):

$$\frac{\partial \phi}{\partial x} \approx D_{oi}\phi_{ij} \equiv (\phi_{i+1,j} - \phi_{i-1,j})/2\Delta x ,$$

$$\frac{\partial \phi}{\partial y} \approx D_{oj}\phi_{ij} \equiv (\phi_{i,j+1} - \phi_{i,j-1})/2\Delta y ,$$

$$\frac{\partial^2 \phi}{\partial x^2} \approx D_{+i}D_{-i}\phi_{ij} \equiv (\phi_{i+1,j} + \phi_{i-1,j} - 2\phi_{ij})/\Delta x^2$$

and $$\frac{\partial^2 \phi}{\partial y^2} \approx D_{+j}D_{-j}\phi_{ij} \equiv (\phi_{i,j+1} + \phi_{i,j-1} - 2\phi_{ij})/\Delta y^2 ;$$

while, first-order backward differencing, which is used at $i = N$ to approximate certain derivatives with respect to x, is denoted as

$$\frac{\partial \phi}{\partial x} \approx D_{-i}\phi_{ij} \equiv (\phi_{ij} - \phi_{i-1,j})/\Delta x .$$

The weighted centered-upwind finite-difference formulation used to approximate axial convection terms, as described in the body of this report, is written using the above notation as

$$W \frac{\partial \phi}{\partial x} \approx (W_{ij}D_{oi} - \alpha_i |W_{ij}| \frac{\Delta x}{2} D_{+i}D_{-i})\phi_{ij} .$$

This formulation makes clear the introduction of artificial diffusion for non-zero values of α_i; the artificial viscosity at grid point i,j is $\alpha_i |W_{ij}| \Delta x/2$.

As a result of their definition on a staggered grid system (with grid points denoted as $i+\frac{1}{2}, j+\frac{1}{2}$) the x and y derivatives

of P at grid point i,j are approximated by averaged centered differences so that

$$\frac{\partial P}{\partial x} \approx (D^*_{oi}P)_{ij} \equiv \Big[(P_{i+\frac{1}{2},j+\frac{1}{2}} - P_{i-\frac{1}{2},j+\frac{1}{2}}) + (P_{i+\frac{1}{2},j-\frac{1}{2}} - P_{i-\frac{1}{2},j-\frac{1}{2}})\Big] /2\Delta x \ ,$$

and

$$\frac{\partial P}{\partial y} \approx (D^*_{oj}P)_{ij} \equiv \Big[(P_{i+\frac{1}{2},j+\frac{1}{2}} - P_{i+\frac{1}{2},j-\frac{1}{2}}) + (P_{i-\frac{1}{2},j+\frac{1}{2}} - P_{i-\frac{1}{2},j-\frac{1}{2}})\Big] /2\Delta y \ .$$

Finally, the values of the coefficients f(y) , g(y) , h(y) , s(x) , and t(x) are denoted at the grid points by f_j , g_j , h_j , s_i , and t_i , respectively.

D.2 Mean-Flow Equations

As discussed in Section 3.2.2 of this report, the ADI procedure introduces two half time-steps each of length 1/2 $\Delta\tau$. During alternate steps, appropriate y and x derivatives of mean-flow quantities in Equations (3.13), (3.14) and (3.15) are differenced implicitly. The implicit differencing results in sequences of tridiagonal matrix equations for U_{ij} , V_{ij} , and W_{ij} which are easily solved. Note that in the equations presented below, the Reynolds stress terms are approximated at the appropriate time level and at grid point i,j by

$$\text{TURBU} = s_i D_{oi} R_{rz} + F_j D_{oj} R_{rr} + h_j (R_{rr} - R_{\theta\theta}) \ ,$$

$$\text{TURBV} = s_i D_{oi} R_{\theta z} + f_j D_{oj} R_{r\theta} + 2h_j R_{r\theta} \ ,$$

and $$\text{TURBW} = s_i D_{oi} R_{zz} + f_j D_{oj} R_{rz} + h_j R_{rz} \ .$$

In the above difference expression and those which follow, the i,j subscripts are omitted.

D.2.1 ADI First Half Time-Step

During the first half time-step, which advances the solution from time level n to $n+\frac{1}{2}$, y derivatives of the mean velocities U, V, and W are treated implicitly. The following finite-difference equations are thus obtained:

$$\frac{U^{n+\frac{1}{2}} - U^n}{\Delta\tau/2} + f_j U^n D_{oj} U^{n+\frac{1}{2}} + s_i (W^n D_{oi} - \alpha_i |W| \frac{\Delta x}{2} D_{+i} D_{-i}) U^n - h_j (V^n)^2$$
$$= -f_j (D^*_{oj} P)^n + Re^{-1} \left\{ \left[f_j^2 D_{+j} D_{-j} + (g_j + f_j h_j) D_{oj} - h_j^2 \right] U^{n+\frac{1}{2}} \right.$$
$$\left. + (s_i^2 D_{+i} D_{-i} + t_i D_{oi}) U^n \right\} - TURBU^n \ ,$$

$$\frac{V^{n+\frac{1}{2}} - V^n}{\Delta\tau/2} + f_j U D_{oj} V^{n+\frac{1}{2}} + s_i (W^n D_{oi} - \alpha_i |W| \frac{\Delta x}{2} D_{+i} D_{-i}) V^n + h_j U^n V^n$$
$$= Re^{-1} \left\{ \left[f_j^2 D_{+j} D_{-j} + (g_j + f_j h_j) D_{oj} - h_j^2 \right] V^{n+\frac{1}{2}} \right.$$
$$\left. + (s_i^2 D_{+i} D_{-i} + t_i D_{oi}) V^n \right\} - TURBV^n \ ,$$

and

$$\frac{W^{n+\frac{1}{2}} - W^n}{\Delta\tau/2} + f_j U^n D_{oj} W^{n+\frac{1}{2}} + s_i (W^n D_{oi} - \alpha_i |W^n| \frac{\Delta x}{2} D_{+i} D_{-i}) W^n$$
$$= -s_i (D^*_{oi} P)^n + Re^{-1} \left\{ \left[f_j^2 D_{+j} D_{-j} + (g_j + f_j h_j) D_{oj} \right] W^{n+\frac{1}{2}} \right.$$
$$\left. + (s_i^2 D_{+i} D_{-i} + t_i D_{oi}) W^n \right\} - TURBW^n \ .$$

As a result of the use of implicit differencing in the y direction only, these three difference equations may be rearranged as independent systems to the form

$$A_{ij} \phi_{i,j-1} + B_{ij} \phi_{ij} + C_{ij} \phi_{i,j+1} = D_{ij} \ ,$$

where $2 \le j \le M - 1$, for each value of i, $2 \le i \le N - 1$. The quantity ϕ_{ij} represents $U^{n+\frac{1}{2}}_{ij}$, $V^{n+\frac{1}{2}}_{ij}$ or $W^{n+\frac{1}{2}}_{ij}$, and the

coefficients A_{ij} , B_{ij} , C_{ij} and D_{ij} are evaluated using the known values of the solution at time level n . It should be noted that A_{ij} , B_{ij} , C_{ij} and D_{ij} differ depending on whether ϕ_{ij} represents U_{ij} , V_{ij} or W_{ij} . The boundary conditions at j+1 and j = M are incorporated, and the equation systems are solved suing the Thomas algorithm (see Roache, 1972) at each value of i for ϕ_{ij} where $1 \leq j \leq M$.

D.2.2 ADI Second Half Time-Step

During the second half time-step which advances the solution from time level $n+\frac{1}{2}$ to n+1 , x derivatives of U , V , and W are treated implicitly. The following equations result:

$$\frac{U^{n+1} - U^{n+\frac{1}{2}}}{\Delta\tau/2} + f_j U^{n+\frac{1}{2}} D_{oj} U^{n+\frac{1}{2}} + s_i (W^{n+\frac{1}{2}} D_{oi} - \alpha_i |W^{n+\frac{1}{2}}| \frac{\Delta x}{2} D_{+i} D_{-i}) \times U^{n+1} - h_j (V^{n+\frac{1}{2}})^2 = -f_j (D^*_{oj} P)^{n+\frac{1}{2}} + Re^{-1} \left\{ \left[f_j^2 D_{+j} D_{-j} + (g_j + f_j h_j) D_{oj} - h_j^2 \right] \times U^{n+\frac{1}{2}} + (s_i^2 D_{+i} D_{-i} + t_i D_{oi}) U^{n+1} \right\} - TURBU^{n+\frac{1}{2}} ,$$

$$\frac{V^{n+1} - V^{n+\frac{1}{2}}}{\Delta\tau/2} + f_j U^{n+\frac{1}{2}} D_{oj} V^{n+\frac{1}{2}} + s_i (W^{n+\frac{1}{2}} D_{oi} - \alpha_i |W^{n+\frac{1}{2}}| \frac{\Delta x}{2} D_{+i} D_{-i}) \times V^{n+1} + h_j U^{n+\frac{1}{2}} V^{n+\frac{1}{2}} = Re^{-1} \left\{ \left[f_j^2 D_{+j} D_{-j} + (g_j + f_j h_j) D_{oj} - h_j^2 \right] V^{n+\frac{1}{2}} + (s_i^2 D_{+i} D_{-i} + t_i D_{oi}) V^n \right\} - TURBV^{n+\frac{1}{2}} ,$$

and

$$\frac{W^{n+1} - W^{n+\frac{1}{2}}}{\Delta\tau/2} + f_j U^{n+\frac{1}{2}} D_{oj} W^{n+\frac{1}{2}} + s_i (W^{n+\frac{1}{2}} D_{oi} - \alpha_i |W^{n+\frac{1}{2}}| \frac{\Delta x}{2} D_{+i} D_{-i}) \times W^{n+1} = -s_i (D^*_{oi} P)^{n+\frac{1}{2}} + Re^{-1} \left\{ \left[f_j^2 D_{+j} D_{-j} + (g_j + f_j h_j) D_{oj} \right] W^{n+\frac{1}{2}} \right.$$

$$+ \left(s_i^2 D_{+i} D_{-i} + t_i D_{oi}\right)^{n+\frac{1}{2}} \Bigg\} - \text{TURBW}^{n+\frac{1}{2}} \quad .$$

As is the case during the first half-step, these equations can also be rearranged as independent tridiagonal systems but of the form

$$A_{ij}\phi_{i-1,j} + B_{ij}\phi_{ij} + C_{ij}\phi_{i+1,j} = D_{ij} \ ,$$

where $2 \le i \le N - 1$, for each value of j, $2 \le j \le M - 1$. Here ϕ_{ij} represents U_{ij}^{n+1}, V_{ij}^{n+1} or W_{ij}^{n+1}, and the coefficients A_{ij}, B_{ij}, C_{ij} and D_{ij} are evaluated using the known values of the solution at time level $n+\frac{1}{2}$. When the boundary conditions at $i = 1$ and $i = N$ are incorporated, the systems are solved at each value of j for ϕ_{ij} where $2 \le i \le N$ (remember that U_j, V_j and W_j are specified).

D.3 Turbulence Model Equations

The turbulence model equations which determine the seven turbulence model quantities contain second derivatives in the y direction. They are, therefore, treated implicitly only in the y direction, and, as a result, identical finite-difference formulations are used to advance the solution from time step n to $n+\frac{1}{2}$ and from time level $n+\frac{1}{2}$ to $n+1$.

Since the difference equations for the seven quantities are all quite similar, only the equation for $R_{rr_{ij}}$ is presented here; the equation is written as follows

$$\frac{R_{rr}^{n+\frac{1}{2}} - R_{rr}^{n}}{1/2\tau} + f_j U^n D_{oj} R_{rr}^{n+\frac{1}{2}} + s_i\left(W^n D_{oi} - \alpha_i \left|W^n\right| \frac{\Delta x}{2} D_{+i} D_{-i}\right) R_{rr}^{n}$$

$$- 2h_j V^n R_{r\theta}^{n}$$

$$= P_{rr}^{n} - \frac{2}{3}\varepsilon^n + \tilde{\phi}_{rr,1}^{n} + \tilde{\phi}_{rr,2}^{n} + Df_{rr}^{n} \ ,$$

where

$$P_{rr}^{n} = -2\left\{\left[f_j R_{rr}^{n} D_{oj} + s_i R_{rz} D_{oi}\right] U^n - h_j R_{r\theta}^{n} V^n\right\} \ ,$$

$$\tilde{\phi}_{rr,1} = -C_1 \frac{\varepsilon^n}{k^n}\left(R_{rr}^{n} - \frac{2}{3}k^n\right) \ ,$$

$$\tilde{\phi}_{rr,2} = -C_3(P^n_{rr} - \frac{2}{3} P^n_k) - 2C_4 k^n f_j D_{oj} U^n - C_5(D^n_{rr} - \frac{2}{3} P^n_k) ,$$

and

$$D^n_{rr} = -2f_j \left\{ R^n_{rr} D_{oj} U^n + R^n_{r\theta} D_{oj} V^n + R^n_{rz} D_{oj} W^n \right\} .$$

The finite-difference approximation to the turbulent diffusion expression Df_{rr}, is

$$Df^n_{rr} = (2n + 1)C_{sn} h_j f_j D_{oj} \left\{ h_j^{-1} \frac{k^n}{\varepsilon^n} \left[f_j R_{rr} D_{oj} R^{n+\frac{1}{2}}_{rr} - 2h_j (R^n_{r\theta})^2 \right] \right\}$$

$$- 2C_{sn} h_j \frac{k^n}{\varepsilon^n} \left\{ (n + 1) \left[f_j R^n_{r\theta} D_{oj} R^n_{r\theta} + h_j R^n_{\theta\theta} \cdot (R^n_{rr} - R^n_{\theta\theta} \right] \right.$$

$$\left. + n \left[f_j R^n_{rr} D_{oj} R^n_{\theta\theta} + 2h_j (R^n_{r\theta})^2 \right] \right\} .$$

(The quantity n which appears as a <u>coefficient</u> in the above expression does not refer to time level. It is, instead, simply a parameter which may take on the values zero or one. See the discussion of the turbulent diffusion model formulation in Appendix B for details.)

At $i = N$ we replace the weighted centered-upwind convection by the simple first-order expression $s_N W_{Nj} D_{-i} R_{rr_{Nj}}$ so that the difference equations are defined for $2 \le i \le N$, $2 \le j \le M$.

The difference equation for R_{rr} presented above (with the slight modification at $i = N$) is rearranged into independent tridiagonal systems of the form

$$A_{ij} R_{rr_{i,j-1}} + B_{ij} R_{rr_{ij}} + C_{ij} R_{rr_{i,j+1}} = D_{ij} ,$$

where $2 \le j \le M - 1$, for each value of i, $2 \le i \le N$. As in the case for the mean-momentum equations during the first half time-step, these equations are solved at each i for $1 \le j \le M$ after the boundary conditions at $j = 1$ and $j = M$ are incorporated.

The difference equations for the other six turbulence models quantities are similar and are solved in identical fashion.

D.4 Poisson Pressure Equation

The transformed Poisson pressure equation (Equation 3.16) is solved numerically for $P_{i+\frac{1}{2},j+\frac{1}{2}}$ at each half time-step following the calculation of both the mean velocities and the turbulence quantities. The finite-difference formulation of the pressure equation at time step n is written as follows

$$\left[f^2_{j+\frac{1}{2}} D_{+j} D_{-j} + (g_{j+\frac{1}{2}} + f_{j+\frac{1}{2}} h_{j+\frac{1}{2}}) D_{oj} + s^2_{i+\frac{1}{2}} D_{+i} D_{-i} + t_{i+\frac{1}{2}} D_{oi} \right] P^n_{i+\frac{1}{2},j+\frac{1}{2}} = F^n_{i+\frac{1}{2},j+\frac{1}{2}} ,$$

where

$$F_{i+\frac{1}{2},j+\frac{1}{2}} = f^2_{i+\frac{1}{2}} (D^*_{oj} C_y)^n_{i+\frac{1}{2},j+\frac{1}{2}} + (g_{j+\frac{1}{2}} + f_{j+\frac{1}{2}} \times h_{j+\frac{1}{2}}) C_{y_{i+\frac{1}{2},j+\frac{1}{2}}} + s^2_{i+\frac{1}{2}} (D^*_{oi} C_x)_{i+\frac{1}{2},j+\frac{1}{2}} + t_{i+\frac{1}{2}} C^n_{x_{i+\frac{1}{2},j+\frac{1}{2}}} - D^{n-\frac{1}{2}}_{i+\frac{1}{2},j+\frac{1}{2}} \Delta\tau/2 .$$

The D^*_{oj} and D^*_{oi} operators have been defined above; and

$$C^n_{y_{i+\frac{1}{2},j+\frac{1}{2}}} = \frac{1}{4}(C^n_{y_{i+1,j+1}} + C^n_{y_{i+1,j}} + C^n_{y_{i,j+1}} + C^n_{y_{ij}}) ,$$

and

$$C^n_{x_{i+\frac{1}{2},j+\frac{1}{2}}}$$

is a similar 4-point average. The quantities $C^n_{y_{ij}}$ and $C^n_{x_{ij}}$ are approximated as follows:

$$C^n_{y_{ij}} = -f_j^{-1} \left\{ \left[-f_j U^n D_{oj} - (s_i W^n D_{oi} - \alpha_i |W^n| \frac{\Delta x}{2} D_{+i} D_{-i}) \right] U^n + h_j (V^n)^2 + s_i D_{oi} R^n_{rz} + f_i D_{oj} R^n_{rr} + h_j (R^n_{rr} - R^n_{\theta\theta}) \right\} ,$$

and

$$C_{x_{ij}}^{n} = -s_i^{-1}\left\{\left[-F_j UD_{oj} - (s_i WD_{oi} - \alpha_i|W^n|\frac{\Delta x}{2} D_{+i}D_{-i}\right]W^n + s_i D_{oi}R^n + (f_j D_{oj} + h_j)R_{rz}^n\right\} .$$

The finite-difference approximation to the divergence of the mean velocity field at n is computed from

$$D^n_{i+\frac{1}{2},j+\frac{1}{2}} = h_{j+\frac{1}{2}} f_{j+\frac{1}{2}} (D^*_{oj} u^{n-1})^n_{i+\frac{1}{2},j+\frac{1}{2}} + s_{i+\frac{1}{2}} (D^*_{oi} W)^n_{i+\frac{1}{2},j+\frac{1}{2}} .$$

As mentioned in Section 2.2 of this report, we use the NCAR BLKTRI direct Poisson solver to solve the above difference equation for $P^n_{i+\frac{1}{2},j+\frac{1}{2}}$.

D.5 East Boundary Conditions

During the first half time-step, y derivatives in the transformed and "unsteady" versions of Equations 3.10 and 3.11, which apply at the East boundary, are differenced implicitly, and x derivatives in the axial convection terms are approximated with first-order backward differences. The following equations, which apply at $i = N$, then result:

$$\frac{V^{n+\frac{1}{2}}_{Nj} - V^n_{Nj}}{\Delta\tau/2} + f_j U^n_{Nj} D_{oj} V^{n+\frac{1}{2}}_{Nj} + s_N W^n_{Nj} D_{-i} V^n_{Nj} + h_j U^n_{Nj} V^n_{Nj} = Re^{-1}\left[f_j^2 D_{+j}D_{-j} + (g_j + f_j h_j)D_{oj} - h_j^2\right] V^{n+\frac{1}{2}}_{Nj} - \left[f_j D_{oj} + 2h_j\right] R^n_{r\theta_{Nj}} ,$$

and

$$\frac{W^{n+\frac{1}{2}}_{Nj} - W^n_{Nj}}{\Delta\tau/2} + f_j U^n_{Nj} D_{oj} W^{n+\frac{1}{2}}_{Nj} + s_N W^n_{Nj} D_{-i} W^n_{Nj} = -s_i (P^n_{N,j+\frac{1}{2}} + P^n_{N,j-\frac{1}{2}} - P^n_{N-\frac{1}{2},j+\frac{1}{2}} - P^n_{N-\frac{1}{2},j-\frac{1}{2}})\Delta x^{-1} + Re^{-1}\left[f_j^2 D_{+j}D_{-j} + (g_j + f_j' h_j)D_{oj}\right] W^{n+\frac{1}{2}}_{Nj} - \left[f_j D_{oj} + h_j\right] R^n_{rz_{Nj}} .$$

Both of these finite-difference equations can be expressed in the tridiagonal form

$$A_{Nj}\phi_{N,j-1} + B_{Nj}\phi_{Nj} + C_{Nj}\phi_{N,j+1} = D_{Nj} .$$

These tridiagonal systems are solved for $V_{Nj}^{n+\frac{1}{2}}$ and $W_{Nj}^{n+\frac{1}{2}}$ after incorporation of the boundary conditions at $j = 1$ and $j = M$. The transformed version of Equation 2.12 is then integrated numerically from the axis (since $U_{N,1} = 0$) to obtain $U_{Nj}^{n+\frac{1}{2}}$. After the turbulence quantities are computed at time level $n+\frac{1}{2}$, Equation 3.9 is integrated numerically for $P_{N,j+\frac{1}{2}}^{n+\frac{1}{2}}$, which is used as the East boundary condition in the calculation of $P_{i+\frac{1}{2},j+\frac{1}{2}}^{n+\frac{1}{2}}$.

During the second half time-step, x derivatives are differenced implicitly, and the following difference equation results for V_{Nj}^{n+1} with a similar one for W_{Nj}^{n+1}:

$$\frac{V_{Nj}^{n+1} - V_{Nj}^{n+\frac{1}{2}}}{1/2} + f_j U_{Nj}^{n+\frac{1}{2}} D_{oj} V_{Nj}^{n+\frac{1}{2}} + s_N W_{Nj}^{n+\frac{1}{2}} D_{-1} V_{Nj}^{n+1}$$

$$= Re^{-1}\left[f_j^2 D_{+j} D_{-j} + (g_j + f_j h_j) D_{oj} - h_j^2\right] V_{Nj}^{n+\frac{1}{2}}$$

$$- \left[f_j D_{oj} + 2h_j\right] R_{r\theta_{Nj}}^{n+\frac{1}{2}} .$$

This equation can be rearranged and expressed in the form

$$A_{Nj}\phi_{N-1,j}^{n+1} + B_{Nj}\phi_{Nj}^{n+1} = D_{Nj}$$

for each value of j. The application of this kind of condition to the tridiagonal equations for V_{ij}^{n+1} and W_{ij}^{n+1} $(i < N)$ is straightforward. The procedure is discussed in Roache (1972). Following the calculation of V_{ij}^{n+1} and W_{ij}^{n+1} $(2 \leq i \leq N)$, Equation 3-12 is integrated to obtain U_{Nj}^{n+1} which is used as a boundary condition in the calculation for U_{ij}^{n+1} $(i < N)$. Finally, after the calculation of the turbulence

quantities, Equation 3-9 is integrated for $P^{n+1}_{N,j+\frac{1}{2}}$ which is used as a boundary condition in the calculation for $P^{n+1}_{i+\frac{1}{2},j+\frac{1}{2}}$.

DISTRIBUTION LIST FOR ICWAKE REPORTS

Defense Advanced Research
Projects Agency
1400 Wilson Boulevard
Arlington, VA 22209
Attn: P. A. Selwyn, TTO
F. A. Koether, TTO

Defense Intelligence Agency
Deputy Director for Scientific
and Technical Intelligence
The Pentagon, Room 1E864
Washington, DC 20301

Department of the Navy
Washington, DC 20390
Attn: CAPT W. Perdum (NSP), SP 202

Assistant Secretary of the Navy
(Research, Engineering, and Systems)
The Pentagon
Washington, DC 20360
Attn: R. Hoglund

Naval Intelligence Support Center
4301 Suitland Road
Washington, DC 20390
Attn: W. M. Hubbard
B. Leven

Office of Naval Research
800 N. Quincy Street
Arlington, VA 22217
Attn: R. Cooper, Code 438
R. Mindak, Code 438
S. Reed, Code 100B
CDR E. O'Brien, Code 222

Mr. James Probus
Director of Naval Laboratories
Washington, DC 20360

Naval Ocean Systems Center
San Diego, CA 92135
Attn: R. Buntzen
G. Donohue

Central Intelligence Agency
Washington, DC 20505
Attn: H. Farmer
G. Goodrich

USD(R&E)
The Pentagon
Washington, DC 20301
Attn: R. Ruffine, Room 3E1082

Defense Documentation Center
Cameron Station
Alexandria, VA 22314

Chief of Naval Operations
The Pentagon
Washington, DC 20350
Attn: NOP-09
NOP-095
NOP-095T
NOP-02
NOP-212E
NOP-009
NOP-00KB

Naval Research Laboratory
Washington, DC 20390
Attn: J. O. Elliott, Code 8300
J. Witting, Code 8340
J. Dugan, Code 8340
E. Rudd, Code 8310

Naval Air Systems Command
Washington, DC 20360
Attn: NAIR-370E

Commander
Naval Undersea Systems Center
Newport, RI 02840
Attn: G. Garosi

National Security Agency
Ft. George G. Mead, MD 20755

Battelle Memorial Institute
505 King Avenue
Columbus, OH 43201
Attn: TACTEC Office

TRW Systems
One Space Park
Redondo Beach, CA 90278
Attn: Dr. J. Chang

Flow Research Company
P. O. Box 5040
Kent, WA 98031
Attn: Dr. J. Riley

JAYCOR
1401 Camino Del Mar
Del Mar, CA 92014
Attn: Dr. J. H. Stuhmiller

Poseidon Research
11777 San Vicente Blvd., Suite 641
Los Angeles, CA 90049
Attn: Dr. S. C. Crow

The Johns Hopkins University
Applied Physics Laboratory
Johns Hopkins Road
Laurel, MD 20910
Attn: H. Gilreath
R. Gasparovic
L. Crawford
J. Austin (2 copies)

Science Applications, Inc.
P. O. Box 2351
La Jolla, CA 92038
Attn: Dr. K. Victoria

The Aerospace Corporation
O. O. Box 92957
Los Angeles, CA 90009
Attn: Dr. T. D. Taylor

Dynamics Technology, Inc.
3838 Carson Street, Suite 110
Torrance, CA 90503
Attn: Dr. D. R. S. Ko

Hydronautics, Incorporated
7210 Pindell School Road
Laurel, MD 20810
Attn: Dr. T. R. Sundaram

Arete Associates
2120 Wilshire Boulevard
Santa Monica, CA 90403
Attn: Dr. F. Fernandez

Science Applications, Inc.
8400 Westpark Drive
McLean, VA 22101
Attn: Dr. G. O. Roberts

Virginia Polytechnic Institute
and State University
P. O. Box 290
Blacksburg, VA 24061
Attn: Dr. J. A. Schetz

SRI International
1611 N. Kent Street
Arlington, VA 22209
Attn: Dr. LeVine

Operations Research, Inc.
1400 Spring Street
Silver Spring, MD 20910
Attn: E. Holmboe

Institute for Defense Analyses
400 Army-Navy Drive
Arlington, VA 22202
Attn: J. C. Nolen
W. Wasylkiwskyj